University of Huddersfield Repository

Rahmatinia, Ali

Intrinsic Fibre Strain Sensor Interrogation Using Broadband Interferometry

Original Citation

Rahmatinia, Ali (2021) Intrinsic Fibre Strain Sensor Interrogation Using Broadband Interferometry. Masters thesis, University of Huddersfield.

This version is available at http://eprints.hud.ac.uk/id/eprint/35566/

http://eprints.hud.ac.uk/

INTRINSIC FIBRE STRAIN SENSOR IINTEROGATION USING BROADBAND INTERFEROMETRY

ALI RAHMATINIA

This thesis submitted to the faculty of the University of Huddersfield in fulfilment of the degree of Master of Science in Electronic Engineering

The University of Huddersfield

May 2021

Abstract

Strain measurement is an essential part of quality control and monitoring for many engineering purposes. One of the best types of strain sensors is a fibre optic strain sensor.

Optical fibre sensors have the exclusive upper hand and unique features compared to more traditional sensors, which make them very enticing for various purposes, notably those with demanding conditions where other conventional electrical sensors normally fail. Due to the harsh environment, explosion risks, durability, and massive electromagnetic noises, well-known electrical sensors are impermissible in numerous technical and industrial applications. The fibre optic sensors can endure severe conditions (pressure, high temperature) and offer complete electromagnetic immunity. Thus, fibre optic sensors are a viable alternative for these types of purposes.

This thesis talks about:

- What are the strain and different types of strain sensors?
    - Traditional mechanical and electrical strain sensors as well as some backgrounds to what a fibre optic is, and various kinds of fibre optic gauges.
- The advantages and disadvantages of fibre optic gauges.
- Different methods of fibre sensing and their modulation and demodulation techniques.
    - Various interferometry sensors and techniques like Michelson, Fabry-Perot, Mach-Zehnder and Sagnac.
- Commercial research about the Fabry-Perot.
    - Choosing the Fabry-Perot (Intrinsic Fabry-Perot interferometer) sensor, its advantages over other fibre optic sensors.
- Setting up the testing system and various test steps that were taken, such as building two plastic jigs for the test.
- Data analysis of the system, signal processing (Takeda method), different cropping and filtration of the signal to achieve the slope, and consequently calculate the strain, error%, stability, and various sensor characteristics.
- The conclusion explains the need for the research, how the test was done and what it achieved.

Testimony of authenticity

I herewith declare that I am the sole author of this Thesis, and there are no tendered or distributed portions of this thesis anywhere else.

I validate, to the best of my knowledge, my dissertation does not contravene upon anyone's copyright nor infringe any intellectual property rights/ideas, methods, or any other element of the effort of other individuals. This dissertation is entirely in consonance with the traditional referencing disciplines.

I state that this is a genuine transcript of my dissertation, covering all revisions and updates, being recognized by my Project board and the Graduate Studies department. This dissertation has not been proffered for a higher level to any school or university.

1 Table of Contents

List of Figures

1 Introduction

1.1 Motivation

High accuracy system monitoring is one of the most important aspects of any project or product. Sensors are one crucial part of these systems. Monitoring temperatures, strain, or pressure could identify problems early, reduce unnecessary costs, and allow proper steps to be taken before a significant incident or costly maintenance. Strain sensors provide a long-life span and high efficiency by delivering precise strain data to ensure improvement in the implementation of many applications such as bridges, tunnels, power stations, etc., which led to time and cost savings. [62] Several methods have been applied to build strain gauges, such as mechanical, electrical, and fibreoptic sensors.

Among these technologies, electrically based strain sensors are primarily used in practice due to their exceptional reliability, high precision, and low cost; nevertheless, every electrical sensor requires its dedicated interrogation device and electrical connection. In conventional strain sensors (electrical), the sensor network is complicated and costly to maintain. Besides, these sensors have the problem of electromagnetic noise since they operate based on the electrical current.

On the other hand, fibre-optic sensors have different characteristics, making them lucrative and sometimes the only go-to option. The excellent optical bandwidth, low power dissipation, and good resistance to electromagnetic noise enable the implementation of several types of sensors in one fibre optic cord.

Simplified maintenance, wire connection, and reducing the cost per sensing point could be achieved using fibre optic sensors (multiplexed sensors). Additionally, fibre-optic gauges have other benefits like low power consumption, small size, lightweights, high sensitivity, wide bandwidth, passive operation, resistance to electromagnetic interference, and environmental ruggedness. The motivation of this study is to satisfy the growing need for fibre strain systems with robustness, economic benefits, high resolution, and easy fabrication that can be run dependably in rigid circumstances or extended structures.

This work examines an Intrinsic Fabry-Perot Interferometric (IFPI) strain sensor to find a more commercially reasonable priced sensor with practical sensitivity and resilience that can monitor strain on a fibre optic.

1.2   Aims & Objectives.

The purpose of this research is to establish the market size and primary competition for high-resolution strain sensing. Contact potential commercial partners (the UK focus initially), develop the laboratory apparatus into a robust yet portable demonstrator and Develop a test rig to enable improved test capability with the current apparatus and establish a full 'marketable' performance specification.

Make technical improvements in some aspects of the signal analysis to allow for further marketable features such as multi-sensor interrogation.

Deliverables of this research are:

- Market survey about different competitors and <u>Strength, Weakness, Opportunity, and Threats</u>
  (SWOT) analysis of the Intrinsic Fabry-Perot Interferometric (IFPI) and potential compotators.

- Enhancing the test rig so proper measurements can be performed to find the sensor attributes such as linearity, precision, accuracy, and pointing out the potential noise and uncertainty sources in the process.

- Improving the signal processing and try to find the best way to demodulate the signal.

1.3   Thesis' structure

1.3.1 First chapter

In this chapter, the thesis introduction, aim, objectives, and project deliverables are discussed, plus presenting the thesis outline.

1.3.2 Second chapter

The second chapter finger on the literature review, which debates examining present Fibre Optic Sensors (FOS) techniques and their specifications. It comprises SWOT analysis of FOS and their architecture, specifically Intrinsic Fabry-Perot sensors (IFPS). It compares the available FOS in a table and several graphs based on their range, accuracy, resolution, etc.

1.3.3 Third chapter

This chapter depicts the design and methodology. In other words, it gives a comprehensive account of taken actions to produce the sensor. It also demonstrates the sensor capabilities, operation, and integration.

1.3.4 **Fourth chapter**

The appraisal Chapter argues about how the sensor could serve various sectors of society. It illustrates the essence of the technology through a few case studies such as airline, oil, and construction industries.

1.3.5 **Fifth chapter**

The fifth chapter pays attention to analysis, testing, and the outcome of the project. It consists of Hardware and software testing. It shows the flaws and impediments of the system and its solutions. At the end of this section, the project's overall design is discussed, plus future work, which exhibits the potentialities of later developments.

1.3.6 **Sixth chapter**

Summarizing all the findings, discussing all restrictions, and presenting the most significant decisions made during this project are the building blocks of the final chapter (conclusion).

2   Literature review

2.1   Stress and Strain brief presentation

Stress and strain are central concepts showing how a body replies to external forces.

These concepts will be explained using the simple example of a loaded bar. Here is a solid metal bar that is loaded by two equal but opposite forces.

Since all the exerted loads act along the same axis, it is called uniaxial loading.

The two opposite forces are dragging the pole resulting in a stretch of the bar. Developed internal forces oppose these applied forces.

In this case, the effect of the internal forces acting on the cross-section created by our cut will be equivalent to the impact of the applied outer force. Here the inner powers are represented as four separate forces, but they could have been described as one or even 20 forces.

The inner energies are scattered across the whole surface of the object. Therefore, it does not matter to discuss particular inner forces. Rather, it is more helpful to discuss stress further.

Stress defines the spreading of inner forces inside a body.

The amount of inner energy by total area is called stress.

Looking at the axially loaded bar, the inner energies act vertically in the direction of made cut. This is termed normal stress.

The bar's normal stress could be evaluated as the exerted force (F) divided by the bar area (A)

$(\boldsymbol{\sigma} = \dfrac{\boldsymbol{F}}{\boldsymbol{A}}$ **(Pa or N/m2)**); it is expressed by sigma.
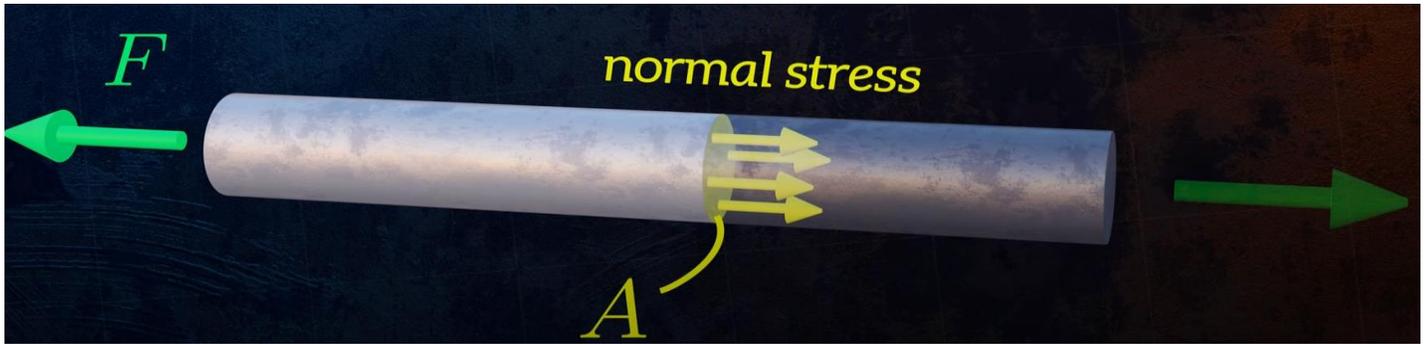
Figure 1 An object under stress

Measuring stress is very useful in our daily lives as it allows us to predict when an object will fail under specific amounts of stress.

Assume the bar diameter is 20 mm, it could be calculated that it will fail if the applied force is larger than 79 kN. Normal stress can be either tensile or compressive. In this case the stress is tensile because the forces are stretching the bar. If the forces result in shortening the bar, compressive stress will happen.

The accepted sign convention is positive for tensile stresses and negative numbers for compressive stresses.

In the case it is reasonable to assume that the stresses are distributed uniformly across the cross-section and along the length of the bar, but this is a straightforward scenario.

The stress distribution in a bent beam is more involved. Stresses are compressive on one side but tensile on the other. The deformations that happen within an object is called <u>strain</u>.

If force get applied to the bar at one end and gets secured at the other end, the force results in deformation of the bar.
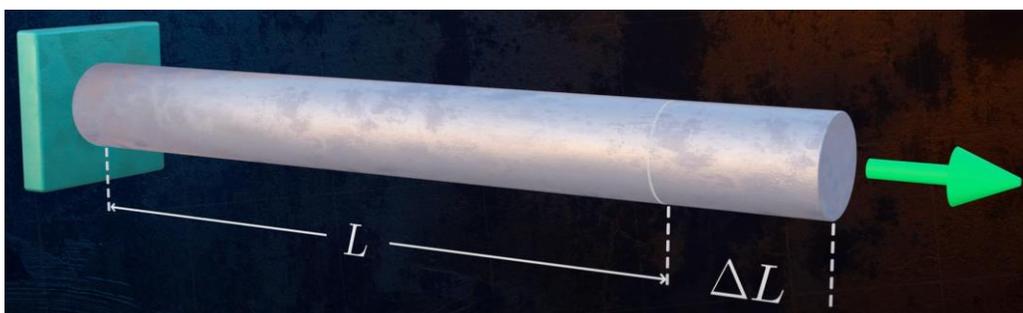
Figure 2 Strain on an object

This deformation could be measured as the length's change of the object $\boldsymbol{\Delta L}$ divided by L (the initial object length).

$$\boldsymbol{\varepsilon} = \frac{\boldsymbol{\Delta L}}{\boldsymbol{L}}$$

Strain is often stated as a percentage since it is a non-dimensional quantity.

Normal strain could be compressive or tensile. A stress-strain diagram is usually used to elaborate more about the connection between the two.

Hooke's law defines this linear relationship between stress and strain. $\sigma = E\varepsilon.$ This is only true for minor strains as a large amount of strain causes plastic deformation, which means the relation between stress and strain is no more linear.

The percentage between strain and stress is termed Young's modulus.

Another form of stress is called shear stress.

Shear stresses could be illustrated by examining the bar stresses acting on a small element.

There is a shear stress on one side of the object; however, the object must be in balance; therefore, there should also have shear stress in the opposing path.

Keeping rotational balance, having two extra shear stresses are necessary.

Shear stresses cause a rectangular object to deform. When there is a deformation, it will result in strain.
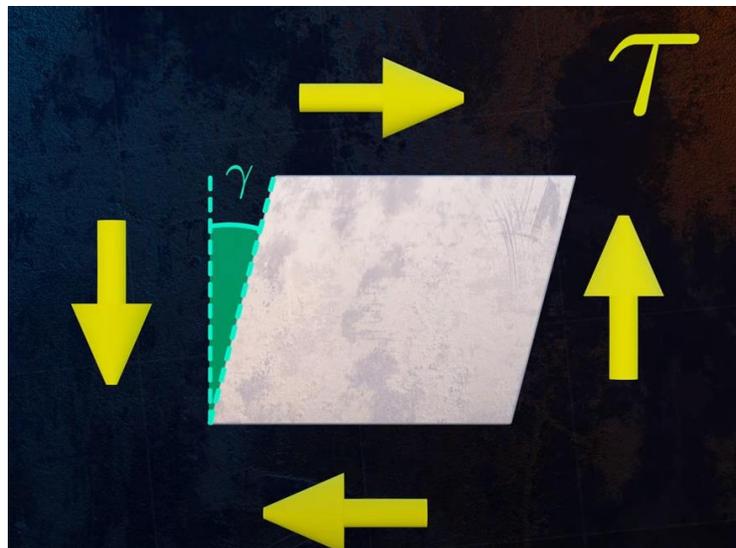
Figure 3 Shear strain on an object

The change in angle is shown here could be described as shear strain and is represented by gamma.

Shear stresses and shear strain relation is also based on Hooke's law, except the ratio between them is not Young's modulus but shear modulus G.

Although normal and shear stresses have been discussed separately, at a single point within a body, the stress state will have components in both the normal and the shear directions.

The amount of the shear and normal components will rely on the plane's angle to observe the stresses.

In the bar with uniaxial loading, the plane we used to make the imaginary cut was perpendicular to the axis of the bar, and so there was normal stresses but no shear stresses.

If instead using an inclined plane to cut the bar, there will be both normal and shear stress components. The stress element is usually representing the stresses applying at a particular point within an object. This is the stress element showing the normal and shear stresses acting at a single point for a two-dimensional case.

2.2 Non-Optical Strain detection

Strain measurement is commonly accomplished by planting a sensor inside the object of interest or securely fastening it on the host substance; then, the material deformation is conveyed to the strain gauge, that helps to measure the strain.

Mechanical sensors were used initially to measure the strain by directly amplifying the length alteration. For instance, extensometers utilizing a series of levers to accomplish the task; extensometer mean extension-meter. They are in two main classes, contact and non-contact [2]. Being one of the primary methods of strain measurements, mechanical strain sensors still have a good amount of accuracy, sometimes as high as most recommended resistant strain gauges if they are designed carefully. Despite the challenges in operating these devices, they are utilized to calibrate other types of strain sensors. A new set of compact sensors has been generated to have a more flexible and more accessible strain evaluation. These strain sensors are specifically developed to interpret strain into alternative physical quantities so it could be measured with more ease and accuracy. These quantities can comprise acoustic signals, an electrical quantity such as capacitance, resistance, and inductance, or an optical signal. Some of the existing strain sensors are based on electrical resistance, piezo-resistance, capacitance, inductance, pneumatic sensors, wire vibrations, and optical sensors. These different sensors are utilized based on their suitability for applications as they have unique characteristics compared to one another.[62]

2.2.1 Electrical-resistance strain sensors

Electrical Strain gauges are vastly utilized to measure and test force. The electrical strain gauge was invented in 1938 by Arthur C Rouge and Edward E Simmons.

This sensor is made of a zigzag shape metal strips on a non-conductive material. These metal stripes have a thickness of 3 to 5 µm.

The measuring grid is the common name used for those metal stripes. For comparison, the width of one strand of spiderweb is about three to eight micrometres.

Stress could be described as force divided by unit area. Alternatively, strain is the deformation or change caused by stress. When some force is applied to an object, it causes a variation in its length

(elongation or compression). The sensor's resistance is proportional to the change in the object shape as it is glued to the object surface. To measure the resistance for a conductor, the formula is

R =L/A

Where R = resistance, L = length, and A = area.

Therefore, the strain could be measure as the variation in the resistance divided by the initial resistance.

Strain is shown as ε, and K= gauge factor.

$$K\varepsilon = \frac{\Delta R}{R}$$

In real life, the variation is very small thus a Wheatstone bridge is usually used to measure the strain. The Wheatstone consists of 4 resistors with 1 of them being swapped by a strain gauge. The change in the strain gauge resistant causes a voltage changes which indicates the strain.
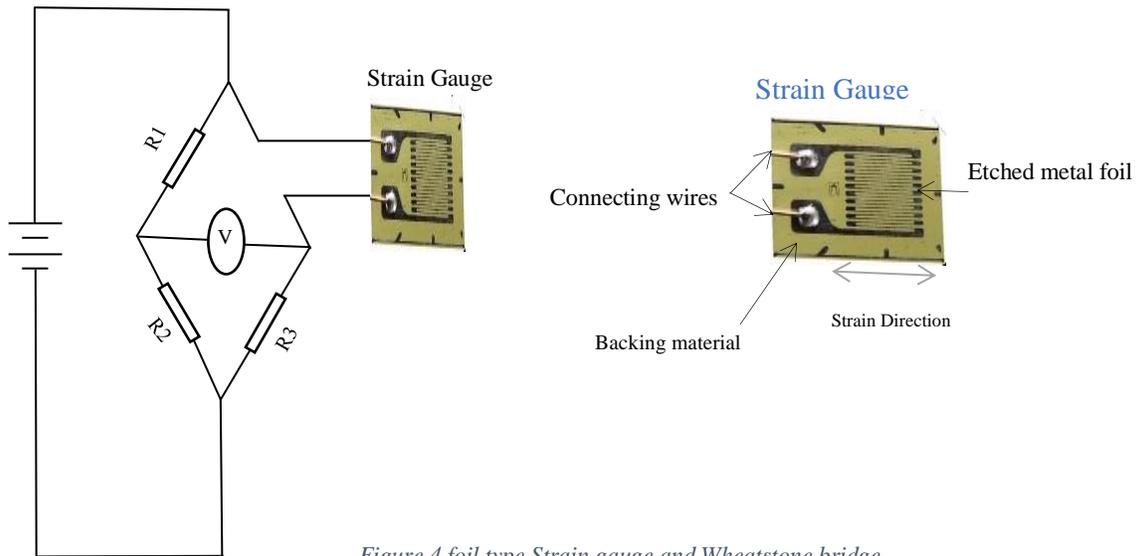
Figure 4 foil type Strain gauge and Wheatstone bridge

When an object is subjected to a force, it can experience either tensile or compressive strain. These changes occur within the limit of elasticity. When a strain gauge is placed on the object, and the object undergoes tensile strain, there is an elongation in the object quantified by a positive change in resistance. However, when the object is subjected to compressive strain, it shows a negative change in resistance; thus, it can detect both expansion and compression of the object.

Strain sensors are hugely employed to observe power plants, dams, bridges to avoid overloading disasters or accidents.

Strain gauges have the following advantages: they have no moving parts, precise, inexpensive, and small. Strain sensors also possess several weaknesses. They are susceptible to temperature, and their demand to be routinely calibrated as well as being nonlinear.

2.2.2 **Piezo-resistive strain gauges**

The piezo-resistive effect of semiconductors is the base of Piezo-resistive strain sensors [3]. As an alternative to employing a metal wire in the role of an electrical resistant sensor, Piezo-resistive sensors with a single crystal of silicon filament are applied. Variation in the filament resistance caused by strain is sensed in the same way as a metal wire; however, the gauge factor is seventy times larger [2]. Consequently, strain sensitivity is more significant yet higher drift, more considerable temperature susceptibility, and the resistance to strain nonlinear correlation, with 10-20% deviation from a straight-line equation, are the impediments of this system. These drawbacks could be compensated for with the help of computers and sophisticated measurement tools. These sensors are widely used, where temperature alteration is small, and the strain variation is minimal.

2.2.3 **Vibrating-wire strain sensors**

Fluctuation in the frequency of tensioned wire made from steel is the basis of these sensor's operation whenever the wire tension level alters. It comprises a tensioned thin steel wire fastened at both ends into flanges (testing equipment). As soon as the gap between two anchors alters owing to the strain of the material under test, the natural frequency and tension of the wire also shift. Throughout the analysis, the wire is stimulated to vibrate, and then the vibration frequency gets identified to quantify the applied strain. The benefit of this model of sensors is their profoundly stable performance, with only a slight drift.
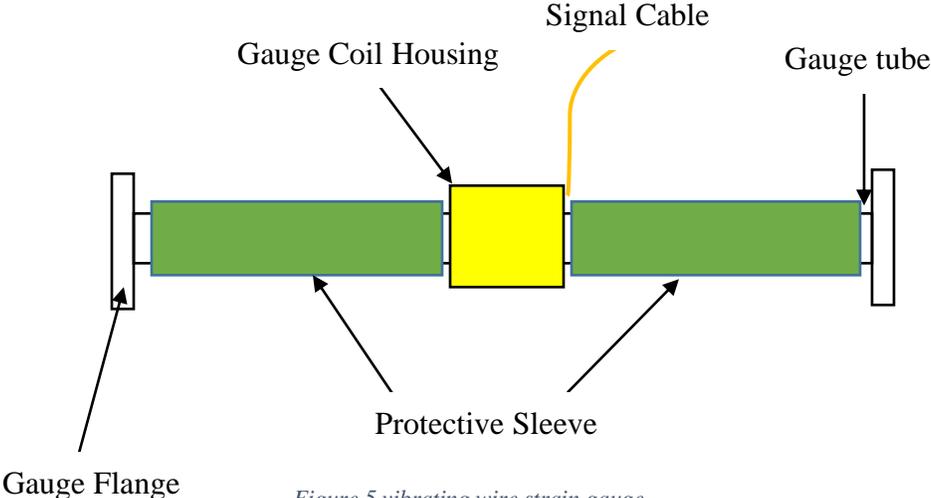
Figure 5 vibrating wire strain gauge

These sensors are costly and extensive, yet these sensors are the most robust solution to observe and control strain in metal and concrete structures due to high reliability and durability.

2.2.4 Disadvantages of Non-optical strain gauges

These sensors experience various deficiencies. One of these pitfalls is that these strain sensors cannot be multiplexed (they are point measurements). Another difficulty of these sensors occurs if a large construction needs to be monitored, as more than a thousand points are needed to be monitored to gather complete and precise data about the situation of the entire construction loading, One more snag is that non-optical sensors commonly operate with the alternating current, which makes them susceptible to be affected by lightning strikes, electrical faults, electromagnetic noise, and the resistance of the wires, which makes the current to be dissipated after a certain amount of length. Despite being cheap (non-optical sensors), their detection system costs, labour, and installation of all those cables make them not desirable for some applications.

2.3 fibre-optic technologies and fibre sensors

To understand how fibre-optics perform, initially, the nature of light as the data (signal) carrier and the fibre itself is described.

2.3.1 The light essence

Light can be described as travelling photons in a vacuum with a speed $c_0 \cong 3 \times 10^8$ And $c_0/n = c$ in a clear (transparent) medium, where n is the refractive index. Additionally, light can be described as electromagnetic waves. The light word usually applies to the visible portion of the spectrum; this could be seen in the figure below.
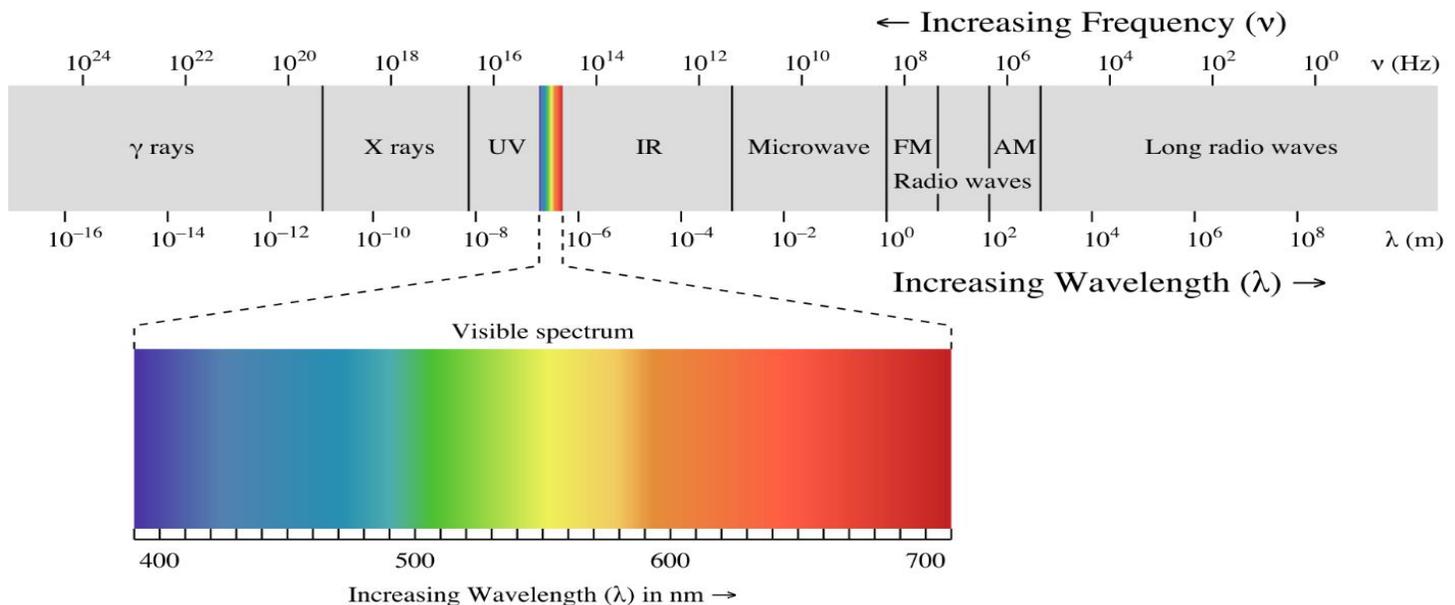
Figure 6 Electromagnetic spectrum and its visible portion.[4]

18

The visible portion of the spectrum, as it could be observed in figure 6, starts from violet colour with the wavelength of 400nm and ends at red with 800nm wavelength. Numerous theories have been proposed to better understand the light phenomena (including mathematical models) of growing intricacy.

Here are some of them in brief.

- Ray optics:

Light needs the least amount of time to travel from one point to another; it conforms to Fermat's principle (also recognized as the principle of least time). Thereupon, light chases straight lines. This argument illustrates refractions and reflections.

- Scalar waves:

Light also satisfies the Huygens mathematical statement; therefore, the general equation is $A = A_0 \sin(\omega t + \emptyset)$. In this theory, diffraction (interference phenomena) is explained besides reflection and refraction. Interference phenomena: the recombination of light after it was split, the intensity may drop from the original level to zero, in reliance on path differences.

- Electromagnetic waves:

It adheres to the Maxwell equations. This theory describes the former phenomena and light polarization.

- Quantum optics:

It reflects the Schrodinger equation. It is required to define their interplay with the matter, absorption, and light emission. The equation is a linear partial differential equation which, explains the state function or wave function of a quantum-mechanical system.

2.3.2 **Optical fibres**

The fibre-optic era began in the 1970s for long-distance telecommunications, and throughout the last four decades, it has encountered exponential advancement. With approximately two billion kilometres positioned globally, optical fibres are the pillars of today's most innovative telecommunications systems. Fibbers are inserted into optical cables that link neighbourhoods, cities, and continents around the world.[52]

A small spin-off from the technology is the sensing function that takes advantage of improvements accomplished for optoelectronic concepts and components. These flexible, thin strands of ultra-pure glass can carry data, voice, and video info in the fashion of light signals at the speed of light. Optical fibre is very thin; one strand of fibre is around the width of a human hair. It is encompassed of two essential parts made of glass: the cladding and the core.

Figure 7 Fibre optic and the light reflection
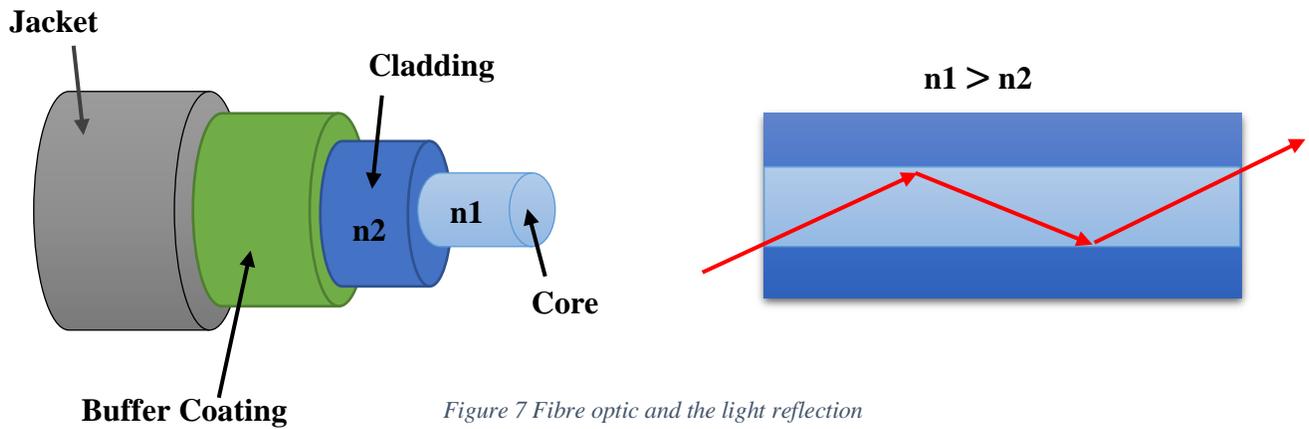
The fibre's core is where the light signals are conducted; surrounding the core is the cladding layer that keeps the light from escaping. Fibbers are in two main modes, multimode or single. The single-mode with a small core diameter allows carrying the light over long distances; it has a small core diameter, low attenuation, a high information-carrying capability, and is the most widely installed optical fibre in the world [47]; which is shown below in Figure 8 a.

Figure 8 Single and Multimode fibre optics
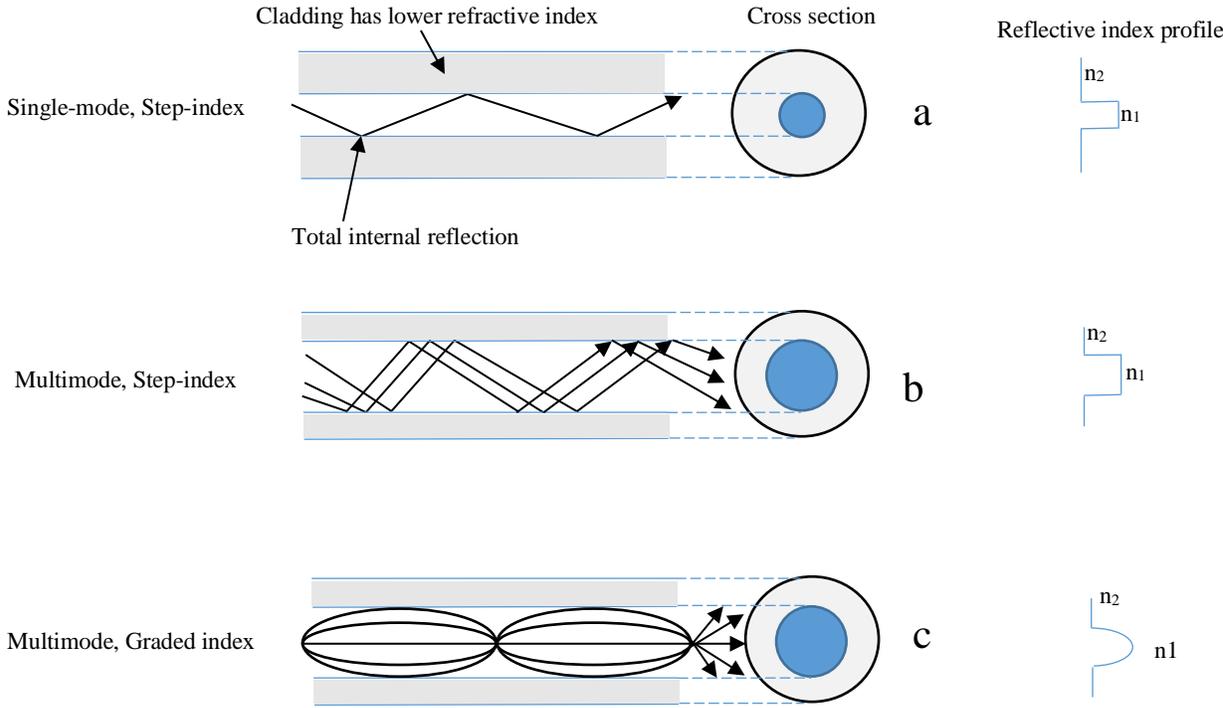
Light can travel through a multimode fibre in many paths concurrently due to the bigger core size of the multimode fibres shown in figure 8 b.

Generally, in data centres, resident area networks, and storing area systems, multimode fibres are installed due to their cheaper cost than single-mode ones [47].

Like any other technology, this one as well has some deficiencies. Attenuation, dispersion, and bend induce loss in shapes of micro bending, and macro bending are three limiting attributes of information capacity or/and speed of any fibre optics. Signal reduction along the length of the fibre is called attenuation. The light loses power as it goes down the fibre, which could be triggered by the quality of the glass or could be caused by bending. Signal distortion and fibre due to difference in the travel speed of different spectral components of a signal are called dispersion. If a fibre is bent from a straight axis, usually two optical effects can happen, macro bending and micro bending. An increase in attenuation triggered by small high-frequency radius bends along a fibre length is called micro bending. Macro-bending is the signal diminution related to wrapping or bending the fibre; in both situations, light can escape the fibre, resulting in the loss of some of the original signals. The macro-bending effect could be reduced significantly using clear curved single-mode and multimode fibre or a bend-insensitive fibre such as corn [47].

Optical fibres work based on total internal reflection, which retains the signal within the core and leads it through the fibre. The bending of light as it goes from an element to another is called refraction. The cladding glass has a less refractive index than the centre of the fibre therefore the light could be confined in the centre by reflecting it at the cladding edge as it propagates down the length of the fibre.

Two other important features of fibres are mode field width and cut-off frequency. Wavelength above the cut-off allows only a single mode, and wavelengths below the cut-off fund two or more modes. The bend of the fibre, length, and cabling process and deployment conditions are encountered during use, and most importantly, the fibbers' refractive index characteristic determines the cut-off wavelength.

Single-mode fibres, a part of the optical power is directed outside the core into the cladding; (in some fibres, up to thirty percent of the light spreads in the cladding layer). This mode field width outlines the magnitude of the optical spreading power in the fibre. [47]

Aperture and core size are two essential numerical characteristics of multimode fibres. Measurement of the angular range of light acceptance into a fibre is called the numerical aperture. Cladding and core glass refractive indices determine the angle over which a fibre receives light. One of the main design parameters of multimode fibres is the core diameter, which means the bigger the core, the fibre can supply more modes of light to circulate along with the fibre. The core size of the multimode fibres is much bigger than single-mode ones. [47]

2.4 Fibre-Optic sensors

Fibre-optic sensors have gained significant attention due to their advantages against traditional sensors, and they operate on evaluating the properties of light carried alongside optical fibres. External influences or movements (like temperature fluctuations or stress) provoke changes in fibre, which prompt the transmitted light signal to vary. This signal variation can be adjusted to the measurand. Employing different physical phenomena to modulate the conveyed light by fibre optic sensors provides each sensor with its unique performance. In other words, various fibre optic sensors are made based on changes in wavelength, phase, and intensity due to external disturbances.

2.4.1 Benefits of Fibre Sensing

Fibre-optic sensors have several advantages over traditional electrical gauges. These are their resolution, sensitivity, and being deployed where conventional electrical sensors are not viable for being nonelectrical; they are insensitive to electromagnetic noise. Besides, these sensors are more resilient to the harsh climate and surroundings. As these sensors are made of glass, they have excellent resilience to most eroding and high-temperature circumstances. Remote sensing is another benefit of fibre optic sensor, thanks to the low loss property of glass.

Some other advantages of the fibre optic sensor

- Flexibility

  Since fibre optics carry light as an alternative to the electrical current, they are immune to

- Lightning strikes
- Electrical faults
- Electromagnetic noise

  Based on the fibre optic benefits, fibre typically cuts maintenance fee and has an established record of consistency in the field; in fact, it is common for clienteles to tell Corning that cables mounted in the late 1970s or the beginning of the 1980s are still functional.

  All in all, Optical fibres are cost-effective, robust, scalable, small attenuation, and it supports the superior communication quality desired for high-speed conveying of voice, data, and video in today's top applications.[47]

2.4.2 Selecting a Fibre optic Sensor

Fibre optic sensors offer various benefits compared to non-optical ones; however, they usually require pricy signal processing systems as well as being complex to be fabricated. These intricacies

limit their viability for some applications, yet fibre optic sensors successfully make their case where utilizing conventional sensors is not an option such as harsh or hazardous situations. Additionally, their ability to be multiplexed can counterbalance their higher cost. Multiplexing gives the ability to implement multiple sensors inside an individual fibre, thus have measurement at different locations, and which can be analysed by a single signal processing unit. Having only one interrogation system prompts a significant reduction in cost per sensing point. Accordingly, multiplexing more sensors in fibre lower the price per sensor. Reducing the cost allows these fibre sensors to be comparable to the traditional sensors or sometimes even with better attributes and low cost. Fibre-optic sensor multiplexing and lowering the cost render an excellent solution to the growing market for temperature and strain measurement through the spatial region.

Various multiplexing systems for fibre optic gauges have been developed. One of these technologies is light scattering inside optical fibres by virtue of fibreglass impurity through the fabrication process. It gives the possibility to process the output (the scattered light) and determine any external perturbation to the fibre. This method is regarded as a fully distributed sensor. Fibre cable itself serves as numerous gauges considering the scattering occurs throughout the fibre; consequently, different parameters could be examined within the whole fibre.

Quasi-distributed sensors are other types of distributed fibre sensors. This type is a network of node sensors built within a fibre. Like fully distributed sensors, external activities modulate their optical signal, but they get extracted separately by the signal processing unit based on their specific characteristics (phase, wavelength, intensity). Quasi-distributed sensor networks, measuring the desired physical quantity only at these discrete sensor spots.

Diverse fibre optic gauges can sense different physical properties such as acoustic sensing, temperature, or strain. Nonetheless, each gauge has its unique characteristics, which makes them more adapted for specific evaluations.

Fibre optic sensors are built based on the modulation of their internal signal triggered by outer activities such as chemical, temperature, or strain.

Fibre-optic sensor configurations could be classified into four main divisions depend on several modulated specifications.

These comprise:

- Intensity

- Polarization

- Phase

- Wavelength/Frequency

The pursuing sections will describe different types of sensors and the way they operate, furthermore, which sensor was adopted for this research.

2.4.3 Extrinsic and intrinsic sensors

Nearly all fibre optic sensors may be categorized into two classes, extrinsic and intrinsic. Extrinsic fibre sensors utilize a different instrument to reflect the light. These types of sensors merely use the fibre to carry the light to the sensing location and consequently to the interrogation instrument. The extrinsic method could be more sensitive than intrinsic since it could benefit from an outer reflector with a lot more sensitivity than fibre optic.

The other method is intrinsic, which employs a section of fibre or the entire fibre as the sensing gadget. Intrinsic sensors pick up on external perturbation on the fibre, which changes the light characteristics; these changes then send back to the demodulators and get translated into strain or temperature based on the sensor type. Intrinsic fibres are the suitable choice for a dirty environment due to the light never leaves the fibre. Intrinsic sensors also have applications in smart structures as distributed sensors.

2.4.4 Fibre sensors based on Intensity [62]

The simplest way to detect strain is by monitoring the signal strength. One of the first marketed fibre-optic strain sensors was the intensity-based strain sensors.

Intensity-based gauges are analogue, as the measured variable is correlated to the intensity of light. These sensors benefits are:

- Adaptability
- Tenacity
- No need for pricey optical accessories due to their simple arrangement.
- Low manufacturing cost

Intensity-based sensors have some fundamental impediments, such as intensity fluctuations, which could be due to unrelated perturbation to the measurand, for instance, the degeneration of optical fibres or the light source fluctuation.

Intensity-based gauges are ordinarily designed to amplify the following modulation methods:

- Signal strength varies because of the reflection and/or transmission loss.
- Fibre micro bending is another reason for the signal intensity loss.
- Signal strength alters based on polarization fluctuations due to the refractive index variation in the encompassing environment.
- Evanescent wave modulation

Intensity-modulated sensors could be characterized as reflective or transmissivity in their physical design.

2.4.5 Transmissive Intensity Sensors

These sensors are considered extrinsic sensors as they are made of two slots in the middle of a fibre. Light enters from one slot and goes to the second, but in between those slots, there is a shutter. The shutter is attached to the object. By moving the object, the shutter moves, which results in the modulation of the light.

The intensity fluctuation in either circumstance identified by the system is proportional to the force exerted on the object. Another way is that the light beam goes to the receiving leg by passing into the transmitting leg and the shutter.

The shutter displacement delimits the amount of light that conveyed to the secondary fibre.

In this sensor, two diffraction gratings replaced the shutter with one adjustable, attached to a diaphragm, and the other being fixed. This mobile diffraction grating modulates the signal (light intensity) [11][12]. Note: the fibre on both sides of the diaphragm is fixed. In other words, when strain is administered to the diaphragm, the grating moves, which cause a change in the transmitted light strength. The sensor sensitivity could be improved by decreasing the grating pitch.

The figure below shows another transmissive fibre gauge depending on the optical signal modulation through the transverse movement prompted by a diaphragm deflection.
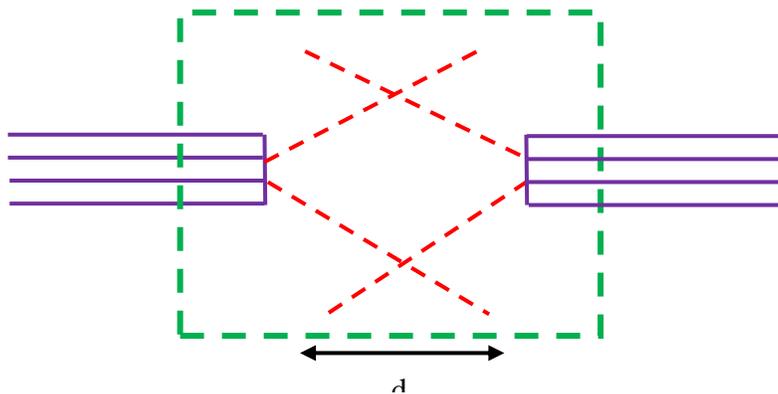
Figure 9 Intensity based Fibre Optic Sensor with transmission

In this structure, the transmission of a maximum mass of light from the radiation source to the detector is guaranteed by properly aligning the two optical fibres. The axial gap and the numerical aperture (NA) connecting the two optical fibres dictate the volume of energy obtained by the receiving fibre. [64]

2.4.5.1 Distributed fibre optic sensor

As it was mentioned before, fibre optic sensors can be intrinsic or extrinsic. Distributed sensors are intrinsic sensors that utilize the whole fibre itself as a continuous sensor. It acts as a communication and sensor at the same time.

Point sensor type.

Detection System

Quasi-distributed sensor

Detection System

Several sensors along a fibre

Detection System

Fully distributed sensor
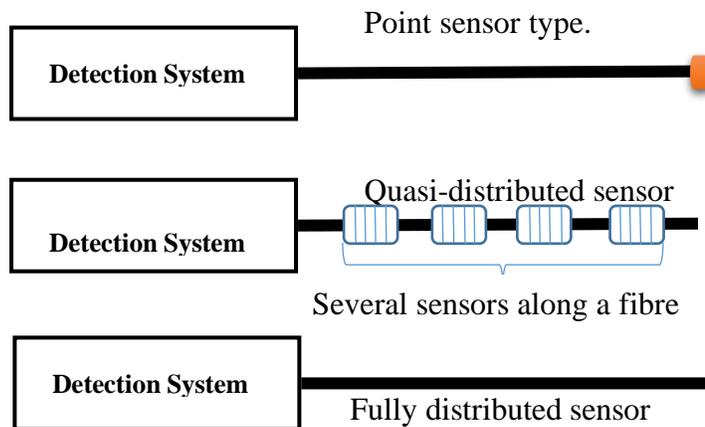
Figure 10 various fibre optic sensing method

With no external devices, costs and complexity are lowered. However, to have some meaningful data, external perturbation such as strain and temperature fluctuations must influence the light characteristics in some way, therefore, making those variations assessable. These different distributed sensors are explained below.

2.4.6 Fully distributed FOS systems

There are different and fully distributed technologies out there like:

- Rayleigh
- Raman
- Brillion.

2.4.7 Rayleigh scattering

There are two major forms of scattering, nonlinear and linear scattering, Rayleigh scattering is a nonlinear scattering. In linear scattering optical power is relocated from one mode to another with no frequency alteration. The Rayleigh scattering take place in all directions. This type of scattering results in attenuation of light rays and is related to $\frac{1}{\lambda^4}$ where λ is the optical wavelength.

The frequency of scattered light and incident light are the same, which means it is an elastic scattering process. In the Rayleigh scattering system Optical time-domain reflectometer (OTDR) is utilized to catch and analyse the backscattered light power, fluctuating with external perturbation. The time changing light-power received by the transmitting-end caused by Raleigh scattering in the fibre is denoted by:

$$P(t) = \frac{1}{2} P_0 WS(z) \, \alpha s(z) Vg \exp \left(-\int_0^t \alpha(z) Vg \, dt \right) \quad [62]$$

Where,

P0 = the injected power to the fibre, **W** = transmitted pulse width, **S(z)** = proportion between the reverse-coupled power at the spot of scattering.

The total scattered power is defined as the refractive index profile and fibre geometry, **αs(z)**= Rayleigh scattering coefficient loss. Vg is the group speed, and **α(z)** is the diminution factor of the fibre. The light travelling time (sending & receiving period) **t**, is directly linked to the **z** distance from the launching-end, and it is defined as $Z = \dfrac{Vgt}{2}$.[62]

These fibres are made by getting the glass temperature to the molten degree, and then there is a dragging and cooling procedure. This procedure renders in thermally induced variations in the density, therefore, the refractive index variations are small, and as a result, these fibres have little scattered light strength variation with the temperature fluctuations; alternatively, liquid-core fibres revealed a substantial Rayleigh scattering sensitivity decrease against temperature instabilities, so, these effects were implemented to create a distributed temperature sensing arrangement [62]

2.4.8 **Raman effect (Raman scattering)**

Temperature detectors built on Raman scattering are well recognized as technically and commercially efficient sensors [14-16]. These sensors have shown low cross-sensitivity to other physical quantities like pressure, strain, and cable nature. The inelastic photons scattering by matter in the fibre silica glass is called the Raman effect. The method entails molecule excitation by absorbing an incident photon releasing it at another rate.

The frequency change magnitude is linked to the molecule discrete vibrational rate. The weaker frequency dispersion is called the Stokes light, resulting from a molecule's excitation from the base state.

In contrast, the excitation of a previously excited molecule generates the anti-Stokes light with higher frequency radiation.

Since the total number of molecules from the exited-state and the ground-state rely on the temperature, Raman radiation could quantify the temperature.[62]

The stoke signal to anti-stokes R ratio level in Raman scattering, seen at same frequency distance from inner excitation line, is presented by [16] [62].

$$R(T) = \left(\frac{\lambda s}{\lambda a - s} \right)^4 exp \left(\frac{-\hbar c \Delta v}{k_B T} \right)$$

Where **R** = ratio, **T** = temperature (absolute), **λs** and **λa-s** are the Stokes and anti-Stokes's wavelength respectively, **k$_B$** = Boltzmann constant, **ℏ** = Planck constant, and **c** = light speed in a vacuum. It could be seen the relation on anti-stokes to stokes backscatter signal magnitudes could render the temperature value of an object regardless of the light power, geometry of the fibre, or launch status.

One of the shortcomings of the Raman Scattering is the inferior signal to noise ratio (20 to 30 decibels (dB) less than Rayleigh) [17]. Nonetheless, comprehensive enhancements have been done on the Raman Scattering systems, such as adopting two-wavelength, so the anti-Stokes and Stokes wavelengths do not endure any differential loss [18]. Gauging from the two terminals to counterbalance the fibre attenuation, Enhancing the spatial resolution to several centimetres, and boosting the ratio of signal-to-noise (S/N) by 20dB utilizing the photon count. [15], [19] [62].

2.5   Brillouin scattering technique.

Brillouin scattering is a sporadic scattering method induced by the refractive index shift stemming from acoustic waves. Brillouin scattered light wavelength change is a function of both temperature and strain throughout the fibre, which is a feature of the acoustic speed in silica fibre. Consequently, it could be utilized for strain as well as temperature sensing.

The frequency variation of Brillouin scattered light is very modest (11 Gigahertz (GHz)) compared to the wavelength shift of the Raman scattering method, which could be tens of nanometres. Since the frequency shift of this method based on light wavelength and the sound velocity in fibre, the frequency relation for anti-Stoke and Stoke's light could be shown as [17]

$$f_B = \pm \frac{2nV_a}{\lambda}$$

Where **λ** = the light wavelength, **n** = refraction index, and **Va** = sound velocity.

To be more precise, it could be mentioned that any physical change such as strain or temperature results in contraction, expansion, or twist in the fibre, which causes sound velocity variation; so, the Brillouin frequency shift analysis could examine this variation.

Brillouin scattering has two main types as stimulated and spontaneous. Both stimulated and spontaneous Brillouin scatterings are employed for distributed temperature and strain sensing with a communication-grade fibre.

One benefit of the Brillouin scattering method is that distributed strain and temperature variations could be observed concurrently.

Brillouin Optical Time Domain Reflectometer (BOTDR) procedure is typically employed for analysis with the spontaneous Brillouin scattering operations; in BOTDR, a light pulse gets injected to the desired fibre, and consequently, backscatter Brillouin light pulse gets measured. This system uses the heterodyne scheme to detect the frequency beating between the incident light and the Brillouin scattering, mixing the local oscillator light with the scattering light. Narrow frequency resolution can be obtained through electrical filtration.

Brillouin optical-fibre time domain is another way to do the measurement analysis; the method operates based on the transmitted light signal rather than the reflection. In this system, a continuous wave (CW) laser and a pulsed laser get transmitted down a fibre with contrary propagation paths. The CW laser encounter increases within the SBS procedure as the CW and the pulsed laser are adjusted to balance the frequency change in the stimulated Brillouin scattering (SBS). It is evaluated like a time function at the end of a pulsated laser [62]; By employing narrowed-linewidth lasers for both CW light and pulsed lights, the high-frequency resolution could be attained.

Testing and measuring distributed sensors:

Testing and assessing the output can be done differently; however, the popular OTDR is briefly explained here.

OTDR denotes Optical Time Domain Reflectometer. It is a device employed to generate a virtual "picture" of a fibre optic cable path. Thus, the integrity of the tested fibres, along with different passive optical components such as splices, multiplexers, and splitters, could be analysed.

The OTDR is additionally the only instrument able to locate any fibre optic cable malfunctions by finding the length of the faulty part and distinguishing the nature of fault-like any excessive loss, bends, or breaks. Although initially planned for long distant fibre-optic purposes, more modern OTDRs could be utilized to analyse a very smaller fibre cable, for example, inside an aeroplane or scattering sensors on the aeroplane's wings.

How OTDR operates?

The OTDR shoots light energy pulses, produced by a laser diode, within the optical fibre until it reaches the end, displaying present graphs and different analyses based on reflected energy and scattered backlight (returning light) over time, which measured by a photodiode. OTDRs examine the position and decline of passive optical network components, also called "events". The round-trip interval of the light pulse moving inside the fibre help to determine the distance or location of every event.

The backscattering effect (returned signal) gets amplified so that the loss could be measured. Most of the current OTDRs auto-select the best acquisition specification for a specific fibre by transmitting out probing pulsations in a method recognized as test auto or auto-configuration. Difficulties and glitches of scattering based fully distributed sensors.

The complexity of getting a very short optical pulse width, which results in low spatial resolution, is a common drawback of scattering-based sensors. If **W** is the duration of the pulse, **v** is the light speed in fibre, so, **δz** (The spatial resolution) of OTDR is:

$$\delta z = \frac{vW}{2} \quad ,$$

for instance, for a 100ns pulse-width, the upper formula returns a ten-meter spatial resolution.

The second deficiency is a weak scattering signal, which prompts a small S/N (signal to noise ratio); thus, having restrictions with quantification resolution and accuracy; although, strain resolution of 10 µε and temperature resolution of 1°c is attainable [13, 20].

Furthermore, significant measurement errors happen sometimes since the scattering-based gauges modulation depends on optical strength; thus, the unwanted power variation due to temperature change or bending loss changes the optical intensity and the result accordingly. [62]

2.6   Wavelength Modulated Sensors

These sensors operations rely on the sensing of light's wavelength change.

It consists of a signal processing unit, a detector, a wavelength modulator and a broadband source.

Wavelength sensing is comparatively not complex if the spectral variations occur from chemical indicator dyes, phosphorescence, black body, or fluorescence radiations.

In those circumstances, the emitted and the incident wavelength are notably distant; consequently, their detection is straightforward. Instances of wavelength modulated gauges are Bragg's grating sensors, black body sensors and fluorescence sensors. [63]

2.6.1   FBG operation method

Germanium doped silica fibre Photosensitivity was identified by K.O. Hill and his colleagues in 1978[23, 24].

The refractive index of the germanium doped fibre, if illuminated by ultraviolet (UV) light, gets amplified as irradiation power and time, which FBG systems functions are based on this effect. FBGs are made of a fibre core with sporadic refractive index modulation inside of it. As all colours of the visible spectrum (white light) travel down the fibre, it passes through a fibre Bragg grating.
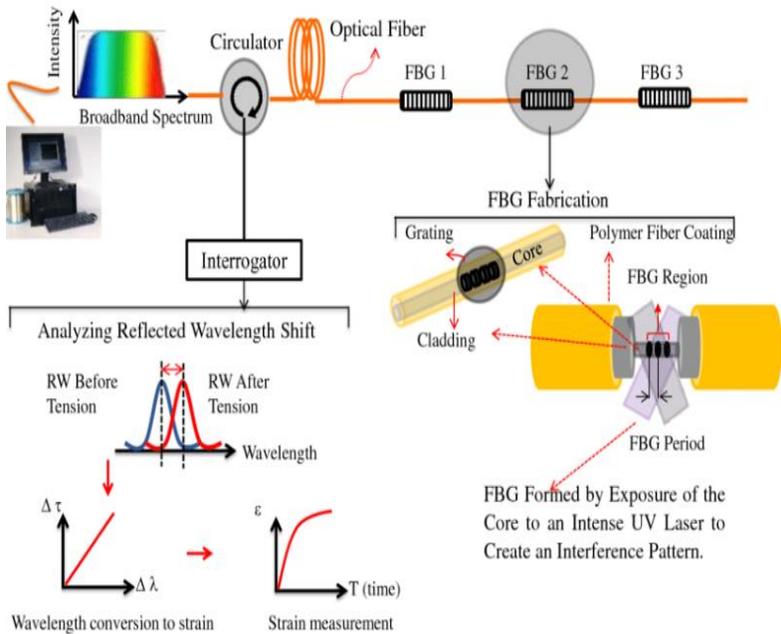
Figure 11 FBG Sensor's measurement principal [41]

Fundamentally, FBG is a sequence of optical filters that could return specific colours or wavelengths while allowing others to get through; this occurs by varying the fibres' refractive index, choosing which wavelengths pass and returning, as displayed in Fig. 11.

FBGs are usually employed in fibre optic telecommunication as drop/add multiplexer for wavelength division multiplexing; they are also used as optical filters based on their wavelength selectivity.

Fresnel reflection principle is the fundamental operating principle behind the FBG. This principle says that a travelling light between different refractive media could both refract or reflect at the

interface. Typically, the refractive index varies over a defined length. The equation below represents the reflection wavelength λB (Bragg wavelength) as:

$$\lambda_{\mathrm{B}} = 2n_e\Lambda$$

Where,

The **λB** (Bragg wavelength), **Λ** = grating period, and the fibre core active refractive index in the grating region is shown by ne.

Outside influences such as temperature and the tremor results in a variation of the reflective light frequency. Those dissimilarities could be interpreted into various units like strain or temperature; with the help of examining the variation of the Bragg grating wavelength.[50]

A lot of FBG sensors have been utilized in civil applications; they are embedded into composite elements as temperature and strain sensors to monitor the structural well-being. Dissimilar to typical electrical gauges, FBG gauges are non-conductive, electrically unreceptive, and invulnerable to electromagnetic interfering, turning them into a harmless and dependable substitute in environments prone to noise, erosion or high voltage.

As FBG gauges are founded on measuring within a designated wavelength or colour range, it is possible to daisy-chain various devices on a single optical fibre.
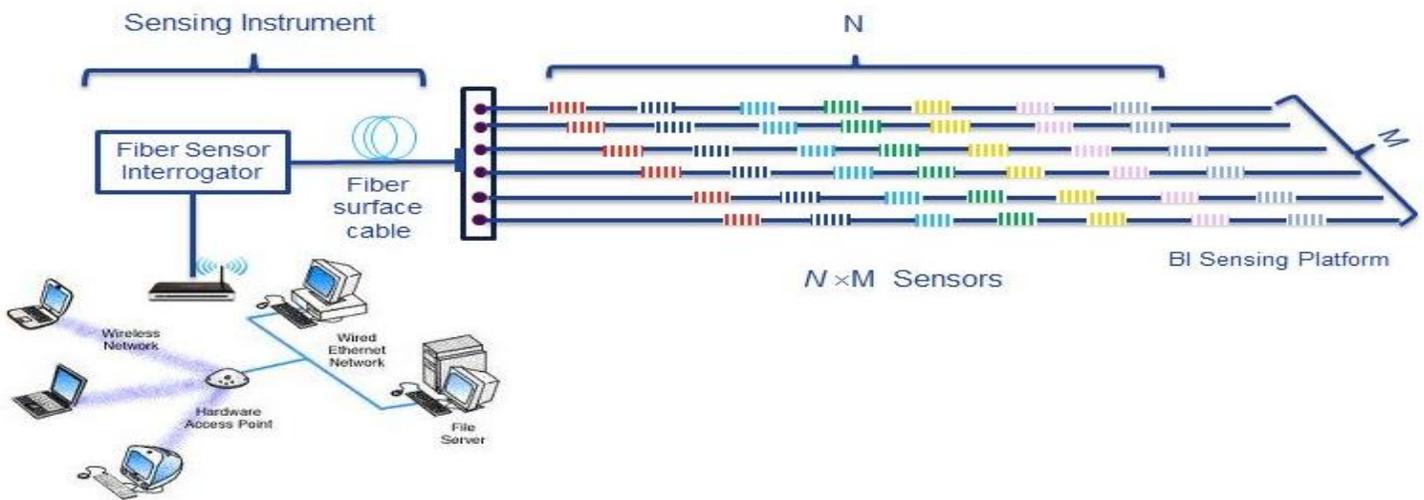
Figure 12 FBG sensors & WDM [42]

FBG (Fibre Bragg Gratings) multiplexing is an instance of sensing application for wavelength-division multiplexing (WDMs). In FBG, Bragg Gratings have dissimilar index period written on the fibre; therefore, echoes a different part of the spectrum. Crosstalk is one of the significant drawbacks of the multiplexed system or even sometimes shadowing, which is another type of crosstalk; shadowing is passing the signal through the first few gratings more than one time.

2.7 Phase Modulated Sensors (Interferometers)

2.7.1 Interferometry

Interferometers are typically connected with phase-modulated optical sensors since the light wave optical phase, or two light waves phase difference is customarily detected with the help of the interferometric method. Usually, coherent light sources are used since they can accurately identify the phase shift generated by the environment variables of concerns. In other words, interferometry is a gauging system utilizing the aspect of waves interferences (typically radio, sound, or light waves).

The analyses might comprise the elements with which the waves interact or those of specific features of the waves themselves.

Additionally, interferometry is applied to explain the methods that utilize light signals for education on variations in displacement. This shift gauging interferometry is broadly utilized in precision machining concerning tuning and mechanical stage motion control.

By utilizing two light rays (typically by dividing one light beam into two), an interference shape could be created when the two light beams interfere. Since the visible light wavelength is very short, little shifts in the optical ways (travelled distance) concerning the 2 light beams could be identified (hence, these variations give notable alteration in the interference shape). Optical interferometry is a vital analysis system in the last 100-years; Its precision has later been enhanced with the laser invention. Interferometric optical fibre sensors could be mainly categorized as

- Mach-Zehnder
- The Michelson
- The Sagnac
- The Fabry-Perot

2.7.2 Mach-Zehnder

Mach–Zehnder interferometer (MZI) is a design utilized to ascertain the pertinent phase shift fluctuations within two collimated rays acquired by dividing the light from a light source. This interferometer has been employed, amid other elements, to gauge shifts in phase within the two beams originated by a sample or a shift in one of the lengths of the paths. Mach-Zehnder interferometry method is based on a two-beam interferometer operating at transmission style. This interferometry style has been adopted by optical modulators, optical fibre sensors, and optical filters.[25][26][27]

The figure below represents a typical Mach-Zehnder interferometer.
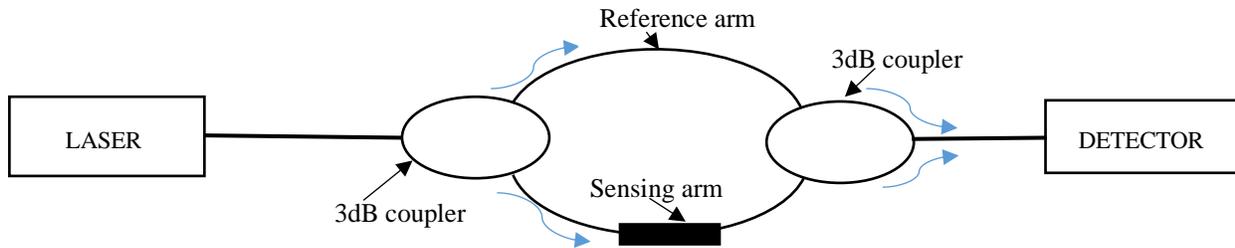
Figure 13 Mach-Zehnder interferometry sensor system.

So how they operate?

The light source emits the light into the fibre, and then the directional coupler split the beam into two rays. Environmental parameters modulate the phase of one arm. Since the second arm light is the same as it was (no interference nor modulation), it gets coupled again with the modulated first arm's light beam with the help of the second directional coupler (half-silvered mirror). The two light beams then interfere with each other; therefore, the phase between two light beams is identified and measured by detectors.

Mach-Zehnder sensors could be multiplexed in a ladder sensor network, tapped sensor array, or other topologies.

All being mentioned, the Mach-Zehnder interferometry has some pitfalls, such as stability given its relatively long fibre arms and temperature fluctuations. The polarization-fading is owing to the birefringence of the optical fibre that results in the random polarization change. Moreover, the Mach-Zehnder multiplexing sensors require several combiners and splitters, which hike the system's total costs and complexity.

2.7.3 Michelson

A Michelson interferometer (MI) main building blocks are two mirrors (reference and measurement mirrors) and a half-silvered mirror called the beam-splitter. As the light beam travels into the beam splitter/ half-silvered reflector (partially reflecting), the ray splits into 2 rays with distinct optical routes (one travelling to the reference reflector and the other moving to the measurement mirror).

After mirrors get the light beams reflected, they get superimposed at the beam splitter prior to landing at the detector. Note: in Figure 14, the directional coupler act as the beam-splitter.
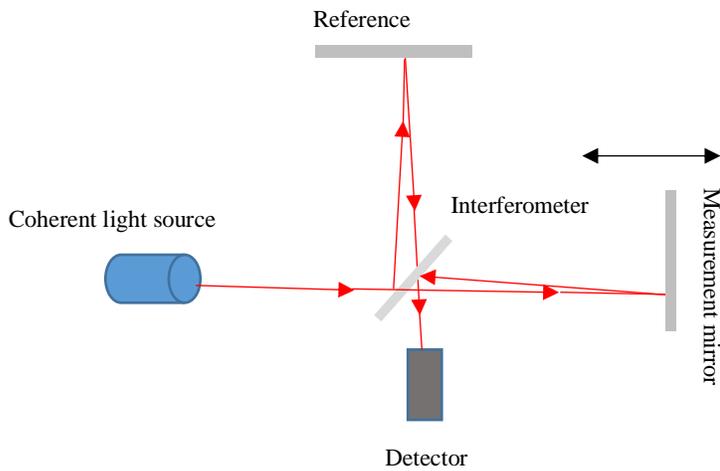
Figure 15 Lab Michelson interferometer setup.
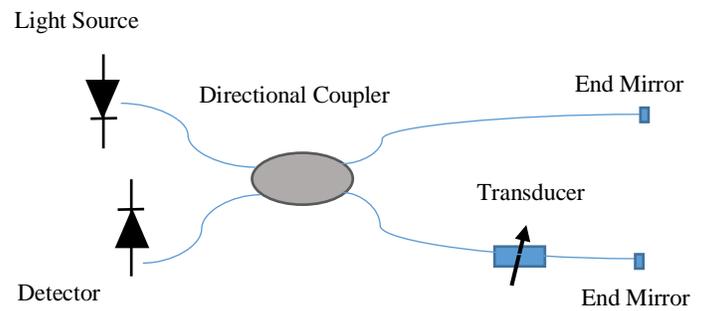
Figure 14 Michelson interferometer sensor system.

An interference fringe pattern appears as two light beams path differences prompt a phase difference. Next, the detector examines the pattern to assess the wave properties, phase difference, or the movement of one of the reflectors.

The principal, in this case, is the same as the above explanation.

Like Mach-Zehnder, this method suffers from environmental temperature variation, which causes unwanted phase change, or the birefringence of the fibres creates the polarization-fading problem.[28] Some scientists stated a process to resolve the polarization-fading intricacy by using Faraday rotation mirrors as the end mirrors that rotate the state of polarization for 90 degrees.[29][30]

2.7.4 Sagnac

The Sagnac system typically exhibits itself in a setting described as a ring interferometer. The first part is like two other methods mentioned above, meaning the light beam is split into two beams, but this time they are transmitted into a ring-fibre; they follow the same route although in opposing directions.
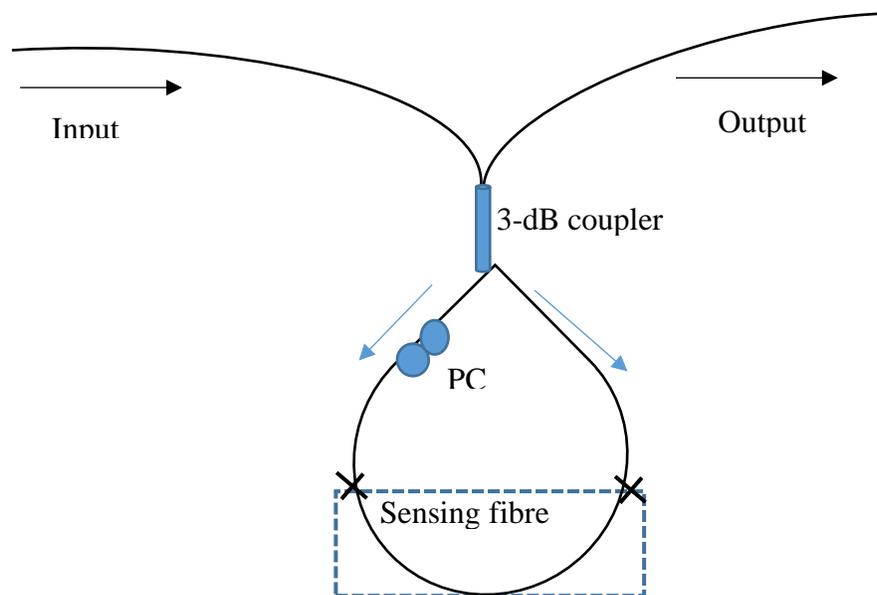
Figure 16 Sagnac interferometer.

35

After completing the circle, both beams come to the splitter and recombine. The recombined light beam then gets detected by the detector. The two exiting beams' corresponding phases, and the location of the interference edges, are changed following the angular velocity of the device. Strictly speaking, while the interferometer is not under any physical pressure concerning a nonrotating structure, the same amount of time is needed for the light beams to travel in the ring in both paths. Nevertheless, if the interferometer arrangement is twisted, one of the light rays will have a longer route to traverse than the other one. A phase variance between the two signals happens due to the difference in travel time in the two beams.

The Sagnac method is broadly adopted as a gyroscope for accurate rotation gauging. The ring formation of Sagnac interferometers has predicaments to be directly multiplexed.

Some scientists utilize a Sagnac arrangement to multiplex in-line Fabry-Perot (FP) sensors in a coherence multiplexing scheme and a loop topology.[31]

2.7.5 Fabry-Perot sensors

These sensors can be extrinsic or intrinsic, as presented in figures 17 and 18. Fabry–Perot interferometers (FPIs) in Fibre-optic sensors render the benefits of compact structure, high resolution, and protection to electromagnetic noise.

FPIs play essential roles in a vast number of sensing operations, for instance, temperature, strain, and pressure.

In FPIs, sensor interference happens based on the several superpositions of both transmitted and reflected stream of light at two parallel mirrors, called etalons
[24][https://www.routledgehandbooks.com/doi/10.1201/9781315369815-4].

The basic configuration of FPI is distinctive from MI or MZI. Production of Fibre-optic FPI could be done by purposely mounting up mirrors either outside or inside the fibres. Therefore, they are categorized into intrinsic FPIs and extrinsic FPIs, as shown in the figures below.

Extrinsic FPI is beneficial for achieving a high-finesse interference signal. It is simple to manufacture and does not demand any high-cost material. Notwithstanding, the low coupling coherence and call for accurate adjustment and packaging are shortcomings contrasted with intrinsic FPI.

In contrast, the intrinsic Fabry-Perot fibre (IFPI) sensors have etalon (reflecting components) within the fibre itself; this is shown in figure 18.
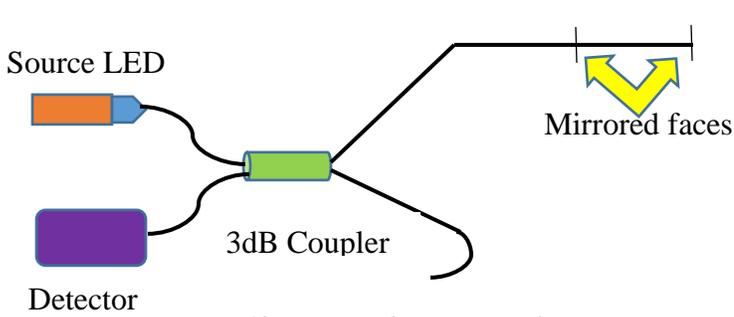
Figure 18 Intrinsic Fabry-Perot interferometer
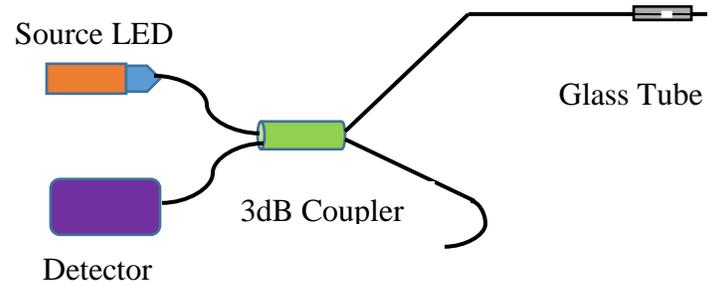
Figure 17 Extrinsic Fabry-Perot interferometer

A series of methods could be used to form the local cavity of the intrinsic FPI, such as fibre Bragg gratings (FBGs) [26], micromachining [25], thin-film deposition [28], and chemical etching [27]. Nevertheless, IFPIs have the difficulty of employing high-cost fabrication tools for cavity configuration. The FPI's transmission or reflection spectrum could be expressed as the intensity modulation susceptance to the input beam spectrum wavelength, particularly generated by the transmitted or reflected beams optical phase difference. The FPI's phase difference is presented as

$$\delta PPI = \frac{2\pi}{\lambda} n 2L \ ,$$

Where,

λ = the incident light wavelength, n = cavity mode or material RI, and L = the physical cavity length. When the sensor goes under perturbation, the phase variance is formed by the difference in the interferometer etalon. For instance, the longitudinal strain exerted on the FPI sensor alters the physical length of the cavity, which causes a phase shift. The exerted strain on the FPI could be quantified by monitoring the variation of the FPI wavelength spectrum.

2.7.6 Multiplexing and Fourier analysis

2.7.6.1 Multiplexing

Multiplexing can be expressed as when multiple or at least two signals simultaneously transmitted through a

channel, in this case, a fibre optic. The conveyed data could be analogue or digital.

Wavelengths, time, and code are the three main multiplexing methods customarily used. In this research, the Fourier analysis has been used to demodulate the interference spectrum, which goes under wavelength-division multiplexing. Here is a brief introduction to some of these multiplexing systems.

2.7.6.2   Time Division Multiplexing (TDM)

Using this method, multiple optical signals concurrently could be transmitted and demodulated based on different received times. Various data channels could be carried in a single fibre by interleaving pulse trains in fibre optic delivery systems [32-34].
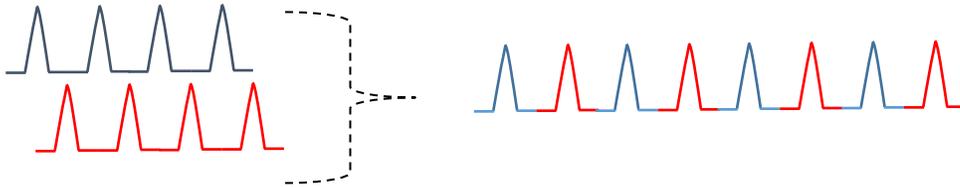
Figure 19 multiplexing of optical time-division. Two interleaving pulse series are joint to a single pulse train.

Employing the multiple channels renders a larger transmission capacity of additional overall data or carrying data of other users concurrently without raising the data rates of a single channel. Nevertheless, the time per bit needs to decrease. The time slot reduction could be accomplished by applying a series of ultrashort pulsations as the modulator input even if the bandwidth of the modulator is restricted.

In a telecommunications system, every pulse could be presented as a "1" (High) or a "0" (Low). Low timing jitter and short pulse duration are the optical time-division multiplexing obligations for data transmitters. Furthermore, a high extinction ratio is a must, i.e., every coupled channel needs to have a low power level among the bit slots, thus, to avoid interference with other channels.

Some types of optical delay lines are required to combine the signals. Sensors are successively addressed in TDM systems by injecting the sensor network by input signal pulses. The transmitted or reflected light from distinctive sensors has unique flight-time delays, which can recognise individual sensors within a network; based on different delays.

TDM scheme can be implemented with various topologies such as the ladder, star, or serial topology. OTDR (Optical Time Domain Reflectometer) based serial array operating at the reflective method is one of the most common configurations for TDM schemes, as shown in Figure (20).
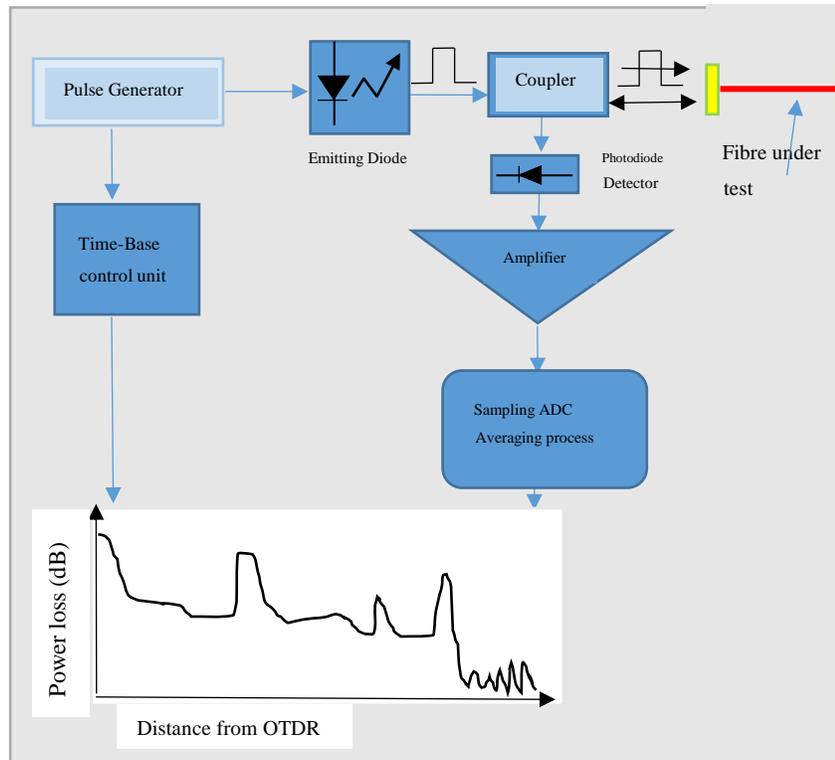
Figure 20 An OTDR configuration

OTDR is an optoelectronic apparatus utilized to qualify an optical fibre. It pulsates a chain of optical signals into the under-assessment fibre and extracts them from the same point. Based on the backscatter or reflected light, the intensity, phase shift, or frequency of returned pulses is assessed and integrated as a function of time and sketched as a function of the fibre size.

The TDM system has been applied for the multiplexing of various sensors, such as interferometric [35] micro-bend,[53], and FBG sensors, working at either reflective or transmissive mode.

2.5.1.2 Wavelength Division Multiplexing (WDM)

This method is applied to divide an optical fibre among dissimilar signals Concurrently. Wavelength-division multiplexing operates since light travels down the fibre in many different light colours without blending or conflicting with one another. It is like the light is separated by a prism where all the various shades of light can travel through the air at once until they reach the prism, which separates them into their component colours. Wavelength division multiplexing was initially used to send two signals over one fibre simultaneously; therefore, to do that, two couplers to couple the light into and out of the fibre, two different light sources, two different receivers, and optical filters are needed. Filters stop one colour of light and let the other through so the two

branches of the colour coupler on the receiver end can carry different signals to detectors simultaneously.

The pond systems (passive optical networks) for fibre-to-the-home work somewhat like this today except for fibre signals are sent in opposite directions at different colours; however, the same technique applies.
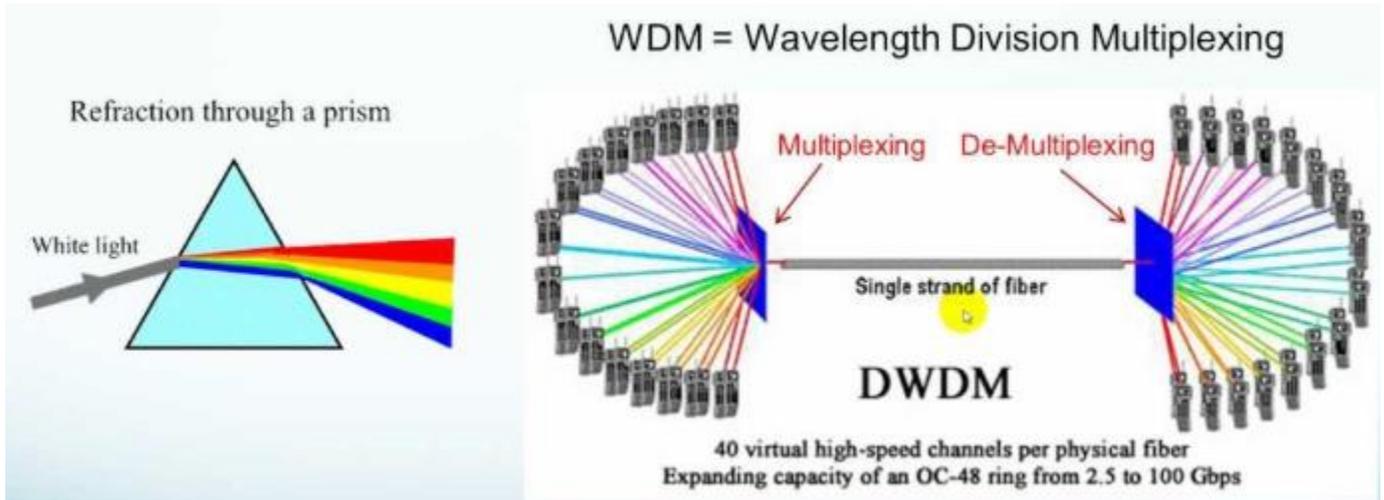
Figure 21 WDM [36]

Nowadays, wavelength-division multiplexing is being used on long-range links and long-distant networks. However, dense wavelength-division multiplexing is used with more than 64 channels tightly spaced with fibre amplifiers for repeaters; we can also use coarse wavelength division multiplexing with fewer channels wider spaced.

In most arrangements, it is preferred to have more wavelengths rather than more fibres; for example, they are used in residential fibres to use a single fibre but being capable of bidirectional communication.

The system has its wavelength range; tightly spaced wavelengths are utilized in DWDMs in the range of approximately 1450 to 1650 nanometres since fibre amplifiers could usually be applied to long-distance modes. Multiplexers utilize a wider-spaced wavelength with a full range of 1280 to 1650 nanometres (The single-mode fibre full coverage) to amplify repeaters' signal. However, to avoid high signal attenuation for crucial signals in the water Peaks, it needs low-water peak fibre. The DWDM and CWDM wavelengths are quite distinct because DWDMs have a lot of channels; the lasers are interval at 0.8 nanometres; these wavelengths' stability demands employing costly DFB lasers.

Coarse wavelength division multiplexing involves lasers at twenty nanometres spacing, making it a lot less critical on all the different lasers' wavelengths.

Fibre amplifiers are used in long-distance networks to regenerate the signal; it is not a repeater; it is just an amplifier; it does not convert the signal to an electrical signal and then back to an optical signal. It works more like a fibre amplifier. The incoming signal goes into some erbium-doped fibre pumped by a pub laser and gets stimulated emission along with the fibre amplifier fibre itself. These erbium-doped fibre amplifiers work in that 1450 to 1650 nanometre range used for dense wavelength-division multiplexing.

When systems are under testing that uses wavelength division multiplexing, it is not uncommon on longer lengths of fibre to test spectral attenuation because it needs to be ensured that over the entire band, that wavelength division multiplexing the fibre can transmit the signals with roughly equal attenuation. Systems tested this way are generally checked with full wavelength sources to cover the entire wavelength range. Testing power in a DWDM system or CWDM system is not all that difficult after the wavelengths have been demultiplexed into each wavelength channel; any standard power meter can measure the power. However, the individual sources may be requiring testing for wavelength as the wavelength is critical for making sure that the system operates appropriately if the wavelength changes, the demultiplexing and multiplexing of the wavelength may not work correctly.

2.7.6.3   Code Division Multiplexing [62]

Following securing its place in the broadcasting (radio) field, CDMA has witnessed a new upsurge in the optical domain. Based on its flexibility, fairness, increased inherent security, service differentiation, CDMA is demonstrated to be also fit for Time Division Multiplexing (TDM) and Wavelength Division Multiplexing (WDM). In the fibre optic field, CDMA methods are generally identified as Optical-CDMA. Every CDMA scheme are troubled with the multiple-access interference (MAI) complexity; to deal with this intricacy, the Spectral amplitude coding (SAC) technique is used. The spreading code in the CDMA arrangement is a different approach to secure the data reconstruction at the detector end by depreciating the impact of MAI.

CDM could be utilized to expand the quantity of gauges on LEDs, decrease the overall cost of a sensor system.

By computing the gauge reflection and transmitted code's cross-correlation, the sensor results could be measured.

Varying the sensor fibre length is done to separate the response in time.

Most sensor noises are overcome by averaging and the sensor response with the transmitted code sequence cross-correlation.

A digital oscilloscope and a microcomputer do all the processing.

3 Commercial research & SWOT analysis

Market research and SWOT analysis is a part of this paper since it is part of research deliverables. Different technologies are commercially accessible for strain measurement. These sensors have some advantages and shortcomings, as exhibited in this paper; however, some have found some niche usage where it appears to be the most suitable sensor.

Fibre optic sensors for the market can be categorized as below.
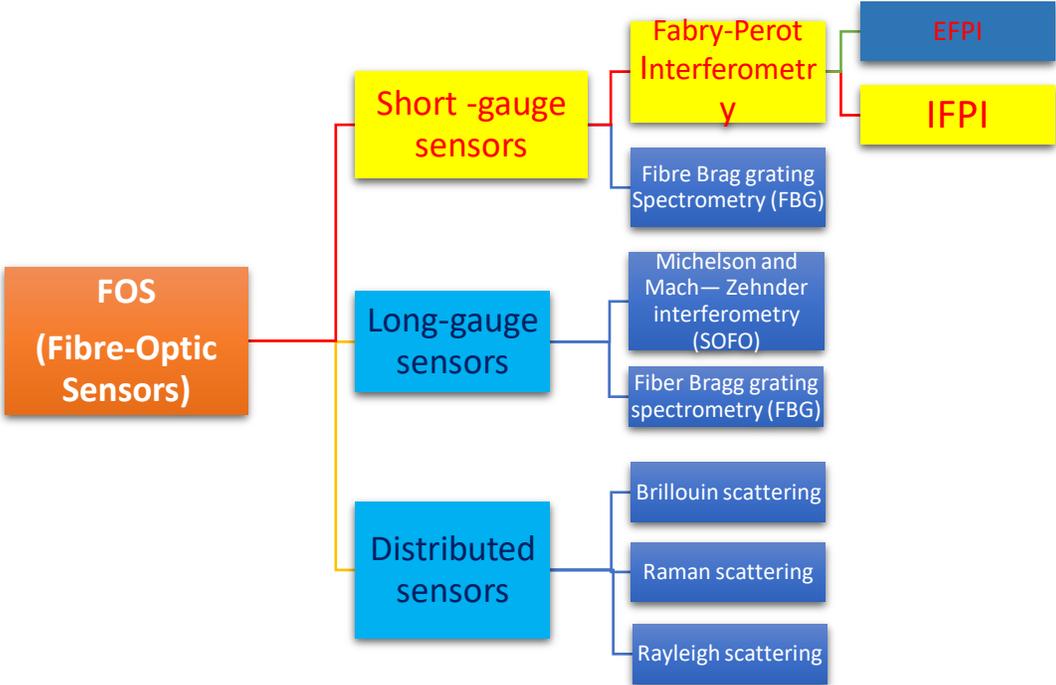
Figure 22 Commercially available types of s fibre optic sensors

Here are some of the commercially available sensors represented in the table below. This table shows various sensors from different companies with several technologies.

The best FBG sensors based on the resolutions from the above table are sensors from Smart fibres. These FBG sensors have an accuracy of 1.2 μ strain with a good range of temperature operation.

From the table above, the best Fabry-Perot strain sensors are from Opsins Solutions' company since it has a better temperature, range, and superior linearity. The best resolution and linearity were 0.15 $\mu\varepsilon$ and 0.15%, respectively.

To better understand the table in section 8.1, the figures (23) is provided. The figure below exhibits ranges vs resolution for FP (Fabry-Perot) and FBG sensors in comparison against each other since they are the most prominent sensors on the market.

To see other graphs about commercial research, section 8.1 can be observed.
The figure below explicitly indicates that if the resolution is higher for the FP (Fabry-Pérot) sensors, the resolution worsens. Between the range and resolution, there is a linear relationship as it was evident that there are gaps in the market in the sense of high-resolution FP sensors that could have a high range at the same time.
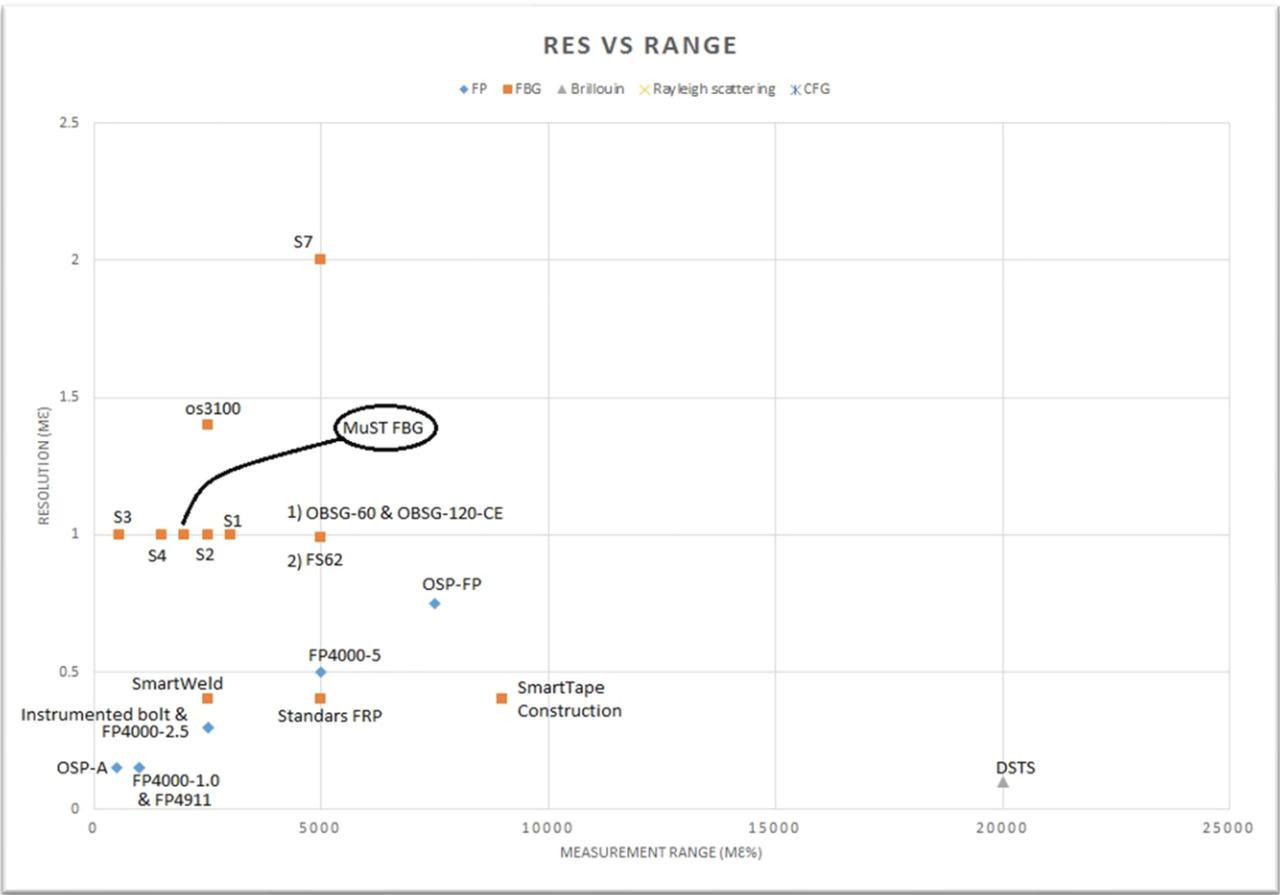
Figure 23 Resolution VS. range in FOS systems

The research shows that FP and FBG have a nearly similar range and accuracy, but FP presents better resolutions and dynamic range.

The other part of the research is the capabilities of the sensors in different applications and scenarios.

3.1.1 What makes FP sensors better than FBGs

Figure 23 & 54 shows that most FP sensors in the market have better resolutions than FBG sensors. FBG sensors usually have a resolution of about 1με, as shown in section 8.1 Fig 54 (Commercially researched fibre optic sensors). On the other hand, FP sensors can be a viable solution for applications that need a better resolution than 1 με since they could potentially obtain n and not be ultra-expensive since they could potentially have strain sensitivity in the nε region.

Also, figure 55 indicates that there is a linear relation between range & resolution for FP sensors. This shows a gap in the market for high resolution, high range FP sensors.

Finally, the researched FP sensor does not need a costly swept laser source, making it a cost-effective system.

3.1.2 SWOT Analysis for IFPI (intrinsic Fabry-Perot Interferometry)

Fibre-optic sensor technology has emerged with unique characteristics as a new sensor technology resistant to electromagnetic interference (EMI) and Radio Frequency Interference (RFI).

Typically, fibre optic sensors are based on the intensity, wavelength, and refractive index modulations.

However, the FPI operates based on phase modulation.

Here is a SWOT assessment of the IFPI, so a decision could be made to choose the desired technology for the research, which would be commercially viable and some niche application in the market.

Strength	Weakness

• Small size & Lightweight
• Great sensitivity, high-frequency response
• Electrical insolation.
• Insusceptibility to EMI noise & RF
• Single-point measurement.
• High spatial resolution
• Simplicity & cost-effectiveness
• Relatively low-temperature cross-sensitivity
• The capability of remote operation
• Survivability in a harsh environment
• Low power consumption
• The strain sensitivity is a lot larger than temperature sensitivity; thus, there is no need for temperature compensation.
  Ability to be embedded in construction.
	• The EFPI sensors' drawbacks are careful alignment, low coupling efficiency, and packaging difficulties.
	• Disability to monitor Temperature and strain simultaneously (Brillouin scattering is capable of that).
	• Low-Temperature sensitivity.
	• Not suitable for multiplexing due to reflection loss from the thin-film coat.
	• Hard to manage the film's thickness and condition through the splicing and coating procedure.
	• Hard to control the cavity length.
	• Complicated alignment process.
	• Packaging problem
	  Expensive equipment for cavity fabrication.

Opportunities	Threats
• Capacity to multiplex multiple sensors within a single fibre. • Mixing the sensor with IoT.	• A lot of similar sensors with good specifications.

This commercial research and the SWOT analysis show that a genuine commercial achievement for such sensors stems from high-volume continuous business, and up to now, applications concerning disposable medical equipment and strain sensors appear to grant such a chance. The Fabry-Perot sensors seem to be one of the most desirable as it gives a reasonable price congruous with the market, high sensitivity gauges with a small size suitable for simplified installation. Based on the presented data, Fabry-Perot sensor technology is the best option for this research since the commercial aspect (being cheap) is a significant factor and has good sensitivity, resolution, and size.

4   Investigational setup

Strain monitoring is an essential exercise in various precision engineering fields where comprehension of structural disfigurement based on thermal and loading impacts is needed to enhance efficiency, for example, in the compensation and characterization of thermal noise in machine apparatuses.

Fibre-optic strain gauges have several distinguished benefits over electrical strain sensors. These include electromagnetic-noise resistance, better longevity in decaying conditions, easier integration/mounting in some embodiments, and enhanced absolute strain susceptibility.

4.1   The need for the rig

This fibre strain sensor invention was formed by applying novel interferometry techniques developed previous research carried out under the EPSRC Centre for Innovative Manufacturing in Advanced Metrology funding to strain measurement using optical fibres. The study push came from the involvement of the CPT in an STFC funded project as part of the High Luminosity Large Hadron Collider upgrade. There was a demand to produce a fibre sensor to facilitate the measurement of strain in beam-line collimator arms under vacuum and high radiation levels.

Fibre strain sensors are the most appropriate solution but are most implemented commercially using Fibre Bragg grating (FBG) technology, which has a fundamental limit on stain resolution of ~1 me. This application required higher strain sensitivity, so a fibre strain sensing system using broadband interferometry was developed (see associated invention disclosure document for further details).

4.2   Key Advantages

This technology provides inherently higher strain sensitivity than commercial FBG based strain sensors. At the same time, it also has similar benefits like FBG sensors: high-speed interrogation, absolute measurement (i.e., constant power-up not required), and an intrinsic fibre sensor package (cheap to produce, small form factor). It may also be able to be supplied at a lower cost than FBG sensors, as the requirement for sources with high wavelength accuracy is not required, leading to an overall reduction in system cost. The shortest length was not a concern since EFPIs have limitations due to the finite air gap length (tens of microns). On the other hand, IFPI (the chosen sensor) is not limited by the length as the light is restrained in the fibre; therefore, the cavity length could be increased to enhance sensitivity.

Note: An Unbalanced Michelson interferometer was used as the interrogation system, which allows the system to be modified for a larger sensor cavity gap by reducing the temporal coherence limitation of the cavity length of the fibre.

4.3 The system setup

An experimental setup was created at the optic lab to evaluate the proposed Fabry-Perot strain sensor.

In order to measure the IFPI attributes, a rig was designed, which could be seen in the figure below (24).
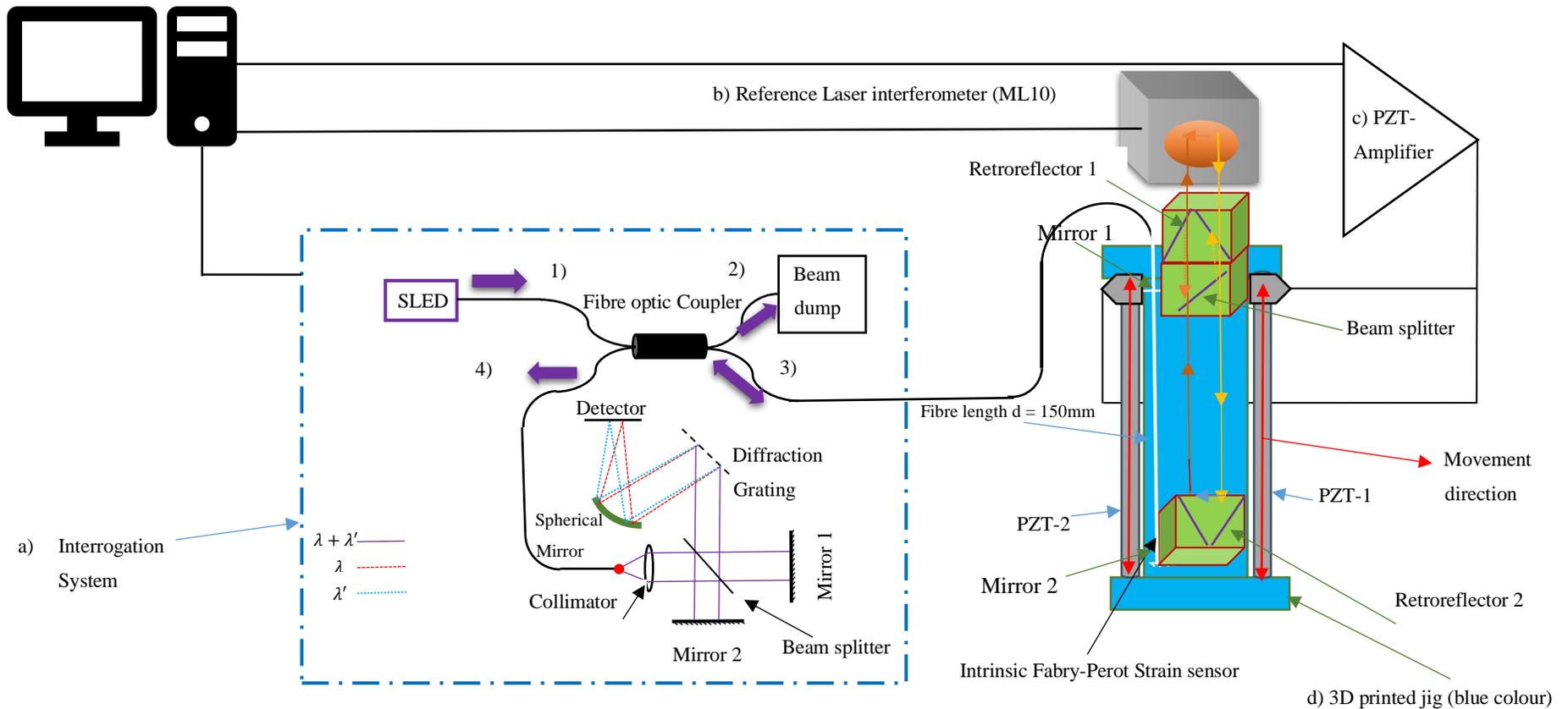

Figure 24 The Setup used for tests and analysis.

- The sensor is glued to the jig, and It is connected to this interferometer. The detector is connected to a computer; thus, data could be observed and recorded simultaneously.
- The system of the interferometer could be seen in the upper figure. To be better familiarized with the system setup comprising parts are explained below. The setup comprising equipment.
- Figure 24 shows the configuration which was utilized to help the analysis of the proposed IFPI sensor. The setup components can be divided into four essential categories:
- a) The interrogation system
- b) The reference interferometer (ML10)
- c) BPC303-apt piezo controller and two PZTs (PAZ015)
- d) 3D printed jig

4.3.1   a) **The interrogation system**

This system had been developed by one of the researchers (Dr James Williamson) at the optical lab to help to investigate the sensor. This interferometer has a source which is called SLD or SLEDs, Fibre Optic Coupler, Beam Dump, Collimator, Beamsplitter, two Mirrors, Diffraction Grating, Spherical Mirror, and a Detector.

SLDs (superluminescent diode) are based on superluminescence, which an edge-emitting semiconductor light source. It couples the brightness and laser diodes with high power and small coherence of LEDs. SLDs emission bands are ranging from 5nm to 700nm. SLDs typically have a bandwidth of 5-100nm, which in this case is 50 nm ($\Delta\lambda = 50nm$) and a central wavelength of 400-1700nm, which for this system was ($\lambda c = 855nm$). SLDs are utilized to direct a light beam into the fibre-gauge, so the spectral reflection ripple could be measured to capture a wavelength change due to any outside influence on the sensor.

4.3.2   **Brief interrogation system operation principle**

SLED emit light signals into the fibre. Then the signal splits into two beams, which one of them gets dumped by the beam dump. The other half of the signal goes to the IFPI proposed sensor (the University of Huddersfield has developed the sensor. It has two mirrors, one 30% TIO_2 (Titanium dioxide) coating, and at the end of the fibre, there is a 100% TIO_2 coated mirror for the maximum reflection).
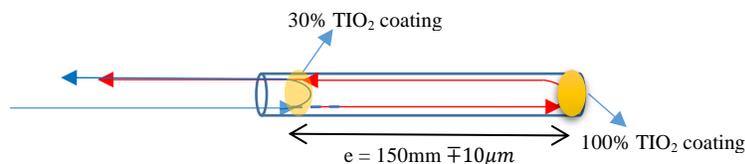

Figure 25 IFPI with TIO₂ coating

The other half of the light signal partially gets reflected at the 30% (partially coated) mirror. The rest of the signal travels and gets to the 100% fully coated mirror and gets reflected as well. Two signals again recouple

into the fibre, but due to their path length difference, there is a difference in phase between the two echoed light signals.

The coupled light then goes back to the interrogation system. It passes the coupler and then gets collimated to a beam splitter (a partial mirror), which splits the beam into two light beams. One of the divided beams moves to the reflector-1, and the other goes to reflector-2 and then get reflected at the beam splitter and get recombined. The recoupled signal then goes to the Diffraction Grating, which diffracts the modulated signal by the IFPI sensor into several beams moving in different directions. These beams then get focused by the Spherical Mirror on the detector. This detector has 8192 pixels.

4.3.3 b) The reference laser-interferometer (ML10)

The ML10 is the reference laser interferometer. The linear displacement of the IFPI was measured with the help of the Michelson interferometer setup shown in figure 24.

How does it operate?

The laser signal-1 emitted from the ML10 laser goes to the beam splitter and gets divided into 2 rays (reflected-2 and transmitted-3. These signals get mirrored from the 2 mirrors, re-join at the beam splitter, and then entering the detector. Retroreflectors ensure that the signals arriving from the measurement and reference arms are parallel when they recouple together at the beam splitter. These re-joined beams interfere with each other destructively or constructively. The ML10 interferometry principles are shown below in figure 26.
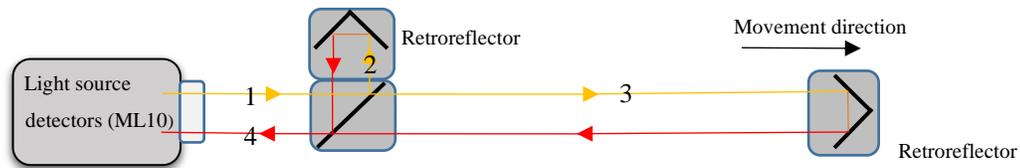
Figure 26 ML10 interferometer

When the 2 light rays are in phase, they add constructively, and the tops of these beams enlarge one another, producing a bright edge. However, when those signals are out of phase, the peaks of beams cancel one another, resulting in a darker fringe.

The signal processing by the ML10 gives the ability to analyse interference produced by those two beams. A change in the measurement arm's length generates changes in the two signals' relative phase.

This sequence of destructive and constructive interruption prompts the strength of the re-joined light to suffer periodic fluctuation. A round of intensity change from dark to light to dark happens each time the retroreflector (the measuring arm) is displaced by half the wavelength of the ML10 laser (316.5 nm). Hence this shift prompts the optical pathway to vary by 633 nm (the laser wavelength); thus, the displacement can be calculated by determining the cycles number with the help of this formula:

$$d = \frac{\lambda N}{2}$$

Where d = the displacement by microns, the λ = the laser wavelength ($\lambda = 0.633\ microns$), and N = the fringes passed number. The result of the ML10, the reference measurement device, was used as the actual measured value against the proposed method. The highest sampling frequency of ML10 (5KHz) was used for this study, so any slight jitter or overshoot could be observed.

4.3.4   c) Piezoelectric Actuator (PZT) and its controller BP303

The BPC303, which is a PZT controller, was used to control the two PZTs at the same time. The actuator controller can synchronize three PZTs concurrently and create different sequences based on the operator's desired function with their software or the LabVIEW software. It can sense the maximum allowed voltage and lock on it so the actuators cannot be overdriven or damaged by high voltage.

By looking at the actuator datasheet (pg.54), the closed-loop scheme was chosen since the hysteresis of the open-loop is not desired, even though open-loop offers a higher bandwidth of the system. The BP303 PZTs are driven with a voltage range of 0 to 75 volts, and they can travel from 0 to 100 µm.

4.3.5   d) The 3D printed jig

TO avoid any twist or jamming of the sensor and being able to apply some strain on the sensor in a controllable manner, two 3D printed jigs were designed by the mechanical department of the university. The first jig did not respond very well. It only showed an almost 9% response to the PZT movements since it was too stiff in the core and too flexible at the PZT holders' positions.

The next jig was designed, which showed a nearly 34% response. Since 34% of 100µm (34 µm) was quite adequate to have the IFPI measurements, the 2nd jig was used for this study.

In the following section, the jig experiments and results are presented as evidence of jigs' responses.

5   Tests and analysis

The Intrinsic Fabry-Pérot (IFPI) sensor was glued inside the 3D printed jig grooves to avoid any undesired twist or any disorderly behaviour. Two PZTs were used to move the 3D printed jig from 0 to 100 µm. The jig only showed movement from 0 to $\cong$34 µm, which was confirmed by the reference interferometer (ML10). The sensor was connected to the interrogation system (chapter 4.4.1 a). The interrogation system monitored and controlled the sensor outcome with the help of LabVIEW. LabVIEW software was already written, but some modifications were done to it to gather a lot of faster data rates. The reference interferometer (ML10)

monitored any jig movement so it could be used as the real (expected) results against the outcome of the IFPI. The IFPI outcome, as interferograms were analysed with the help of MATLAB, which will be discussed more. To avoid any unwanted behaviour and potential calibration, some tests were done without the IFPI, so it could help decide the tests' conditions so it could be defined if the jig was any good for the purpose.

Here are some of those tests can be seen below.

5.1 Equipment's individual tests

5.1.1 ML10 zero-drift testing

To ensure how much the final result was affected by the ML10, the below tests were conducted.

At zero positions (no movement at all) for <u>10 minutes</u>, the displacement was recorded by the reference interferometer (ML10) so that it could be seen if there is any drift in measurement or not.

The saved plot from the ML10 is shown in Figure 27.
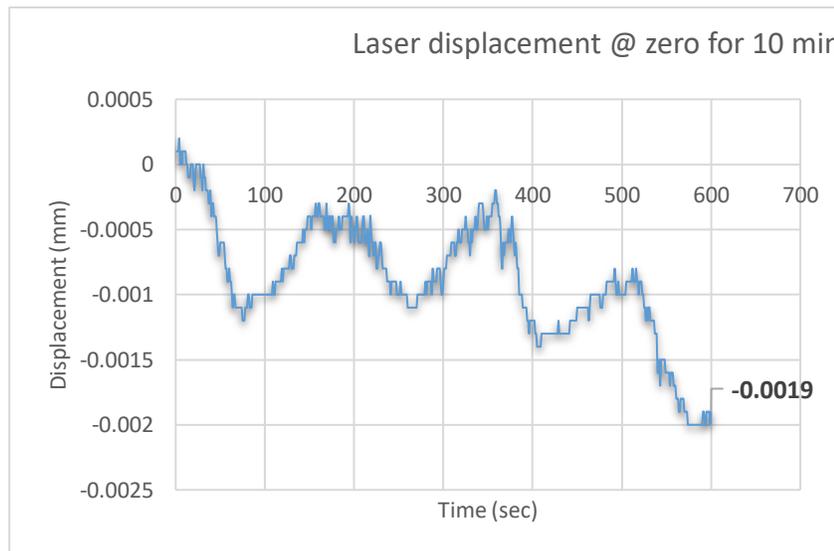
Figure 27 Zero drift _ 10 min

In the 2nd attempt, the test was carried for another <u>100 minutes.</u>

The data in Figure 27 shows after 600 seconds (10 min), Laser measurement recorded $\cong$ 2 µm drift for the 1st attempt. At the 2nd attempt, 100 minutes, it shows almost a 3 µm drift. The PZT amplifier (Figure 28) only showed a 363 nm drift.

5.1.2 **1st developed jig**

The first 3D printed jig was developed and tested to see the

Figure 28 Zero drift _ 100 min

Response of the system. The jig was run by the two PZTs from 0 to 100 µm in 10 steps. The maximum response of the jig was <u>8.443µm</u> against the 100µm PZT.

Here is the response of ten runs of PZT vs the reference laser interferometer.
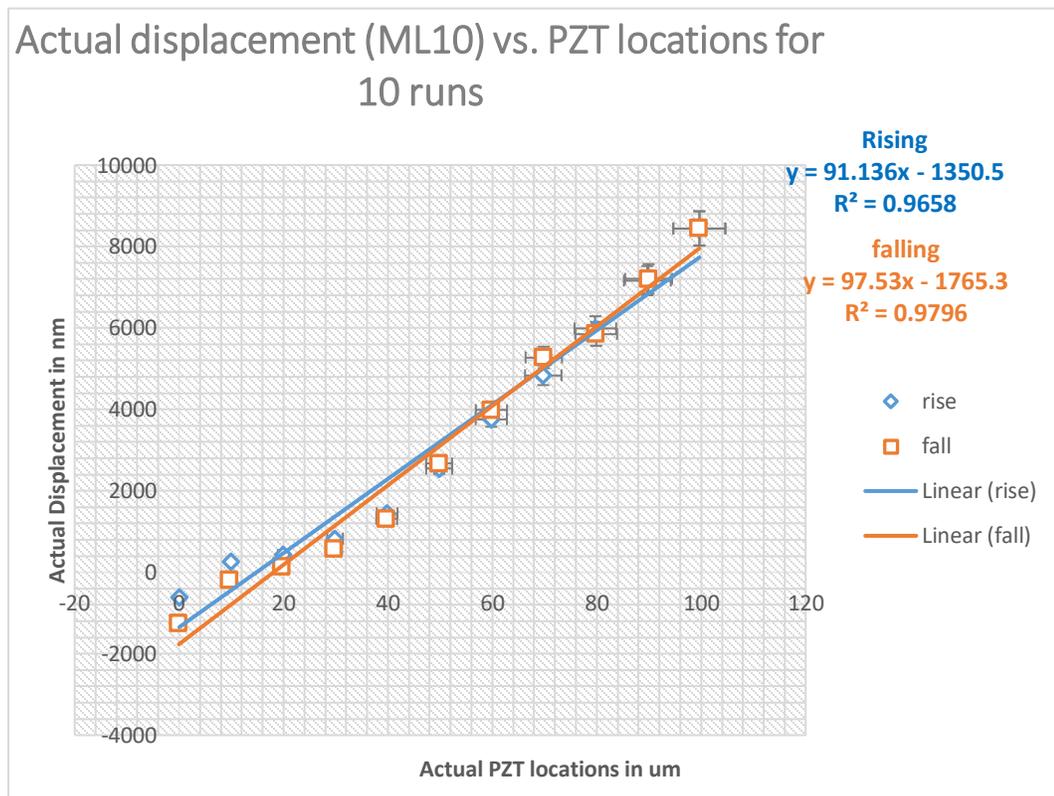
Figure 29 The Actual expansion of the 1st jig vs.

Since the response of the first jig was not desirable due to lack of enough reaction to the PZTs movements, the 2nd jig was developed by some enhancements like de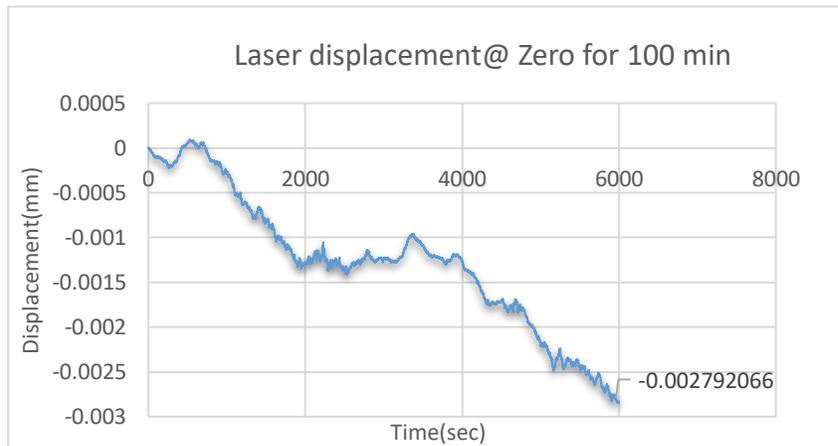signed hollow circles inside the jig so it would be for flexible in the core and put to the metal rod instead of 3D printed PZT holders since they were too flexible, so the jig moved very little until 40µm (only 1.3µm).

5.1.3 **2nd developed jig.**

The 2nd jig was tested with the same conditions of the first jig to be fairly compared against each other. Two sets of 10 runs were performed from 0 to 100µm. This time the jig showed between 33.4µm to 35.3µm response to the PZTs movements. The figure below shows the averaged for every ten runs.

Figure 30 2nd jig test ML10 vs. PZTs

There is another plot where all rising is averaged together and falling averaged together to have only one rising and one falling graph as their total mean.

53

Figure 31 Falling residuals of the 3D jigs.
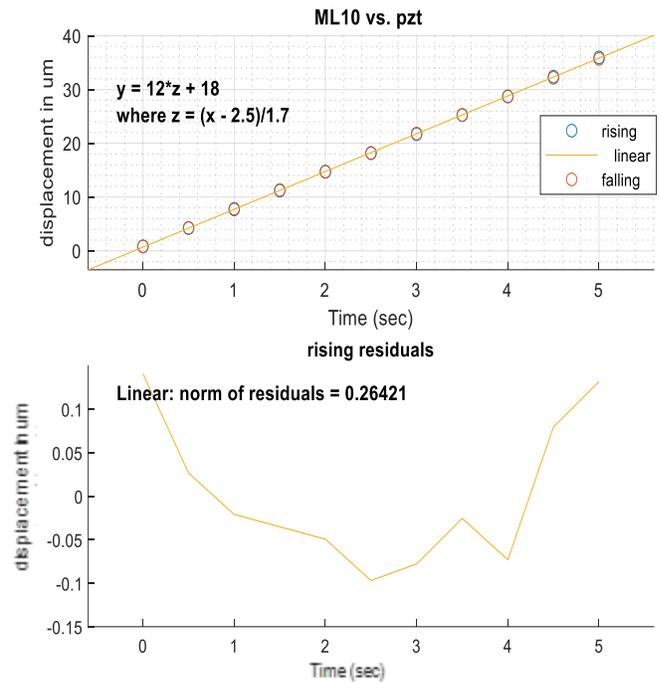
Figure 32 Rising residuals of the 3D jig.

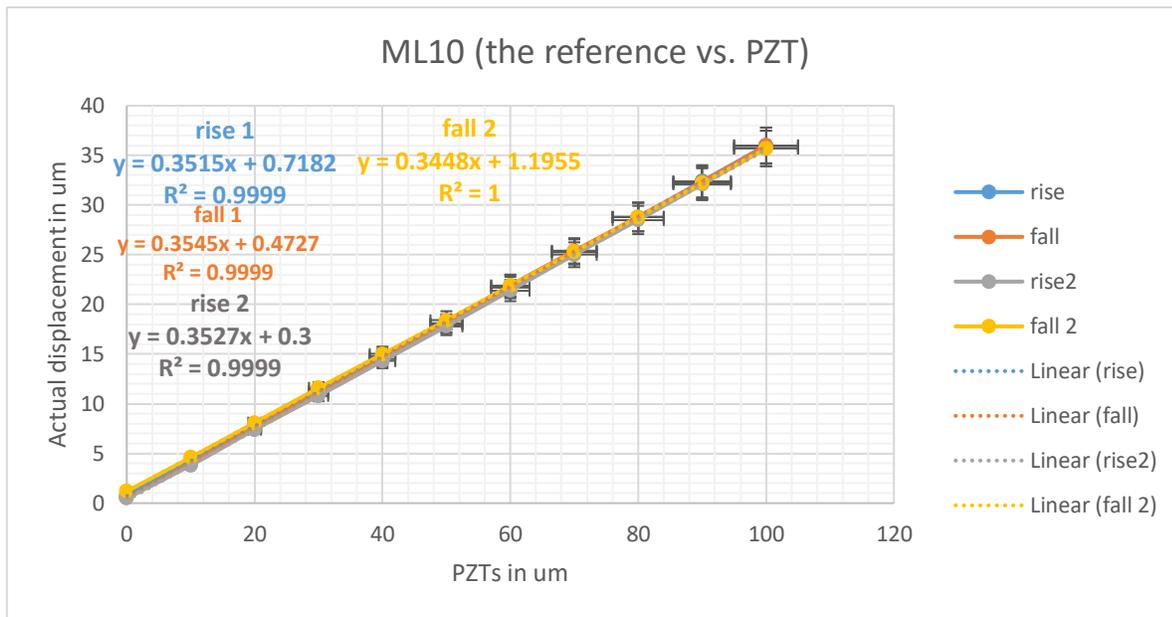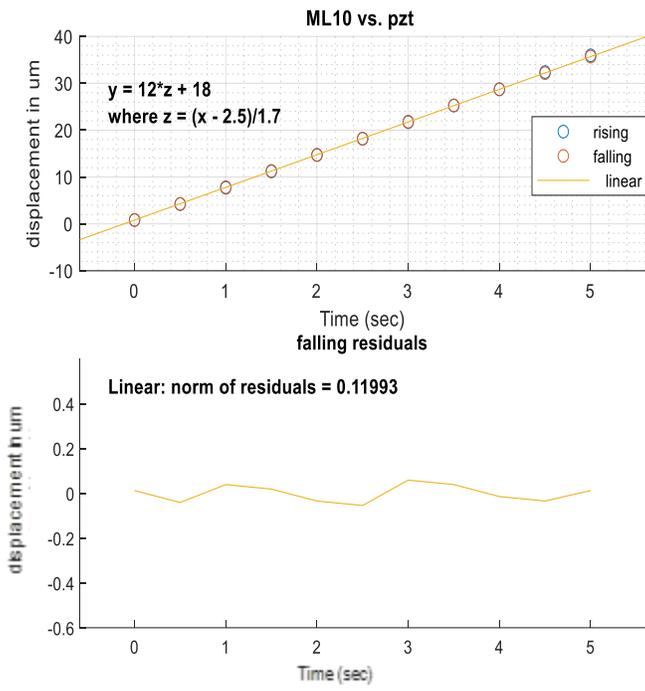As it is presented, the 2nd jig was chosen for the IFPI performance evaluation since it showed a lot better linear response (looking at the correlation coefficient for both graphs) and a nearly 34% response to the PZTs displacement. The schematic of both designs can be seen in appendices (8.5).

The transition is smoother in falling rather than risings based on the residuals of the risings and fallings of the 3D printed jig. By looking at the jig response and their residuals over periods of testing, it was decided that a sweet spot for the test would be from 30µm to 80µm to avoid nonlinearity of the jig in the final IFPI evaluation tests as the jig is only there to help the measurement be performed in a controllable manner.

5.2 Test & Validation of the sensor

5.2.1 Signal processing

The output interferograms of the interrogation system were analysed in Matlab. Here is the method was chosen for the extraction of the data phase and showing the slope as a result.

5.2.1.1 Discrete Fourier analysis [40]

Introduction

In many optical analyses, the fringe pattern is found in the form of:

$$g(x, y) = a(x, y) + b(x, y)\cos\left[2\pi f_0 x + \emptyset(x, y)\right], (1)$$

where the $\emptyset(x, y)$ is the phase which holds the desired information, $a(x, y)$ and b (x, y) describe undesirable irradiance fluctuations stemming from the irregular transmission of light or reflection by a trial piece; in

54

nearly all circumstances, a(x, y), b(x, y) and $\emptyset(x, y)$ change gradually in comparison with the shift initiated by the spatial carrier-frequency f_0.

The traditional procedure has been to produce a fringe-contour record of the phase distribution to extract the phase data. In interferometry, for which the above formula (1) expresses the interfering fringes of tilted wavefronts, the angle is fixed to 0 to attain a fringe form like

$$g_0(x, y) = a(x, y) + b(x, y) \cos [\emptyset(x, y)], \quad (2)$$

that produces a contour map of $\emptyset(x, y)$ with an outlined period of 2π. In the event of moiré topography formula. (1) shows a distorted grating image developed on an item exterior. Additional grating of the similar spatial occurrence is superposed to produce a moiré form, which has approximately the equal order as the above formula (2). Barring that, it affects other high-frequency terms that are in the region of observation. Even though these methods give us direct resources to present a contour map of the distribution of the quantity to be quantified, they have some shortcomings: (1) The phase sign determination is not possible; therefore, it is not possible to differentiate between elevation and depression from a prearranged contour map. (2) The susceptibility is set at 2π as phase deviations of less than 2π cannot generate any contour fringes. (3) Precision is restricted by the undesired changes a (x, y) and b(x, y), especially in the event of broad-contour fringes. Fringe-scanning methods have been offered to resolve these obstacles; however, they demand movable parts, such as a mobile mirror installed on a decoder, that need to be operated with high stability and accuracy. The proposed novel procedure can resolve all those difficulties by a Fourier-spectrum analysis of a non-contour sort of fringe pattern, as presented in the formula. (1)

Principle and Procedure

Initially, a non-contour kind of fringe shape of the type given in the formula. (1) is given into a processor by image-sensing equipment, which holds sufficient resolution to comply with the sampling-theory condition, especially in the x-path. The given fringe outline is reworked in the next form to provide a more straightforward explanation:

$$g(x, y) = a(x, y) + c(x, y) \exp(2\pi j f_0 x) + c^*(x, y) \exp(-2\pi j f_0 x), \quad (3)$$

with $c(x, y) = \left(\frac{1}{2}\right) b(x, y) \exp[j\emptyset(x, y)]$, $\quad (4)$

where * represents a complex conjugate. Next, formula. (3) is Fourier transformed regarding x by utilizing a fast-Fourier-transform (FFT) algorithm that gives

$$g(f, y) = A(f, y) + C(f - f_0, y) + C^*(f + f_0, y), \quad (5)$$

f is the spatial frequency in the x-direction, and capital letters express the Fourier spectra. Because of the spatial fluctuations of a(x, y), b(x, y), and $\emptyset(x, y)$ are quite slow versus the spatial frequency f_0, the Fourier

spectra in the formula. (5) are detached by the f_0 carrier rate. Either of these bands on the carrier is used, suppose C(f – f_0, y), and decipher it by f_0 on the rate of change axis toward the source to get C(f, y). Bear in mind that the undesired background fluctuation a(x, y) has been sifted out in this step. Once more applying the FFT process, the inverse Fourier transform of C(f, y) is computed to f and have c(x, y), characterized by the formula. (4). Then a complex logarithm of Eq gets calculated. (4):

$$\log[c(x,y)] = log\ [(\tfrac{1}{2})b(x,y)] + j\emptyset(x,y). \tag{6}$$

Now the phase $\emptyset(x, y)$ is attained in the imaginary part entirely isolated from the undesired amplitude deviation b(x, y) in the real part. The phase so acquired is unspecified to a factor of 2π. So, for 1D signal, the above 6 can be simplified as

$$\log[c(x)] = log\ [(\frac{1}{2})b(x)] + j\emptyset(x)$$

The phase term $\emptyset$ in the equation is responsible for the fringe modulation. The phase value from the interferogram is obtained as described by Takeda et al. using the 1D FFT applied to the recorded interferograms. But the obtained phase has a 2π discontinuity which is due to the value of the phase exceeding the defined range of -π to π. This causes the phase to wrap at the boundary limits yielding ambiguous results. The wrapped phase needs to be unwrapped, so it becomes continuous. Phase unwrapping is done by Matlab built-in UNWRAP function. After unwrapping the phase, the height/distance is obtained by fitting the phase curve in a phase-wavenumber plot. $Z = \frac{\Delta\emptyset}{\Delta K}$.

Where $\emptyset$ is the phase and K is the wavenumber $K = \frac{1}{\lambda}$.

The mapping from pixel to wavelength and wavenumber was done by calibrating the spectrometer as described in the paper [Reference = Williamson, J., Henning, A., Martin, H., Furness, T., Fletcher, S., & Jiang, X. (2020, November 18). Flexible gauge length intrinsic fibre-optic strain sensor using broadband interferometry [Invited]. Retrieved November 20, 2020, from https://www.osapublishing.org/josaa/fulltext.cfm?uri=josaa-37-12-1950].

Conclusion

The Takeda method has the susceptibility for spotting phase shifts of smaller than 2π and could be utilized to subwavelength interferometry with no need for a fringe-scanning procedure. The accuracy has been enhanced vastly by the whole detachment of the phase from additional undesirable irradiance changes. This technique supports a clear identification between depression and elevation, even from a single fringe sample. The scheme allows fully automated mensuration with no man-machine communication when is applied to topography, which is typically required for the fringe-order project in computer-aided moiré

topography; additionally, since only one designated spectrum is applied, the technique has the extra merit that the calculation is not distressed by higher-order harmonics, that are encompassed in a non-sinusoidal grating sample and cause an increment of spurious moiré fringes in the event of moiré topography.

(Takeda - Fourier-Transform Method of Fringe-pattern Analysis. (n.d.). Retrieved 29, 2019, from

5.2.2 Signal demodulation

5.2.2.1 Software implementation

In this study, LabVIEW was utilized as the data acquisition software and Matlab to analyse and retrieve the spectrum phase to find the slope of the unwrapped phase. The demodulation process flow chart for extracting the slope is shown below.
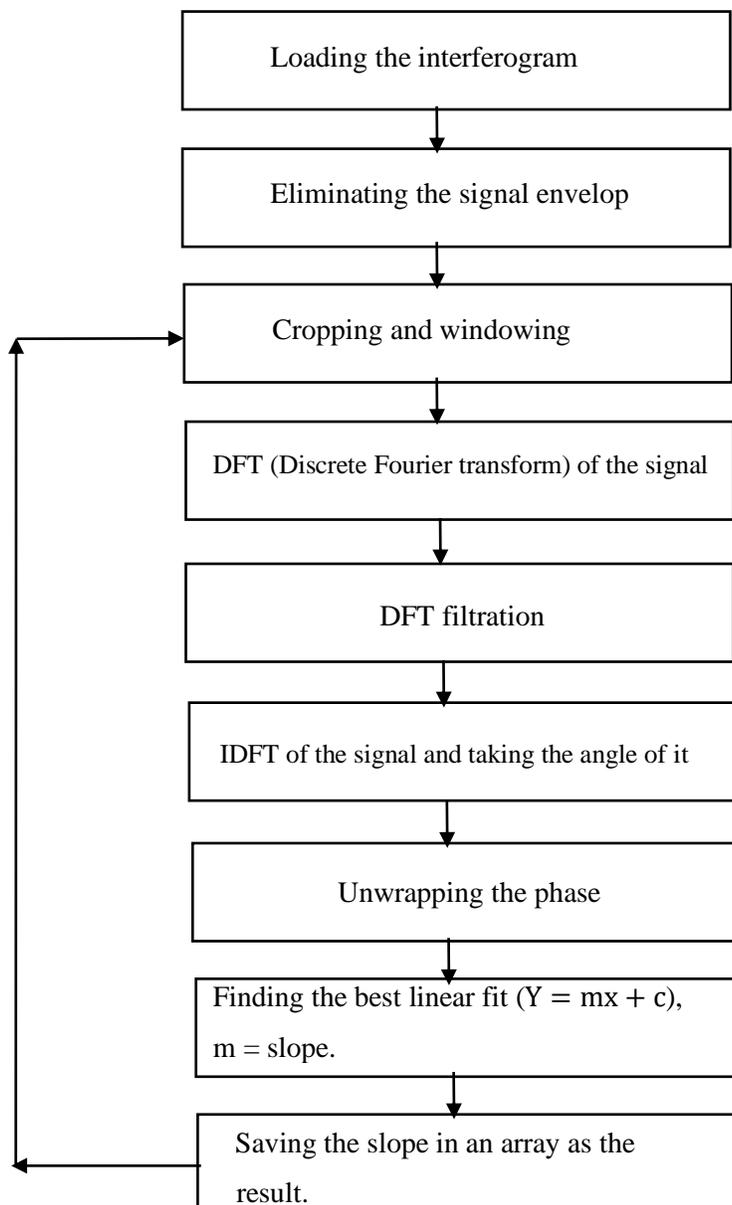

Figure 33 The signal demodulation process flow chart

57

Figure 33 shows the major parts of the demodulation process performed on the interferograms to extract the slopes.

In the following section, some of the critical parts of the flowchart, plus some different tests, are explained.

5.2.2.2 Eliminating the signal envelop

The figure below (34) presents an interferogram inside another sinusoid envelop, which is not desired since the interferograms, in theory, is a single frequency sinewave, so with the help of software, the envelop was removed. The figure below presents an interferogram before and after the envelop removal.
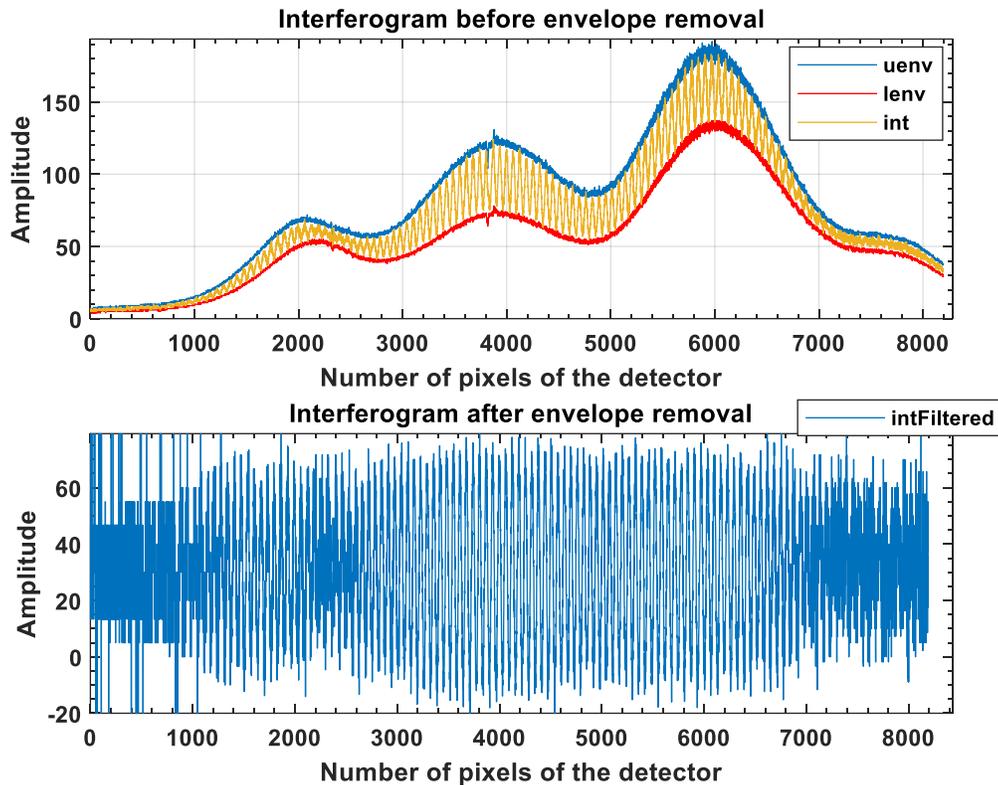

Figure 34 the interferogram of the interrogation detector before and after the envelop removal.

The removal helps detecting the phase correctly without the superimposed sinusoid envelop.

Then the signal processing with the help of Matlab was performed on the signal without any filtration

By looking at the upper figure, it was evident that there are some parts with too much noise and since the frequency of all those sinusoids is one number, so assuming the outcome would not suffer, those parts were removed to see what the result would be or if would improve the outcome in any way.

5.2.2.3 Cropping the undesired part of the interferogram by zero-padding

Several different methods were used, such as cropping different lengths of the interferograms to see the effect of cropping on the data and finding out the least window of the spectrum in which the slope could be deciphered from it successfully. After some initial tests, it became clear that deleting some part of the

interferogram to crop the data was not the optimum method since it changed the centre frequency of the spectrum each time with different cropping length. Therefore, to keep the centre-frequency stable, the input array was zero-padded; hence, zero-padding kept the array untouched. Here is the table showing the different cropping length and their standard and maximum deviation.

No.	Low-Frequency	High-Frequency	Centre-Frequency_ zero-padded	The centre frequency with no zero paddings	Standard-Deviation	Max Deviation
			Several different Cropping lengths on the data			
1	1	8192	129	129	6.59E-06	1.89E-05
2	192	8000	129	126	7.16E-06	2.22E-05
3	400	7800	129	120	8.05E-06	2.09E-05
4	600	7600	129	114	7.17E-06	2.13E-05
5	800	7400	129	108	6.23E-06	1.91E-05
6	1000	7200	129	102	4.93E-06	1.42E-05
7	1200	7000	129	95	3.97E-06	9.87E-06
8	1400	6800	129	89	4.14E-06	1.27E-05
9	1600	6600	129	83	4.70E-06	1.33E-05
10	1800	6400	129	76	6.09E-06	1.79E-05
11	2000	6200	129	70	9.36E-06	2.70E-05
12	2200	6000	129	64	1.11E-05	3.12E-05
13	2400	5800	129	58	6.15E-06	1.66E-05
14	2600	5600	129	48	5.73E-06	1.73E-05
15	2800	5400	129	39	6.11E-06	1.56E-05
16	3000	5200	129	38	7.58E-06	2.30E-05
17	3200	5000	129	33	8.33E-06	2.22E-05
18	3400	4800	129	28	1.07E-05	2.73E-05
19	3600	4600	129	26	1.81E-05	4.80E-05

Figure 35 Cropping table.

59

In the upper figure (35), the difference between the centre frequencies in the case of zero-padded or non-zero padded can be seen.
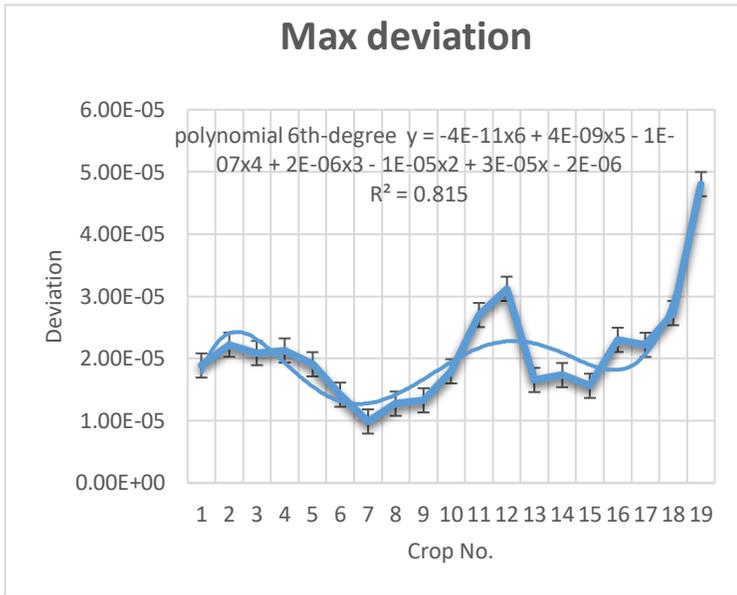

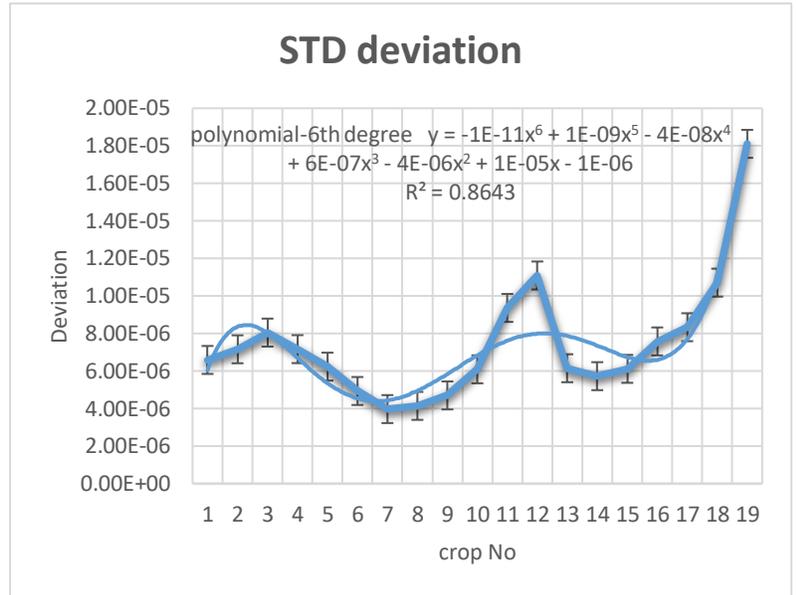*Figure 37 Cropping maximum deviation.*
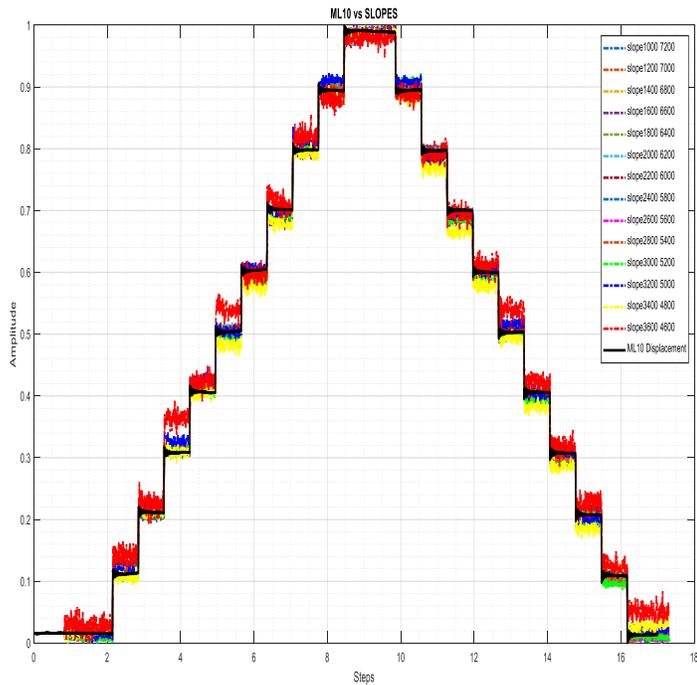

Figure 36 Cropping standard deviation.

Figure 39 Normalized different cropping length slope vs. ML10.
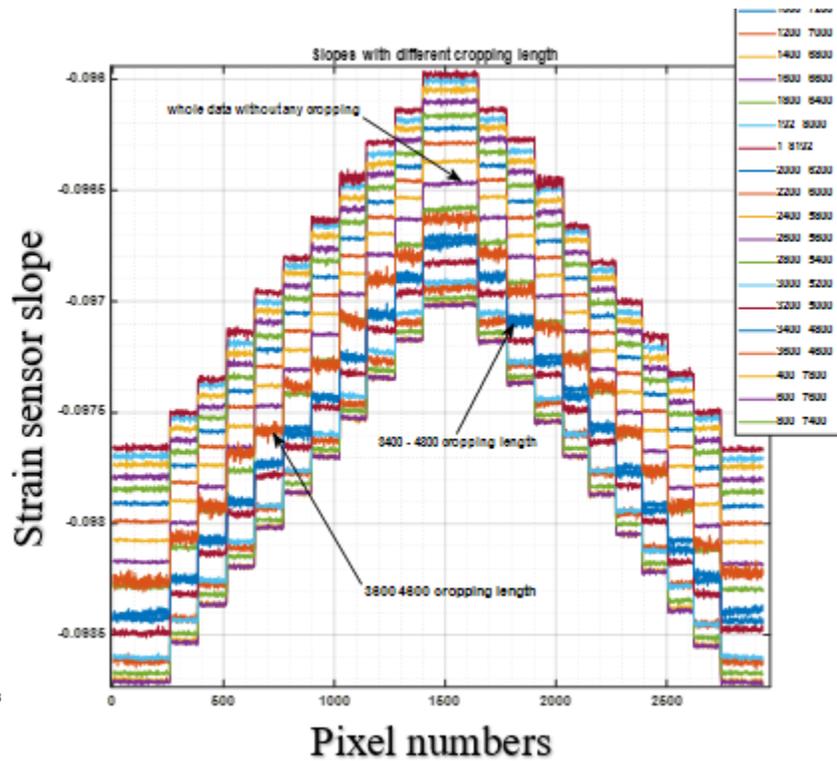

Figure 38 different cropping length without any normalization

These upper tests and so many more showed that different cropping has a dissimilar impact on the outcome. They mostly give an acceptable result but going less than 1400 pixels (length of the cropping) makes the outcome too noisy as it can be seen with the red colour in figure 39 and orange colour in figure 38 also, in figures 36 and 37 it shows going lower than that size dramatically increases the deviations.

5.2.2.4 Windowing the interferograms by the decided cropping length (1400 pixels)

It was determined that 1400 cropping length is the least length of the pixel numbers (signal length), giving a good result. The lower length of data showed that the extracted slope became noisy. In this part was decided to use different windowing with the length of 1400 pixel. The figure below shows the two-best windowing on the interferogram, 4000-5400, and 5000- 6400 pixel are the best windows that generate the best outcomes concerning the slope of the signal.
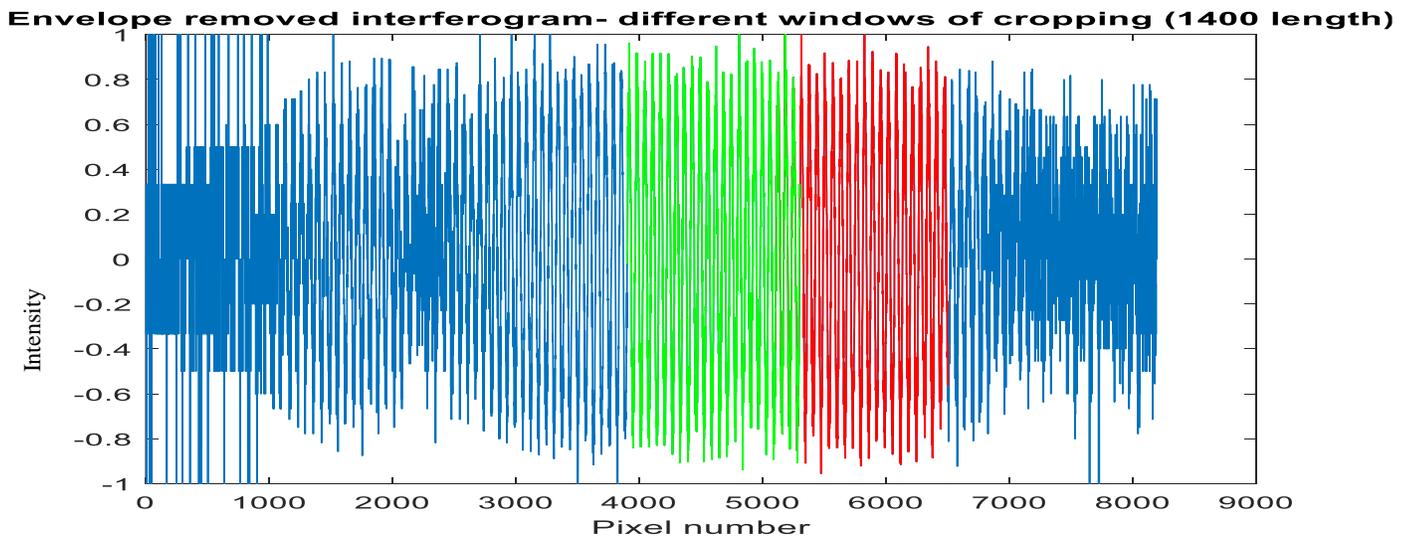

Figure 40 two of best windows for extracting the data.

The table and its maximum and standard deviations for different windowing can be seen in appendices 8.6.

5.2.2.5 Gauge length and strain

Here is the averaged slope vs ML10 for 10-runs (30µm →80µm- PZTs location) so in the residual, it could be seen that it is linear, but 6th-degree polynomial shows to be a lot better fit since it lowers the residuals to less than half the linear regression model for the data.

The lower figure shows 10 averaged runs of ML10 vs slope. Since the interrogation system used was an unbalanced interrogation interferometer, it reduces the temporal coherence of the arrangement, thus enabling the sensor length to be configurable concerning sensitivity for particular purposes.

The fibre length in this research was d(d=150mm) with reflective mirrors at each end mirror 1 & mirror 2 shown in figure 24. Since retroflector 1 is located above mirror 1 (reflecting surface in the fibre) and

retroflector 2 above mirror 2, every measured variation in the fibre length is equal to the change in the distance of mirror 1 & mirror 2 measured by ML10. The figure below shows16.39 µm(∆L) variation in the fibre's length, and since L (length of the fibre) = 150 mm so

$$\text{Strain} = \Delta L/L$$

$$\text{as } \Delta L = 16.39\mu m \text{ (Fig.48) \& } L = 150mm$$

$$\text{Strain} = 16.39\mu m \text{ / } 150 \text{ mm}$$

$$\therefore \text{Strain} = 0.00010926666 \ \varepsilon \text{ or}$$

$$\Rightarrow 109.266\mu\varepsilon$$
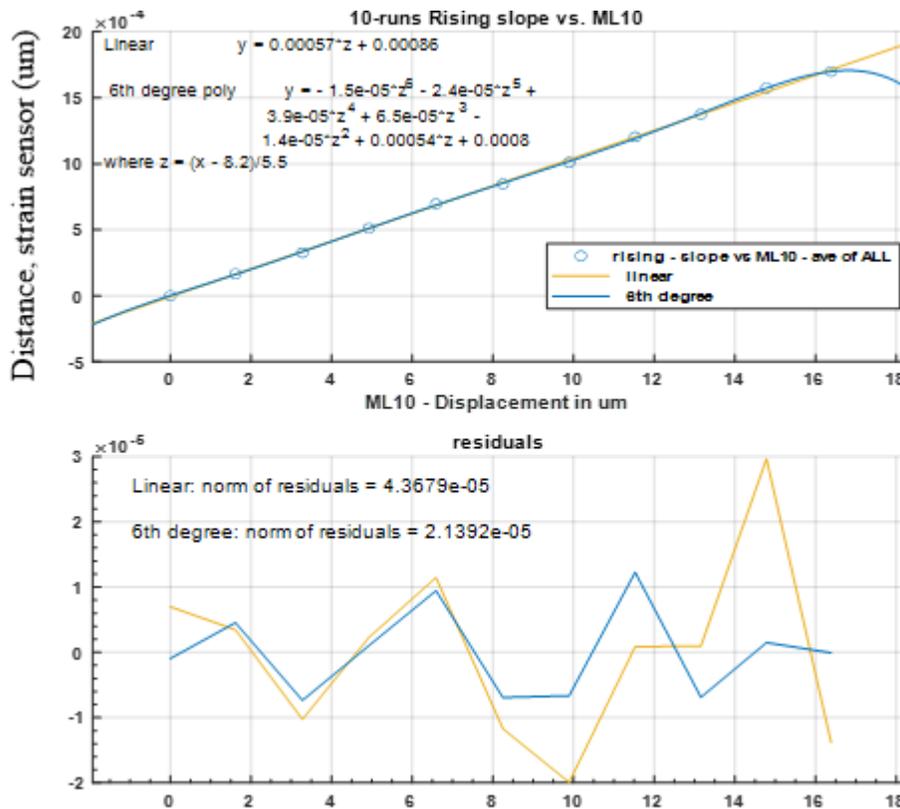
Figure 41 Strain sensor(um) vs ML10 displacement

Note: unwrapping = unwrapping in the Matlab adds multiples of ±2π when the phase variance between consecutive elements of P is equal or bigger than the jump threshold π radians [43].)

The other test that was done in Matlab was to try not to filter anything before unwrapping. Therefore, the test was done without any prefiltration or windowing.

After so many different filtrations and windowing, the final data analysis was decided to be done as below.

The whole data was loaded, and DFT and IDFT carried out; the phase was extracted and unwrapped to see if there is a possibility to filter the undesired parts of the unwrapped phase. Some of the procedures done on the data can be seen below Figure 42.

Initially, the data was loaded as it could be seen as the interferogram (intensity vs Pixels), then removed the envelope and chose the best part of the signal with the least noise (pixels 4000 - 6400), which is shown in green as intensity vs wavelength (superluminescent light-emitting diode (SLED), centre wavelength 850 nm and bandwidth of 55 nm. = 822.5nm→877.5nm). The next step was extracting the phase from the cropped signal, thus used the fast Fourier transform (Fig.42 bottom left), put the negative part of the frequency to zero, inverse Fourier transformed the rest of the signal and used unwrapped function in the Matlab to unwrap the phase (Fig.42 bottom right).

Note Wavenumber = K; where λ is the Wavelength.
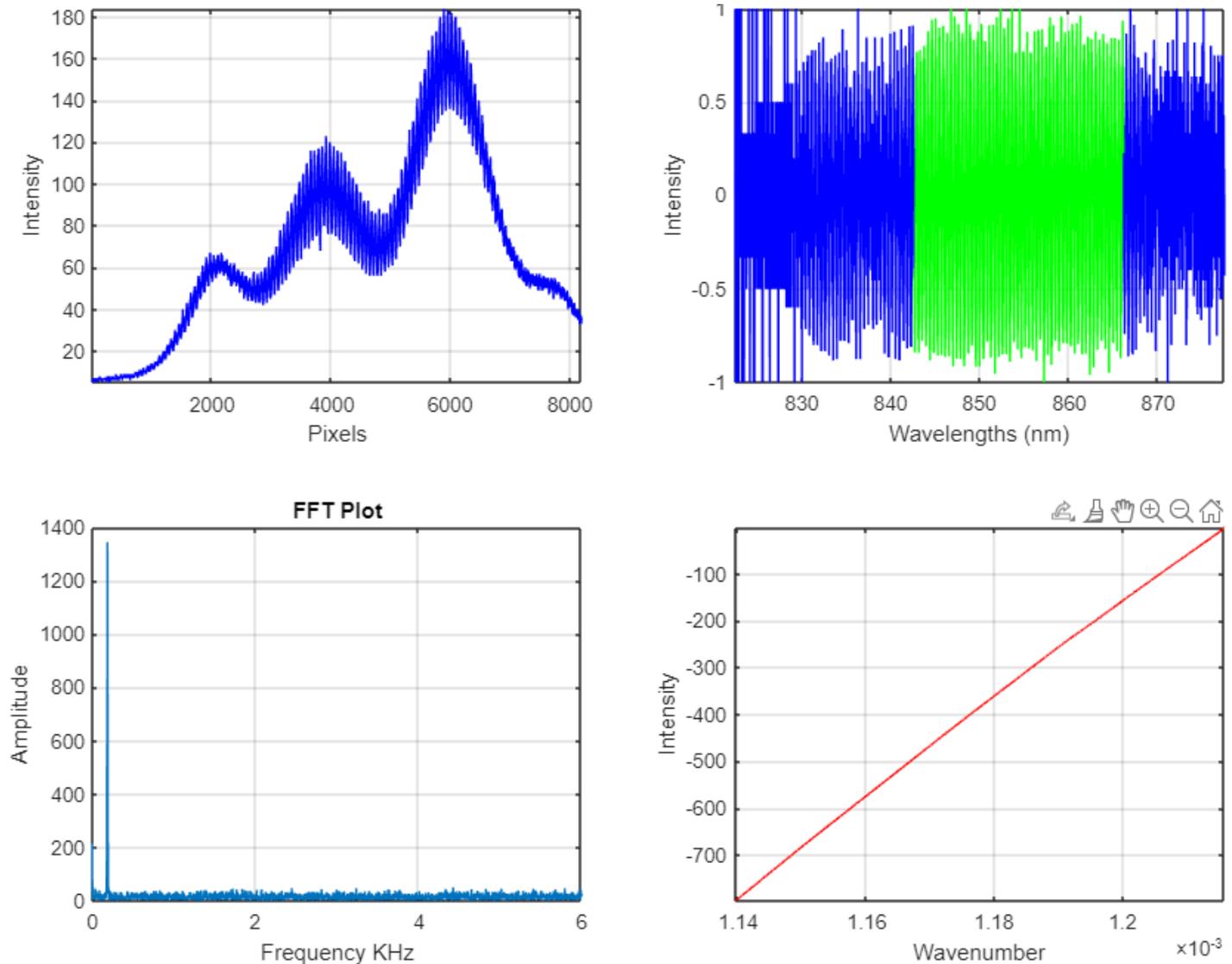
Figure 42 interferogram from removing the envelop and unwrapping the phase.

In the figure below, the extracted slope without any filtration can be seen.

Figure 43 Extracted slope without any filtration.

The upper figure shows the outcome (slope) before the unwrapped phase filtration, and the lower figure shows the slope after the unwrapped phase filtration. This method showed the most precise and accurate way of slope extraction, as is displayed, and explained below.

Figure 44 ML10 vs the slope

Note: black boxes on the graph show the points taken to be averaged and create an array of slopes and another array for averaged ML10 reference to mitigating the error.
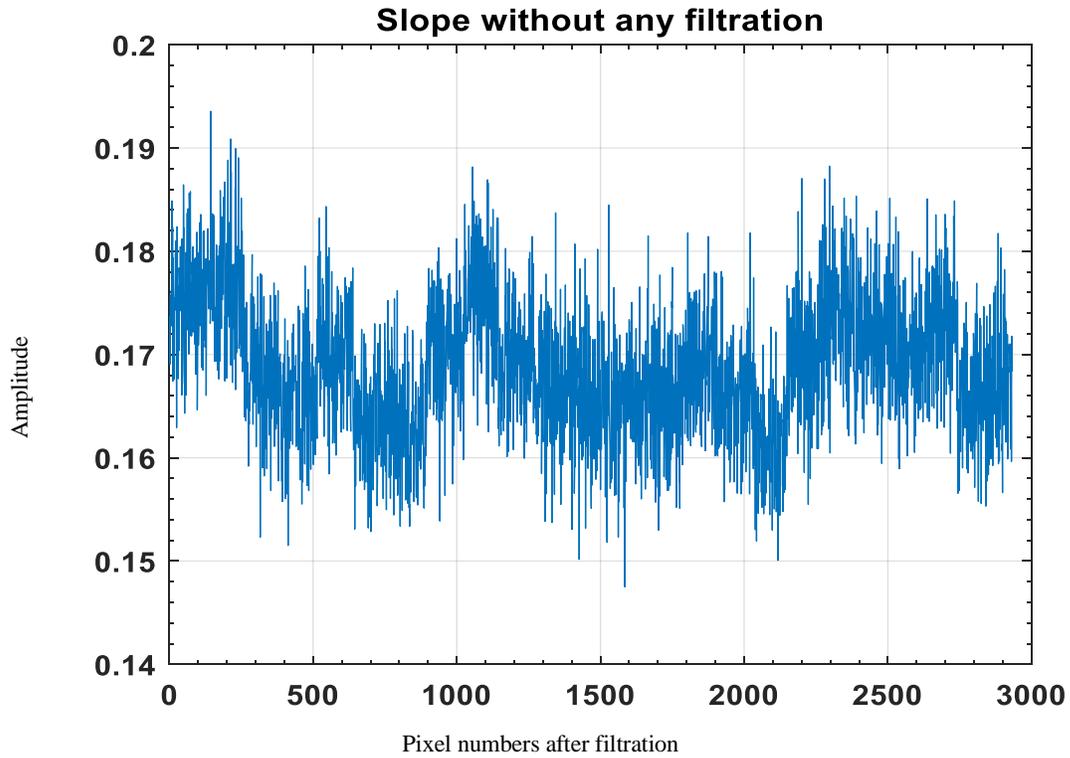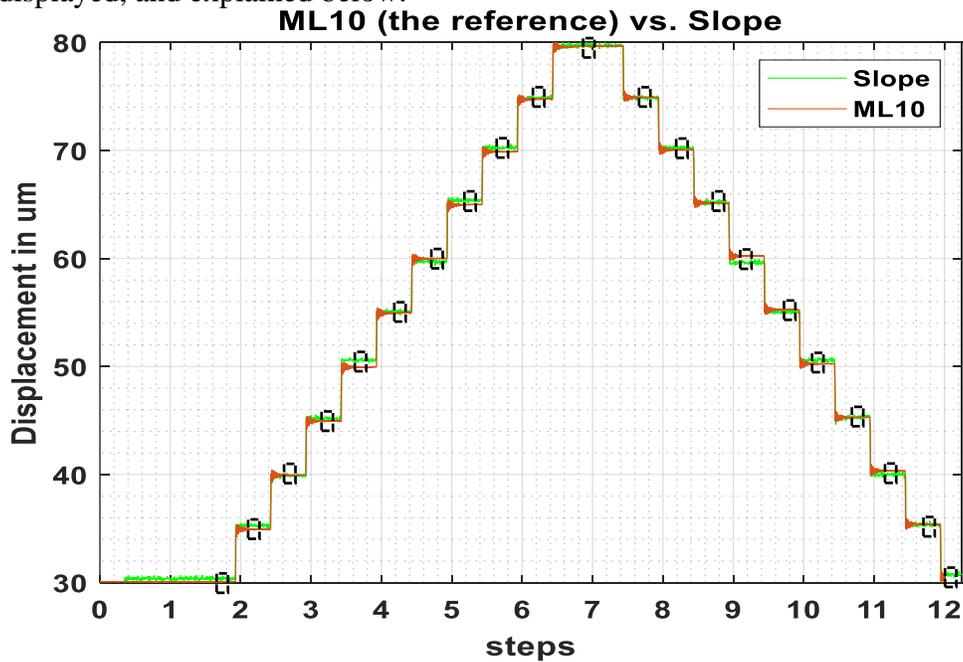
After retrieving the signal, now was the time to show its attributes and qualities. Based on many tests and the overshoots of ML10 for the first four seconds, the rising step time had to be more than 0.4 second and less than one second since after 0.4 seconds, the jittering (overshoots) of each step gets to its settling time (Tay, Maree's and Moore (1998) Determined settling time as "the time needed for the response curve to arrive and stay within a range of specific percentage (usually 2% to 5%) of the final value.")[44].

Avoiding the initial overshoots increased the accuracy of the reference by180nm. Since the pk-pk noise of the overshoot is much higher than the settled region. The overshoot region showed a pk-pk noise of 194nm, but the settled part only showed 14nm. The figure below (45) shows the case of the overshoot region vs the settled region.

Note: Ml10 measured everything in mm, so, for example, 3.4mm shown below actually means $3.4\mu m$.
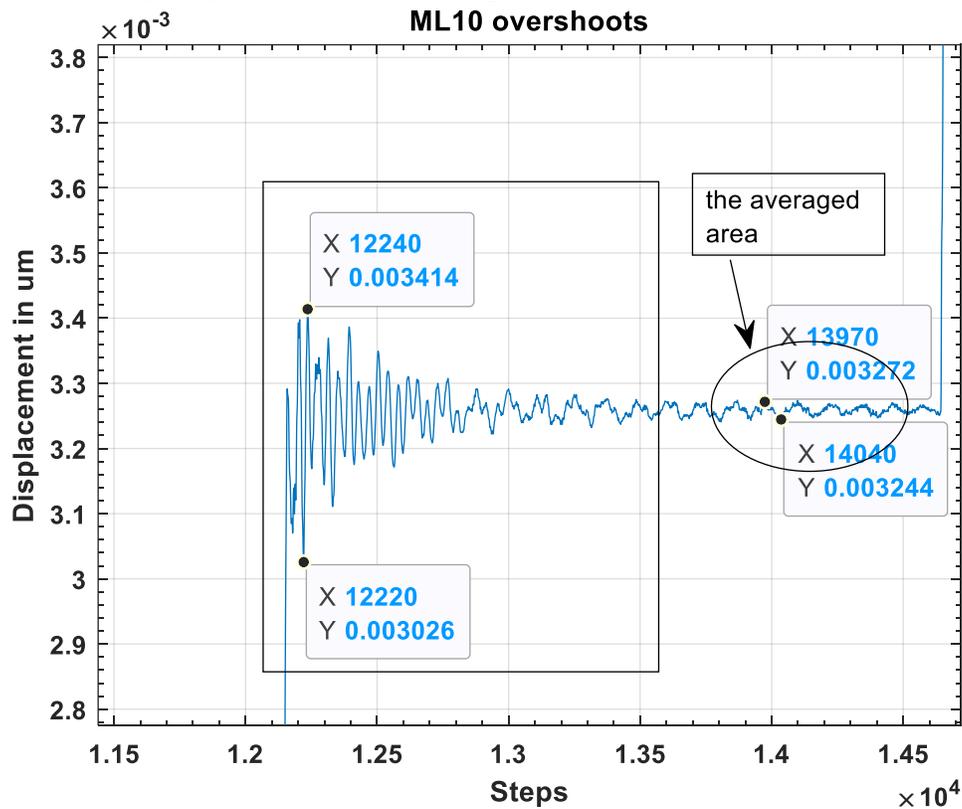
Figure 45 Ml10 overshoot region vs. settled region.

Finally, 0.5 seconds was decided to have enough points to get the data and avoid the zero drift of the ML10, which was discussed in section 5.1.1. As shown in figure 43, after settling time and before the next step-rise, an array from each step was gathered and averaged. This test was done ten times, so different behaviour of the system could be detected. The average of all those ten runs as slope vs ML10 (reference) is shown in figures

49 (rising steps) and 50 (falling steps). ML10 vs slope graph can be seen plus their linear model and 6th-degree polynomial fit. Several graphs of the ten runs can be seen in the appendices section ([8.7](#)).

Figure 46 10-run averaged rising steps before applying any multiplying factor

Figure 47 10-run averaged falling steps before applying the multiplying factor.

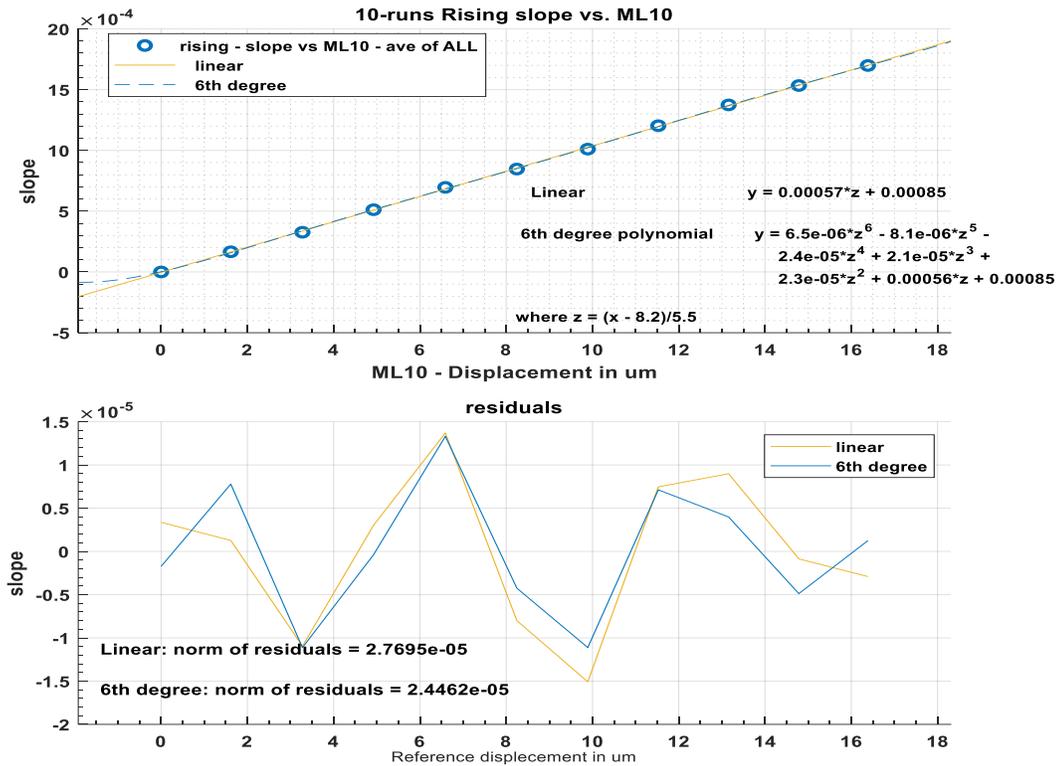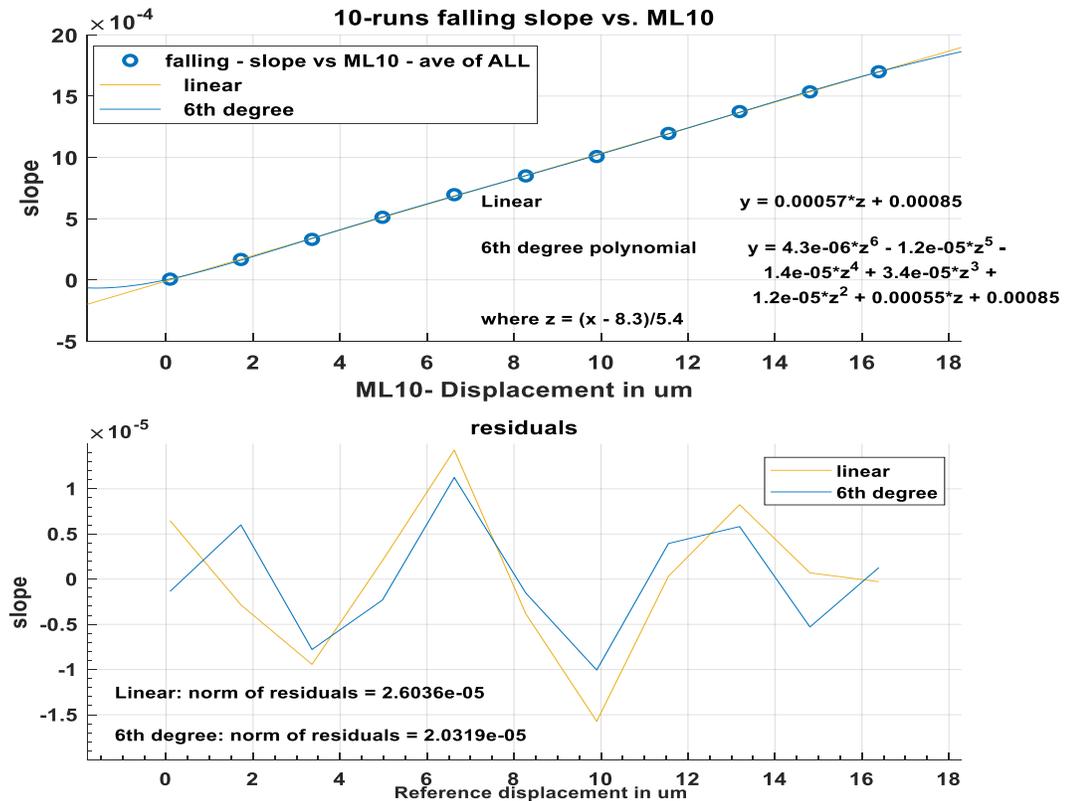The upper figures show the amount of the system's linearity; of course, linearity is proportional; however, the upper graph shows a comparison between 6th-degree polynomial and the linear residuals are very close and quite the same amount and shape.

The upper figures also show dividing the maximum of the ML10 (the reference) by the slope maximum produces the number **multiplication factor** = 9.647062801047454e+03. By multiplying the factor to the slope, its average number became as same as the ML10. This factor can be used for this study to be multiplied to each run and then find out the system's precision. Further research can be done to find a better factor, which perhaps is more than the 7th-degree polynomial based on figures 46 and 47.

Here is the rising slope vs the reference (ML10) in the figure below after applying the multiplying factor.
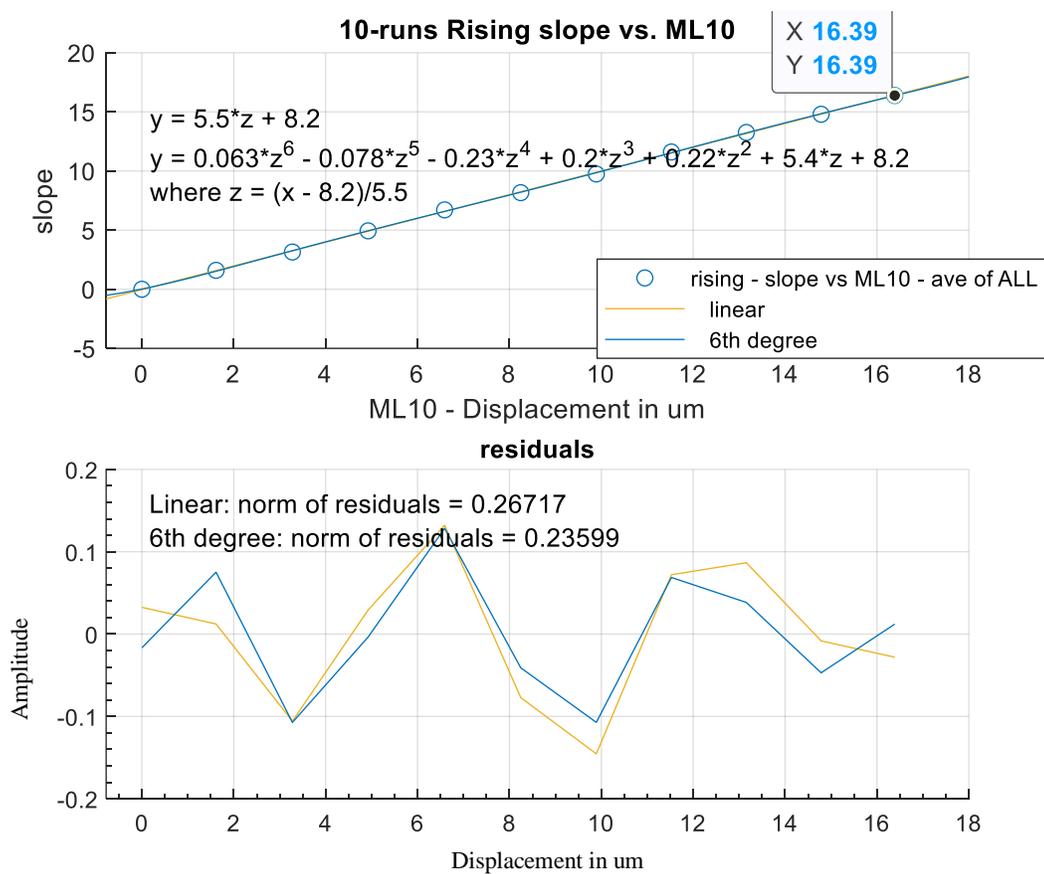
Figure 48 Slope vs. ML10 after applying the multiplying factor.

A comparison between figure 48 and 49 between rising and falling steps (averaged over 10-runs) after applying the factor still shows, they have good linearity. The falling steps show less linearity than the rising steps based on the linear and the 6th-degree polynomial smaller number of residuals.

67
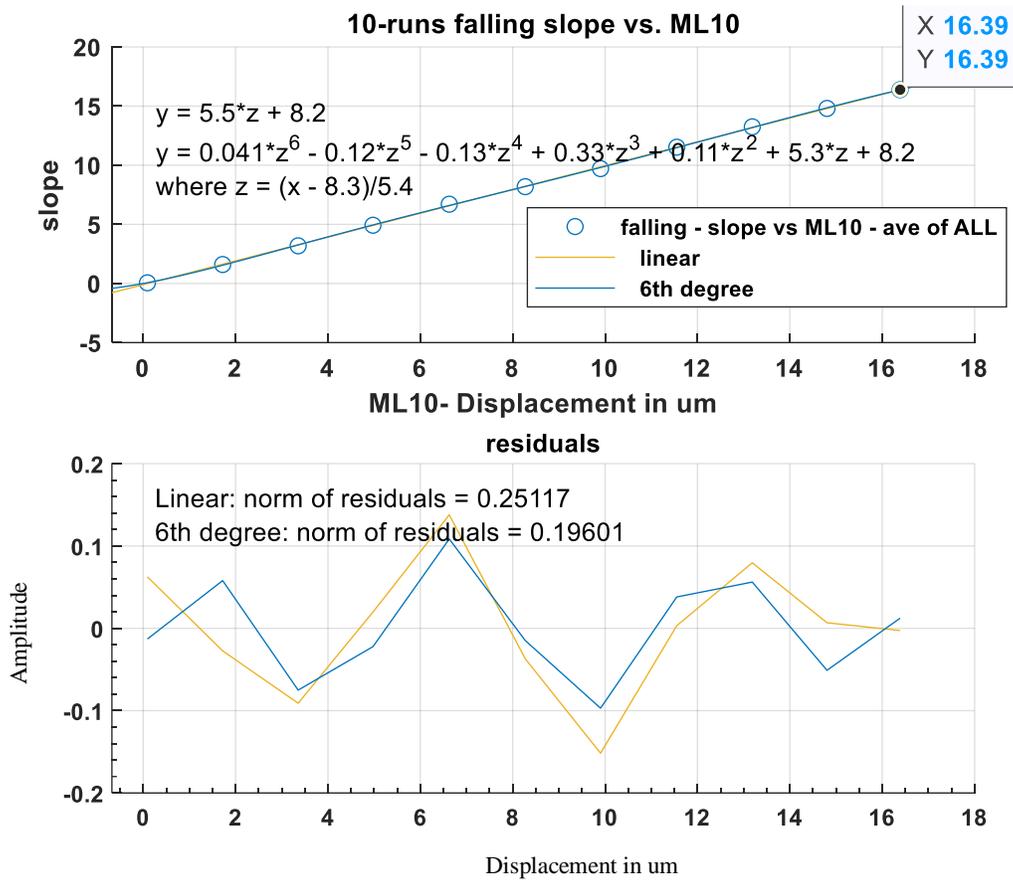
Figure 49 Falling average steps of Slope vs. ML10

After applying the factor to all slopes, the experiment's precision was carried out based on the standard deviation (STD) method. The STD formula is shown below [45].

$$\sigma = \sqrt{\frac{1}{N-1} \sum_{i=1}^{N} (x_i - \bar{x})^2}$$

Where,

σ is the standard deviation, N = the samples' number, x_i is the observed value of samples (slopes in this case), and $\bar{x}$ is the mean value of observation.

Since every step was quite different, STD (standard deviations) were calculated for each step separately which could be seen in the figure below (50). However, the mean of all those STD is equal to ±0.1458μm, which indicates the precision of the results.

68
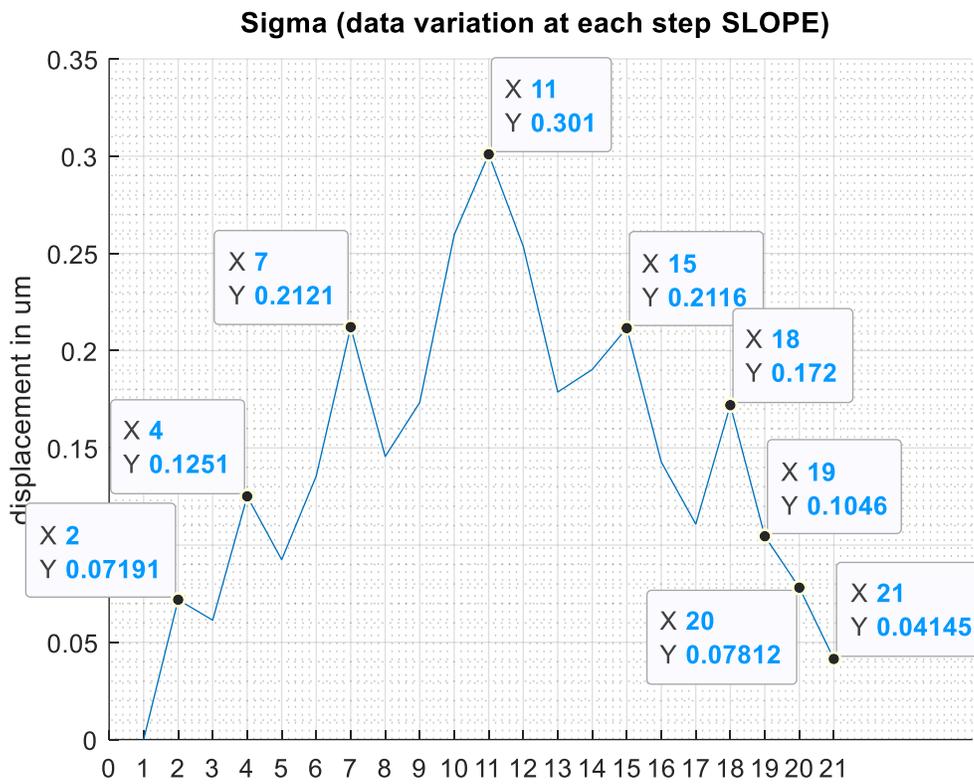
Figure 50 Standard deviation for each step.

The **system's accuracy** was calculated as the error percentage, which is shown below [46].

$$\% \; error = \frac{Measured \; value - true \; value}{true \; value} \times 100$$
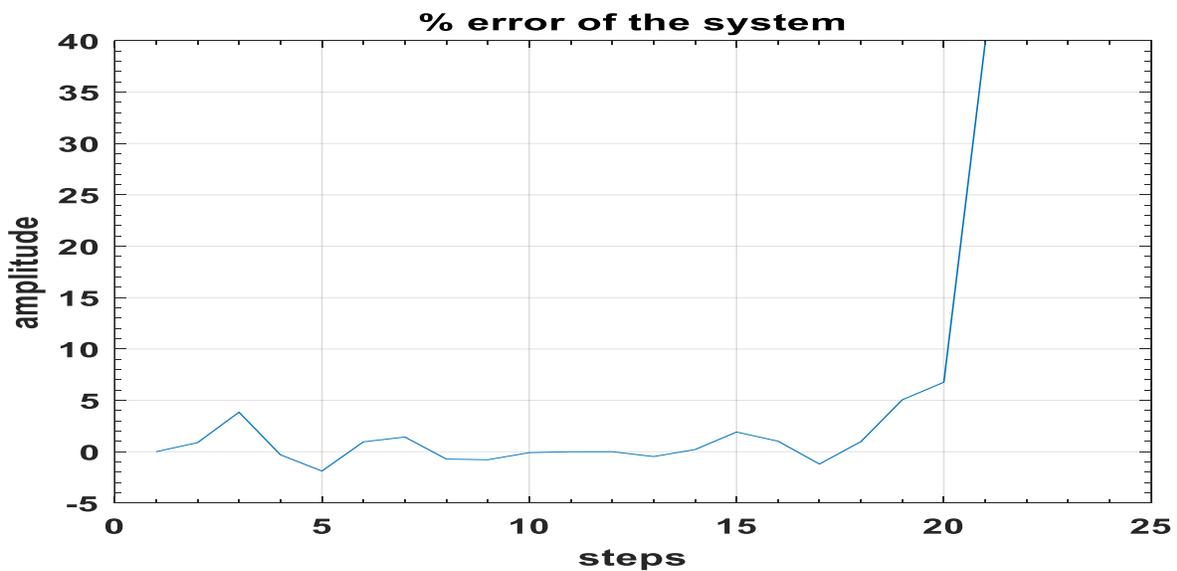
Figure 51 The error percentage for each step

Since the %error was calculated as an array (for each step) rather than a single digit, here is the mean of the error array. % error = 2.74.

The other attribute of any measurement is the stability (peak to peak noise) of the system, and it can be described with the formula below as [46]:

$$Stability = \frac{Highest\ positive\ reading - highest\ negative\ reading}{2}$$

$$Stability = \frac{16.57\mu m - 16.38\mu m}{2} = 95nm\ of\ stability\ (pk - pk\ noise)$$

The figure below shows one of the worst cases of the 10-runs pk-pk noise. As in figure 44, the averaged region for the ML10 showed a pk-pk noise of around 14nm vs the slope around 95nm; therefore, it could be said the system's stability vs the reference is nearly seven times worse.
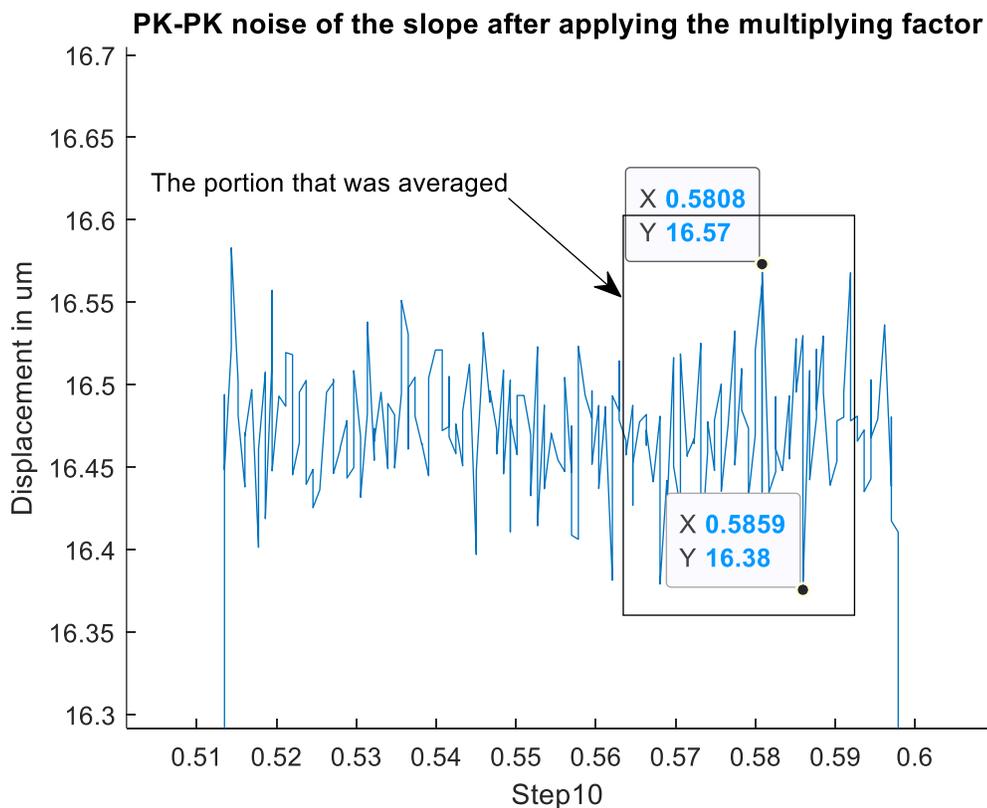
Figure 52 pk-pk noise of the slope readings

6   Conclusion

Commercial research and SWOT analysis were initially done to investigate the feasibility, commercial needs and perhaps to find a gap in the market. There are some gaps in the market in the sense of making cheaper sensors or having a high resolution and a high range, which was not the case for Fabry-Perot sensors.

A rig was developed to make the tests and analysis of the IFPI sensor possible. The platform consists of ML10 (reference) with a maximum 6KHz sampling rate (which was used), an interrogation system controlled by a computer for data gathering and monitoring, and a PZT controller (BP303) and two PZTs (PAZ015) (0 to 100 um movement range). The PZT controller controlled by the same computer so the two PZTs could move concurrently to avoid any twist in the jig.

The optical lab produced a 3D printed jig so the IFPI sensor could be glued into the grooves of the jig so that some force could be applied to the sensor in a controllable manner. The 1st jig was too stiff in the core and flexible and soft at the PZT holder positions; therefore, after exerting 100um extension, it only showed less than %9 of response, plus it had bad hysteresis and showed much nonlinearity. The 2nd jig showed a much better response, 34%, and from 30µm to 80µm showed a good amount of linearity. Therefore, all tests were carried out from 30µm to 80µm.

Signal analysis for the system was carried out based on the Takeda method, but in that paper, a two-dimensional form of data is illustrated, while in this case, a single line of data was used ($fft(g(x)) = G(f)$). Data acquisition was carried out with the help of LabVIEW but initially could not have more than one interferogram in a second. Thus, a queue (producer-consumer design) design was developed to give the ability that two hundred interferograms could be saved per second. Having the ability to have 200 interferograms instead of one was a big help so that the data could be averaged and be able to run much faster tests like the final tests every half second the PZT position increased by 5um and still was able to have more than 80 interferograms.

ML10 was tested at zero position and showed nearly 3um of drift only after 10 min. It also showed the time for each step, increase, or decrease should be under 1 sec to avoid any drift.

The interferogram extracted from the sensor was analysed by removing the envelop, which was superimposed the original sinusoid signal. The signal was then examined with different methods such as cropping the data, filtering the data before or after the DFT process, or loading the data without any filtration, and after the DFT process, filter the data when it is unwrapped. The result of those different filtrations showed that filtering the result after unwrapping gave the best result in the case of the signal residuals or linearity. The senor outcomes were more precise compared to any other methods tried before.

Based on that knowledge, 10-runs of the test were performed from 30µm to 80 µm by 5µm steps every 0.5 sec, and it showed the results of:

It is quite a robust linear relationship between the slope and ML10 since residuals of the 6th polynomial is not very different from a linear fit. A multiplying factor of 9.6471.E3 was identified between the slopes and the ML10. After applying the factor, the precision of the system was calculated based on the standard deviations. The STD of all those runs for the slopes came to ±0.1458µm. The accuracy of the system was calculated based on %error= 2.74. The system's stability was carried out as calculation of PK-PK noises, which was equal to 95nm, which was nearly seven times worse than a settled region of the ML10 (14nm), but ML10 in the overshoot region showed 194nm pk-pk noise. That is why the results were taken after 0.4 sec till 0.5 sec (just before jumping to the next step).

7 Future Work

This study that has been done and explained in this thesis can be modified and studied more. Initially, what comes to mind is adding more sensors to see if they act similarly, as well as being able to monitor two or multi-directional strain. Perhaps one of the sensors not glued to be able to see the temperature effect on these sensors. The thermal expansion could be separated by using another sensor with the same characteristics but not gluing it to the jig.

The mechanical strain could not affect the sensor, but only the temperature since it is not glued to the jig. When the temperature changes were calculated, then they could be deducted from the glued sensor result. To have a more accurate reference like XL80 plus XC-80, which is the temperature and humidity compensator, so more accurate results could be gathered and analysed. Having a metal jig instead of plastic so the response could be seen for different materials as well as metal perhaps shows less hysteresis due to its young modulus. Calibration of the interrogation system would be so helpful. Additionally, being able to control the PZTs, reference interferometer, as well as interrogation system from one program such as LabView help to synchronize the outcome; therefore, dynamic tests will become a viable option for the future.

The researched FP sensor has been investigated for CERN regarding the monitoring and gauging of malformation of the collimator jaws installed in the direction of beams of the Large Hadron Collider (LHC). LHC operates based on clashing beams construct of small particles with unprecedented strengths. Monitoring those collimator jaws are vital Since the potential power in both LHC beams is nearly enough to melt one tonne of copper. Still, the investigated FP sensor needs further investigation to reach less than 0.1µε resolution and measurement rates of several kHz to observe the transient effect efficiently; this is vital for the correction of the collimator jaws. {Collimators: The LHC's bodyguards. (n.d.). Retrieved November 1, 2020, from https://home.cern/news/news/experiments/collimators-lhcs-bodyguards}

8 Appendices

8.1 Commercially researched fibre optic sensors

						Strain Fibre Optic Sensors (FOS)					
Number	Company	Sensor's name	Sensor's Type	Technology	Measurement range (μƐ%)	Resolution (μƐ)	Dynamic range	Accuracy± %	Min Temp Range	Max Temp range
1	Geokon	FP4000-1.0	Strain gauge	FP	1000	0.15	6666.666667	3	-40	80
2	Geokon	FP4000-2.5	Strain gauge	FP	2500	0.3	8333.333333	3	-40	80
3	Geokon	FP4000-5	Strain gauge	FP	5000	0.5	10000	10	-40	80
4	Geokon	FP4911	Strain gauge	FP	1000	0.15	6666.666667	0.25	-40	80
5	Opsens Solutions	OSP-A	Strain gauge	FP	500	0.15	3333.333333	0.15	-40	250
6	Opsens Solutions	Instrumented bolt	Strain gauge	FP	2500	0.3	8333.333333		-40	250
7	Opsens Solutions	OSP-FP	Strain gauge	FP	7500	0.75	10000		-40	250
8	Micron Optics	os3100	Strain gauge	FBG	2500	1.4	1785.714286		-40	120
9	FBGS	SGC-01	Strain gauge	FBG		0.85	0	1.7	-50	130
10	Optromix	S1	Strain gauge	FBG	3000	1	3000	1	-50	80
11	Optromix	S2	Strain gauge	FBG	2500	1	2500	1	-20	80
12	Optromix	S3	Strain gauge	FBG	560	1	560	0.1	-50	80
13	Optromix	S4	Strain gauge	FBG	1500	1	1500	1	-20	150
14	Optromix	S7	Strain gauge	FBG	5000	2	2500	0.1	-50	80
15	ROCTEST	MuST FBG	Strain gauge	FBG	2000	1	2000	2	-20	80

16	Scamie	OBSG-60 & OBSG-120-CE	Strain gauge	FBG	5000	0.99	5050.505051	1.2	-30	60
17	HBM	FS62	Strain gauge	FBG	5000	0.99	5050.505051	1	-20	80
18	nBG	FBGS-01	Strain gauge	FBG				1.2	-20	60
19	Smartfibres	Standars FRP	Strain & Temp gauge	FBG	5000	0.4	12500	1.2	-30	60
20	Smartfibres	SmartWeld	Strain gauge	FBG	2500	0.4	6250	1.2	-270	150
21	Smartfibres	Coated by Acrylate & Polymide	Strain gauge	FBG	9000	0.4	22500	1.2	-270	300
22	Smartfibres	SmartTape Construction	Strain & Temp gauge	FBG	9000	0.4	22500	1.2	-20	50
23	AUSOPTIC	MSS-1700	Strain gauge	FBG	5000				-20	80
24	ozOptics	DSTS (versions F, R & C)	Strain & Temp gauge	Brillouin	20000	0.1	200000	2	-270	1000
25	LUNA	HD	Strain gauge	Rayleigh scattering		1	0		-40	200
26	LUNA	HS	Strain gauge	CFG		1	0		-40	200

Figure 53 Fibre optic strain sensor commercial table

8.1.1 Market size

The fibre optic industry has grown rapidly in the last few years due to Fibre optic resistance to corrosion, EMI (electromagnetic interferences) and RFI (Radio frequency interference).

Fibre optic sensors have many applications such as metrology, defence, construction, transportation, oil and gas, automotive, and healthcare.

Major players in the fibre optic strain sector consolidate the industry by using different strategies. Still, their products are the most expensive, and the technology is mostly around FBG sensors, i.e. Micron Optics (section 8.1 Commercially researched fibre optic sensors) has 1.4με resolution and a tag price between 11000-45000 US dollars (USD).

Based on several market size estimators' oil & gas is leading the fibre optic sensor market. They also report that pressure and strain sensors are the prime players in the industry. Based on geography fibre optic sensor industry could be divided into North America 45%, Europe 30%, Asia 20% and 5% rest of the world.

Fibre optic market forecast between 2018-2023 is anticipated to have a compound annual growth rate (CAGR) of more than twenty-one percent, but the fibre optic strain sector CAGR will be around ten to eleven percent.

The industry is expected to reach a valuation of around four billion USD by the end of 2023, which is promising.

The competition in the fibre optic industry is tough, though, for a good quality (good resolution)

To consolidate a market position for the researched FP sensor having a cost-efficient and high-quality product is very important.

8.1.2 Marketable performance

The researched sensor is currently being assessed for the active sensing of deformation in large collimator jaws positioned in the beamline of the Large Hadron Collider (LHC). The deformation is caused by localized heat generated by accelerated particles impact [3]. This application demands the strain resolutions of less than 0.1 με and measurement frequencies of several kHz to guarantee the transient effects are adequately obtained, so closed-loop compensation could be done by employing piezoelectric components to exert corrective force at various spots on the collimator jaw.

8.1.3 The improvement in the data processing

- Modify an existing LabVIEW program that was logging the unbalanced interferometer output as it could log the data 1/sec. The program was improved to 200/sec.

- Testing the 1st built jig and analysing its characteristics, so the 2nd (final) jig was improved concerning elasticity and movement (The 1st jig could only stretch 8µm, but the second one could go up to 33 µm).
- Finding the sweet spot in the plastic jig 30µm to 80µm (The jig behaviour was linear in this region but before 30 µm and after 80µm was not.)
- collecting the data by LabVIEW as a CSV file
- Analysing the data with the help of MATLAB.
- The student wrote different Matlab codes for analysis of the interferometer output.
- Removal of the data envelope so the "pure" sinewave could be extracted.
- The MATLAB code was improved and changed to find the best window of data concerning pixel numbers 3000-6500.
- A lot of different FFT filtering was tested; thus, the best outcome could be achieved.
- Extracting the slope and unwrapping the phase.
- Filtering the signal after unwrapping.

[Refrences]

1.   {Optical Sensing Market. (n.d.). Retrieved October 25, 2020, from https://www.marketsandmarkets.com/Market-Reports/optical-sensing-market-197592599.html}

2.   {Global Optical Sensing Market Research Report Forecast 2023: MRFR. (n.d.). Retrieved October 22, 2020, from https://www.marketresearchfuture.com/reports/optical-sensing-market-3260}

3.   {Carra, F., et al., The "Multimat" experiment at CERN HiRadMat facility: advanced testing of novel materials and instrumentation for HL-LHC collimators. 2017. 17: p. 76-097.}

4.   {Williamson, J., Henning, A., Martin, H., Furness, T., Fletcher, S., & Jiang, X. (2020, November 18). Flexible gauge length intrinsic fibre-optic strain sensor using broadband interferometry [Invited]. Retrieved November 20, 2020, from https://www.osapublishing.org/josaa/fulltext.cfm?uri=josaa-37-12-1950}
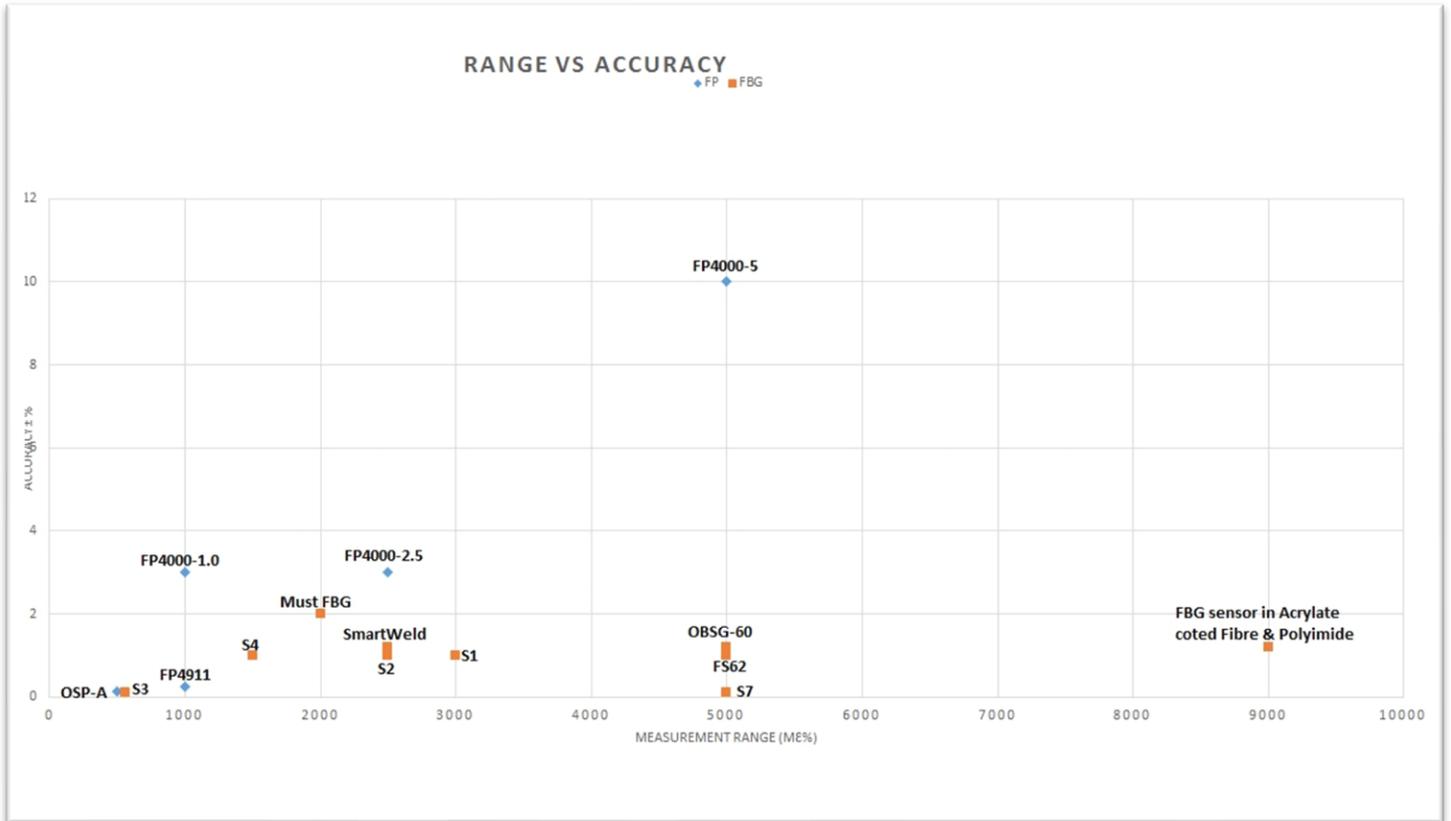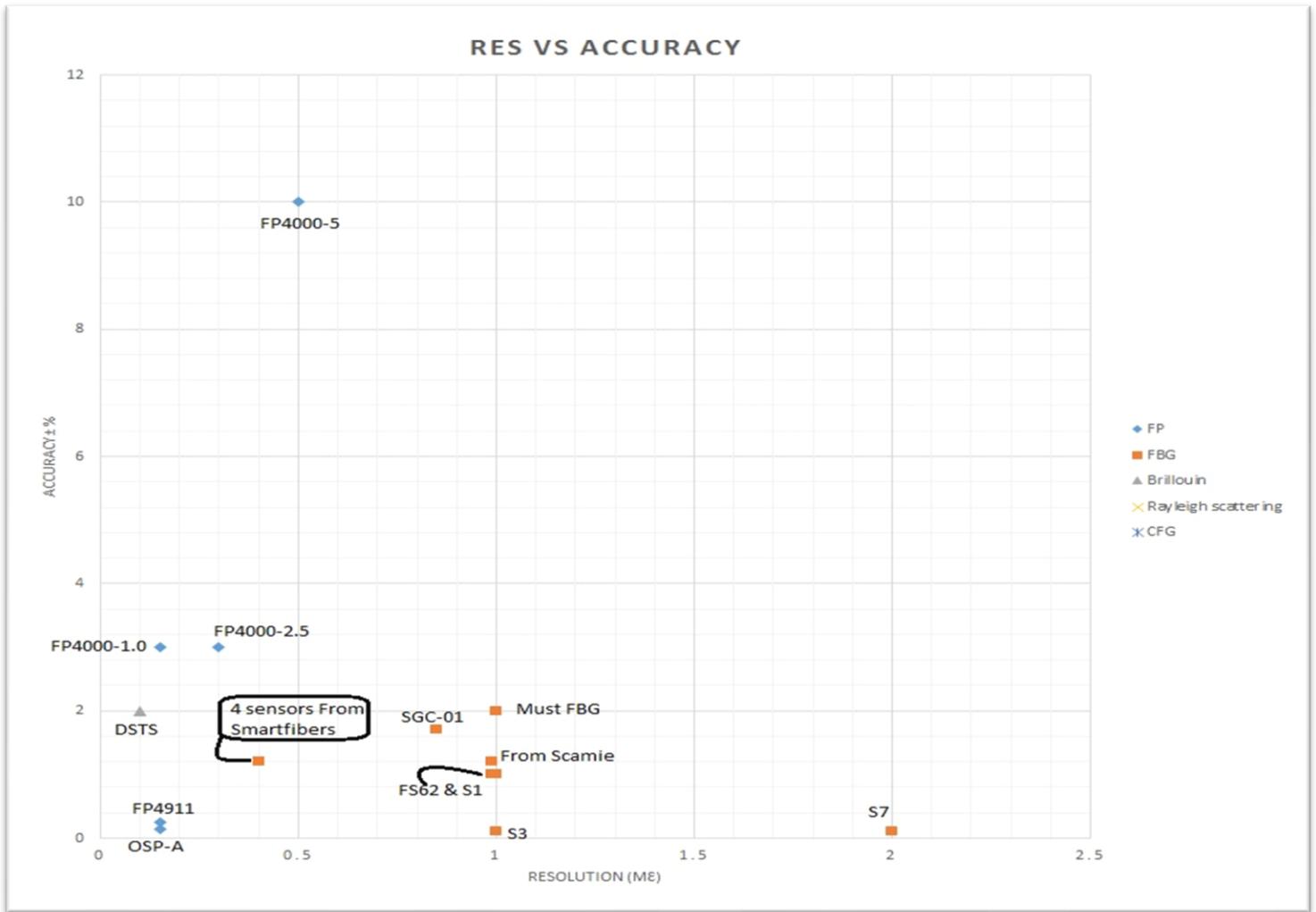
8.1.4   Range vs accuracy graph
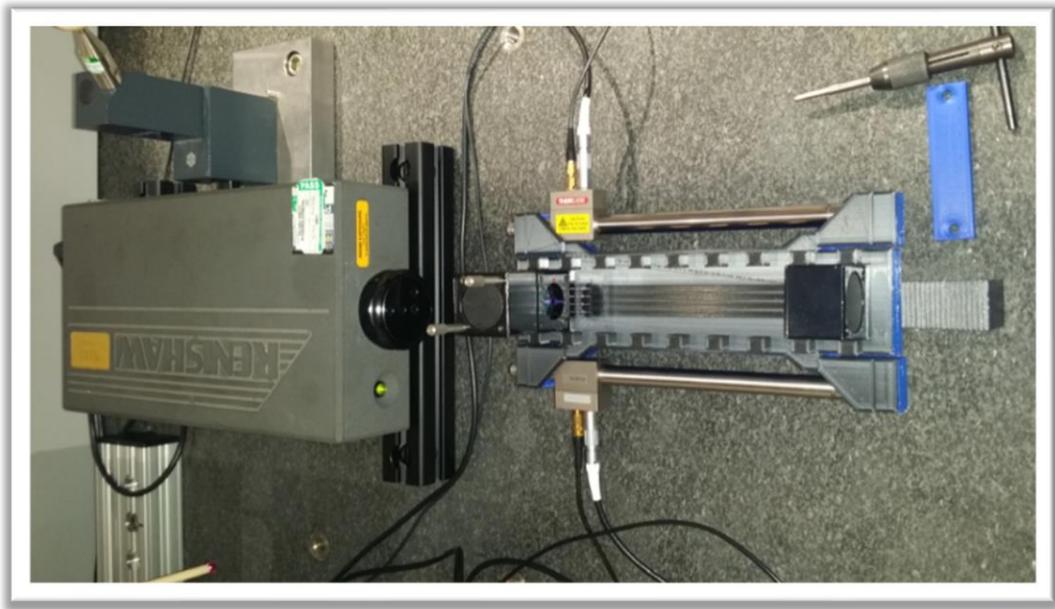

Figure 54Range vs accuracy

8.1.5 Resolution vs accuracy

Figure 55 Accuracy vs. Resolution - commercial research

8.2 The rig in the lab

Here is a photo of the sensor and the rig under the test.

Figure 56 The setup for the test

8.3 PZT actuator used for the movements.

The two PZTs used in this study.

Figure 57 PAZ015 - Piezoelectric Actuator with Feedback, 100 μm Travel

8.4   PZT controller (the amplifier)

8.5   3D printed jigs

Figure 58 *BPC303-apt piezo controller*
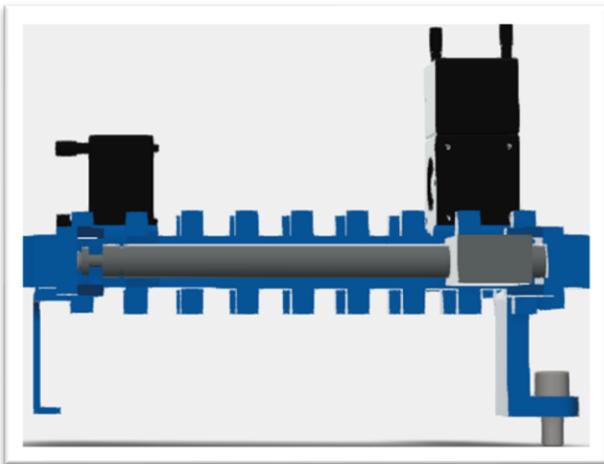
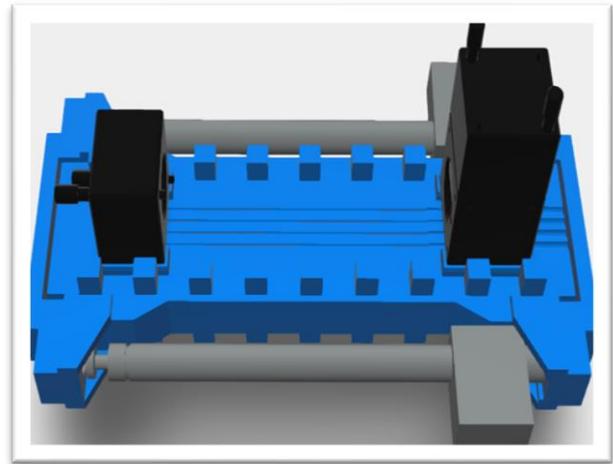### 8.5.1   1st jig

Figure 60 side view of the 1ˢᵗ jig

Figure 59 Top-view of the 1st jig

8.5.2   2ⁿᵈ jig

In the second jig, as it could be seen, the holes in the body and the metal rod PZT-holders helped the jig to be %34 responsive rather than 9
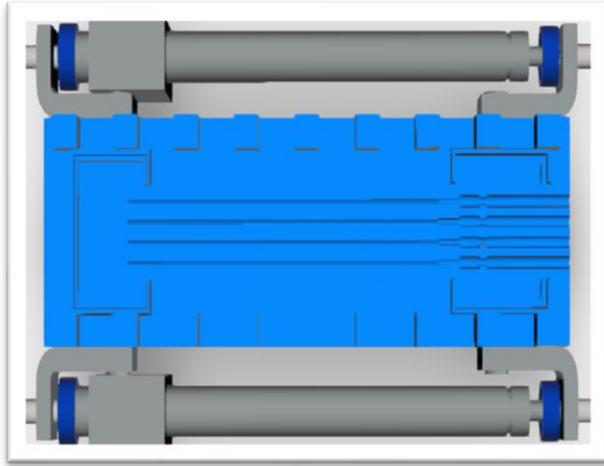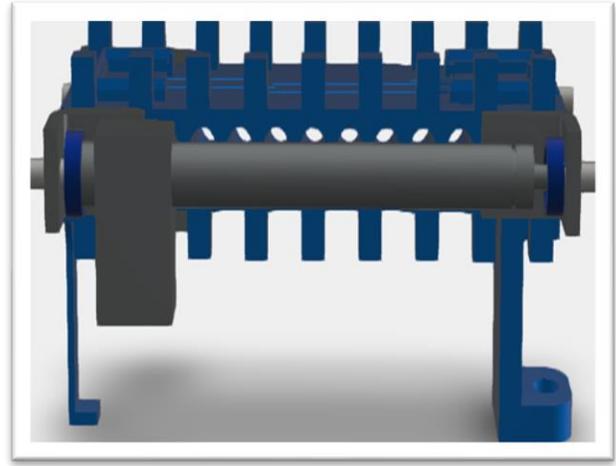
Figure 61 2nd jig sideview

Figure 62 2nd jig top view

8.6 Different windows of cropping

windowing_fft(120-140)					
Test No	lowFreq	highFreq	picFreq	maxRes	stdRes
1	100	1500	126	0.5881	0.2143
2	300	1700	126	0.5463	0.248
3	500	1900	126	0.4241	0.1715
4	700	2100	126	0.2681	0.0881
5	900	2300	126	0.0394	0.0233
6	1100	2500	126	0.4678	0.2244
7	1300	2700	126	0.5869	0.3194
8	1500	2900	126	0.5778	0.3569
9	1700	3100	126	0.9202	0.44
10	1900	3300	126	0.9025	0.5477
11	2100	3500	126	0.9356	0.3133
12	2300	3700	126	0.164	0.0376
13	2500	3900	126	0.2163	0.1039
14	2700	4100	126	0.23	0.0979
15	2900	4300	126	0.2335	0.0976

16	3100	4500	126	0.1507	0.0888
17	3300	4700	126	0.2466	0.1084
18	3500	4900	126	0.2981	0.1235
19	3700	5100	126	0.3119	0.1386
20	3900	5300	126	0.2023	0.1257
21	4100	5500	126	0.1264	0.0584
22	4300	5700	126	0.139	0.0626
23	4500	5900	126	0.2515	0.1544
24	4700	6100	126	0.3661	0.1654
25	4900	6300	126	0.3646	0.1435
26	5100	6500	126	0.307	0.1196
27	5300	6700	126	0.3123	0.1066
28	5500	6900	126	0.274	0.1008
29	5700	7100	126	0.2454	0.0899
30	5900	7300	126	0.2649	0.0817
31	6100	7500	126	0.6289	0.1485
32	6300	7700	126	0.6413	0.2064
33	6500	7900	126	0.3576	0.2098
34	6700	8100	126	0.2033	0.1176

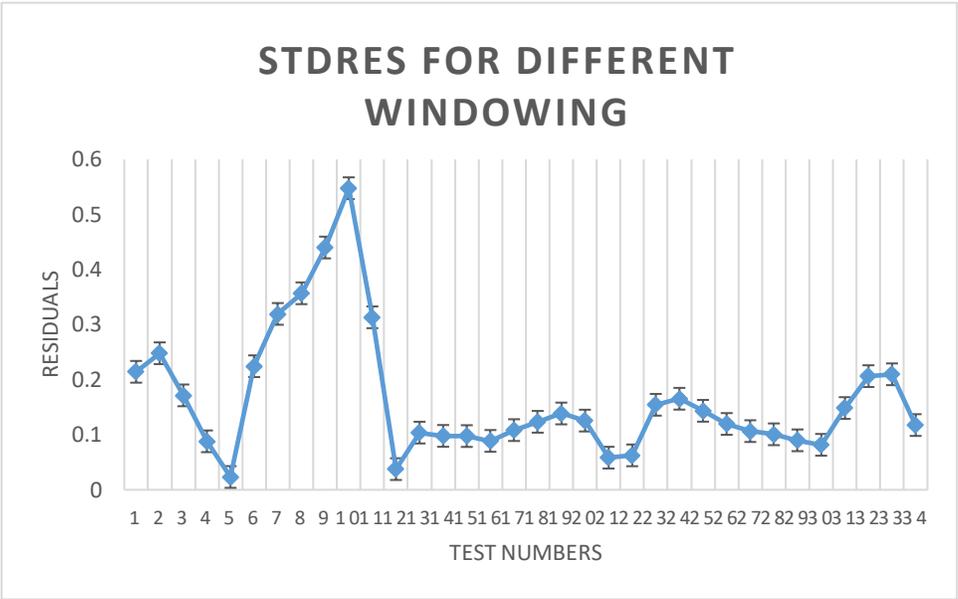*Figure 63 table of different windowing to extract the slope.*

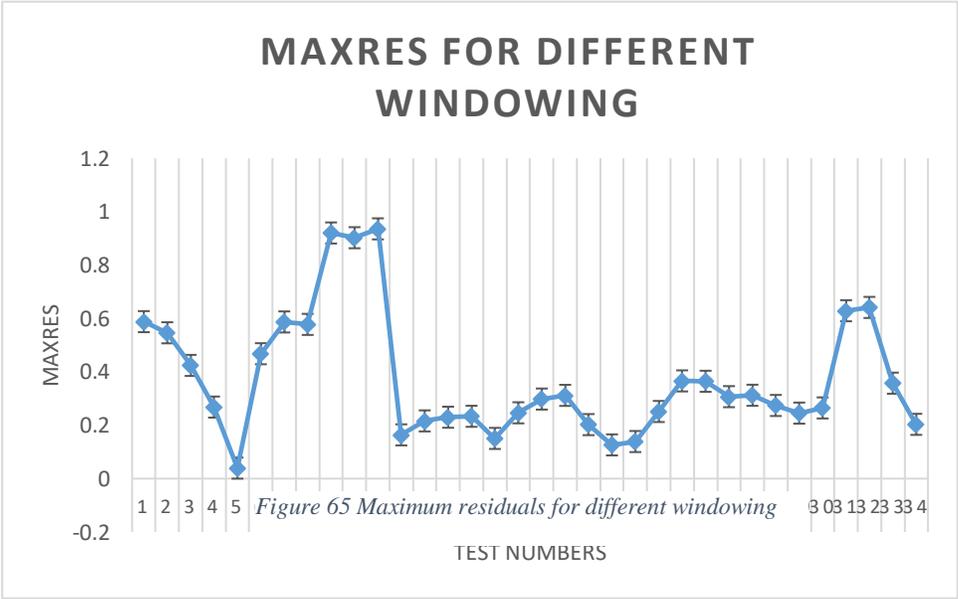*Figure 64 standard residuals for different windowing*

Figure 65 Maximum residuals for different windowing

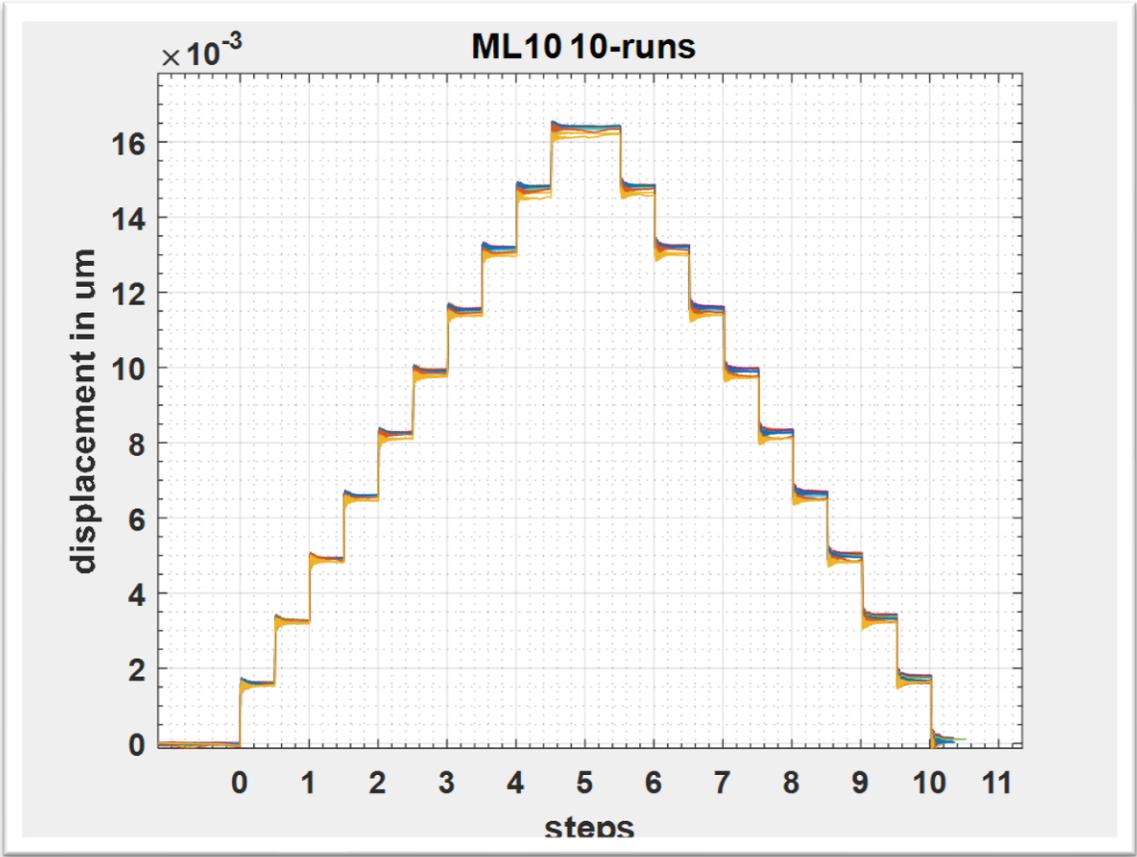## 8.7   10-runs of the final test's graphs and tables
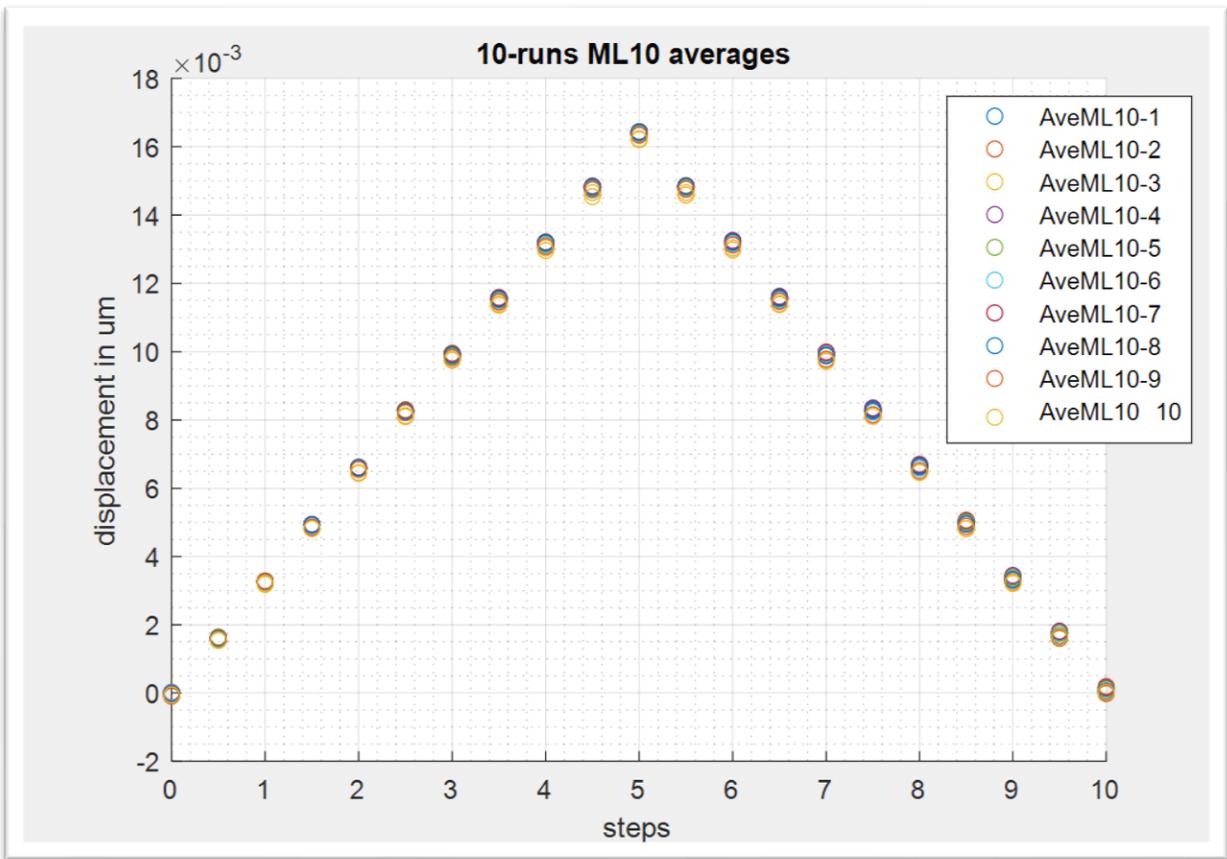
8.7.1   ML10

Figure 66 ML10 10 runs

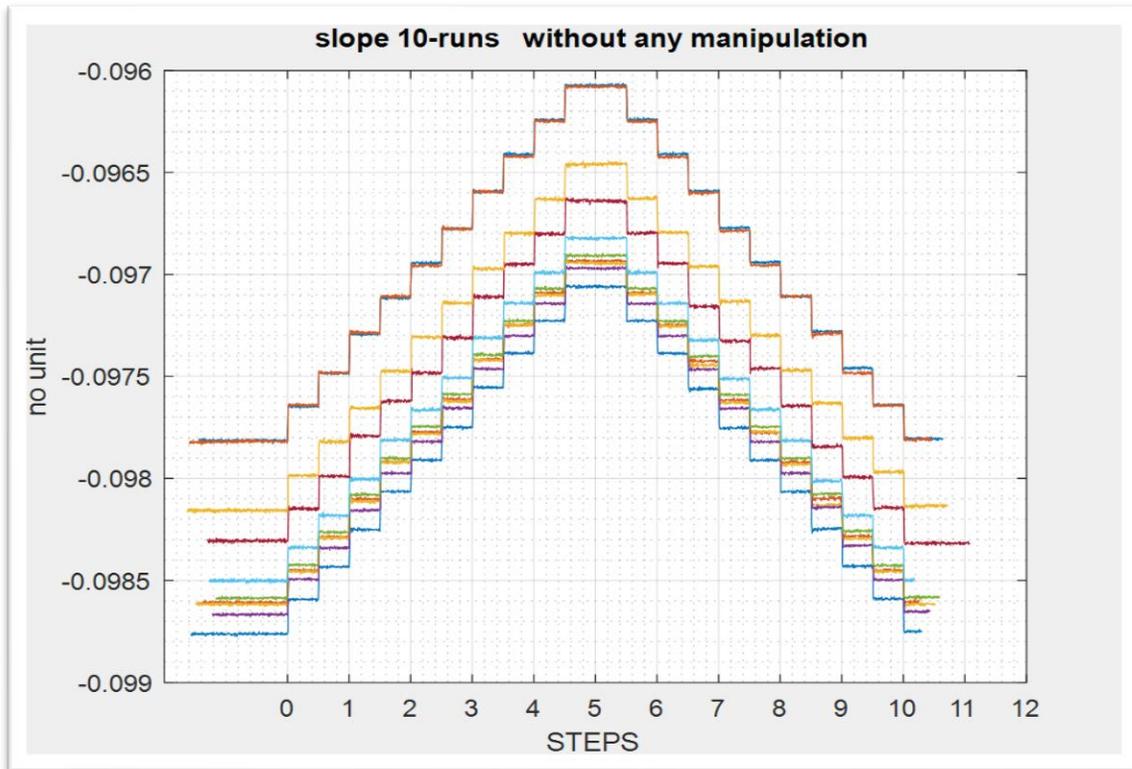*Figure 67 10-runs of averaged ML10.*

8.7.2 Slopes

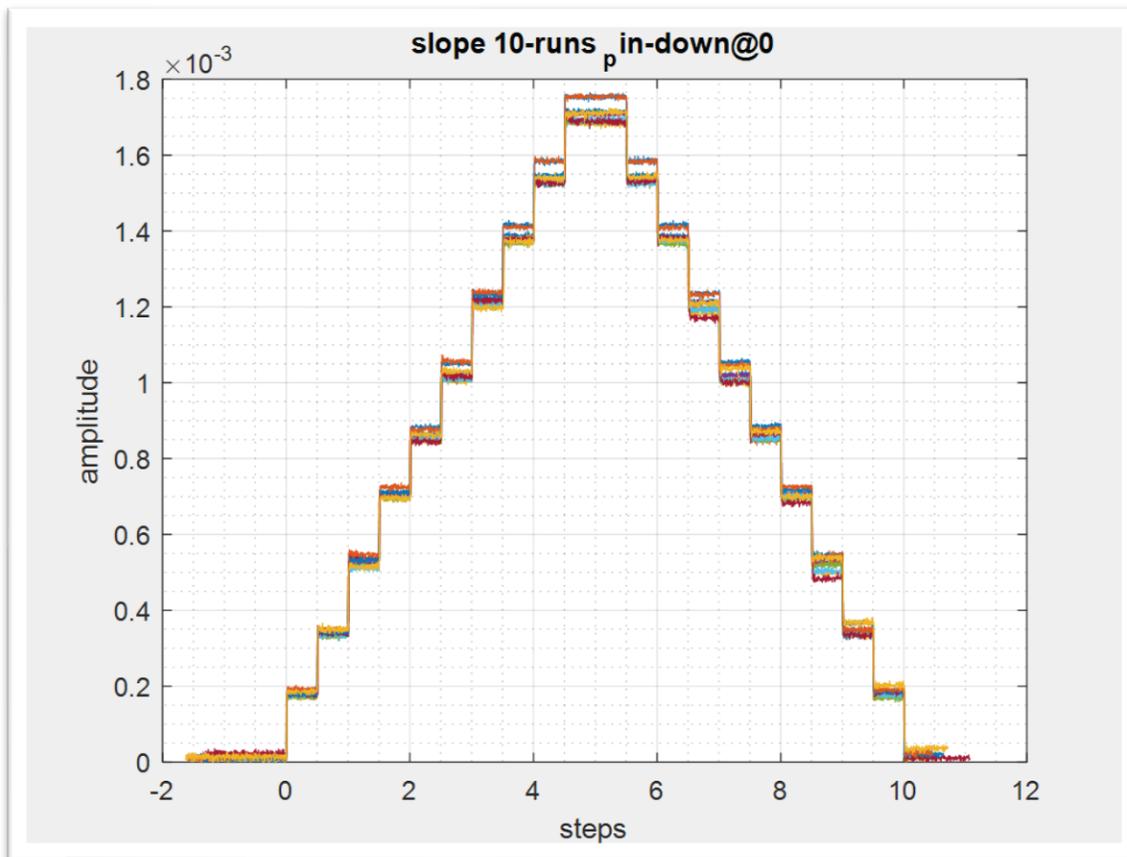*Figure 68 Slopes with no anchoring them down.*
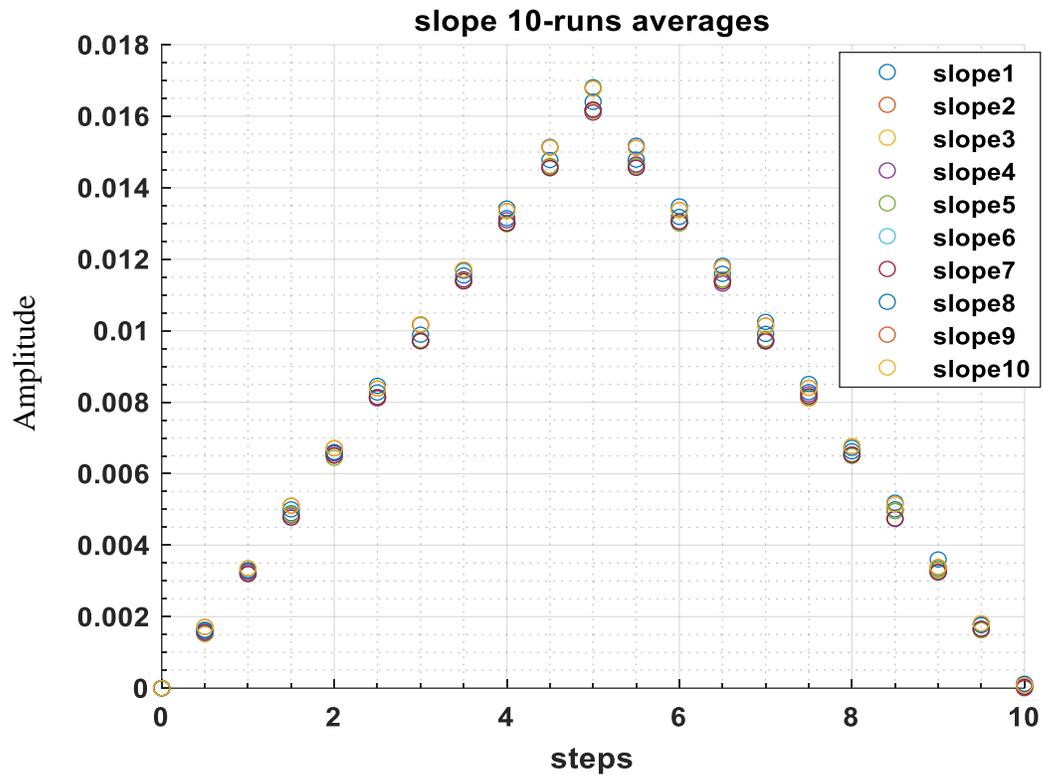

Figure 69 all slopes pinned down at zero.

Figure 70 10-runs step averaged of slopes.

References

1. Pilkey, W. D. (2005). Formulas for stress, strain, and structural matrices. Chichester: John Wiley & Sons.

2. Hearn, E. J. (1971). Strain gauges. Watford: Merrow Publishing Co.

3. Holister,– 1. 1979. Developments in Stress Analysis. London: Applied Science Publishers LTD.

4. Light. (2019, September 12). Retrieved from https://en.wikipedia.org/wiki/Light.

5. Chanzy, A., & Gaudu, J.-C. (2015). Measurement and instrumentation: theory and application. United Kingdom: Auris Reference Ltd.

6. Kimura, M., & Toshima, K. (1998). Vibration sensor using optical-fibre cantilever with bulb-lens. Sensors and Actuators A: Physical, 66(1-3), 178–183. doi: 10.1016/s0924-4247(98)00005-3.

7. Peiner, E., Scholz, D., Schlachetzki, A., & Hauptmann, P. (1998). A micromachined vibration sensor based on the control of power transmitted between optical fibres. Sensors and Actuators A: Physical, 65(1), 23–29. doi: 10.1016/s0924-4247(97)01643-9.

8. Waynant, R. W., & Lowell, J. (1999). Electronic and photonic circuits and devices. New York: Institute of Electrical and Electronics Engineers.

9. Pal, B. P. (2010). Guided Wave Optical Components and Devices: Basics, Technology, and Applications. Academic Press.

10. Optical Fibre Sensors. (1987). doi: 10.1007/978-94-009-3611-9.

11. Krohn, D. A., MacDougall, T., & Mendez Alexis. (2014). Fibre optic sensors: fundamentals and applications. Bellingham, Washington (1000 20th St. Bellingham WA 98225-6705 USA): SPIE.

12. Sperry Corporation. (2019, November 27). Fibre optic small-displacement sensor. Retrieved from https://patents.justia.com/patent/4293188.

13. Hartog, A. (1983). A distributed temperature sensor based on liquid-core optical fibres. Journal of Lightwave Technology, 1(3), 498–509. doi: 10.1109/jlt.1983.1072146.

14. Hartog, A., Leach, A., & Gold, M. (1985). Distributed temperature sensing in solid core fibres. Electronics Letters, 21(23), 1061. doi: 10.1049/el:19850752.

15. Farhadiroushan, M., Feced, R., Handerek, V. A., & Rogers, A. J. (1997). Evaluation of a High Spatial Resolution Distributed Optical Fiber Sensor for High-Temperature Applications. 12th International Conference on Optical Fiber Sensors, 3772–3776. doi: 10.1364/ofs.1997.owd2

16. Long, D. A. (1977). Raman spectroscopy. New York: McGraw-Hill.

17. Horiguchi, T., Shimizu, K., Kurashima, T., Tateda, M., & Koyamada, Y. (1995). Development of a distributed sensing technique using Brillouin scattering. Journal of Lightwave Technology, 13(7), 1296–1302. doi: 10.1109/50.400684.

18. Dakin, J. P., Pratt, D. J., Bibby, G. W., & Ross, J. N. (1986). Temperature Distribution Measurement Using Raman Ratio Thermometry. Fibre Optic and Laser Sensors III. doi: 10.1117/12.949798.

19. Feced, R., Farhadiroushan, M., Handerek, V., & Rogers, A. (1997). Advances in high resolution distributed temperature sensing using the time-correlated single-photon counting technique. IEE Proceedings - Optoelectronics, 144(3), 183. doi: 10.1049/ip-opt:19971183.

20. Bao, X., Demerchant, M., Brown, A., & Bremner, T. (2001). Tensile and compressive strain measurement in the lab and field with the distributed Brillouin scattering sensor. Journal of Lightwave Technology, 19(11), 1698–1704. doi: 10.1109/50.964070.

21. Dakin, J., & Culshaw, B. (1988). Optical fibre sensors. Norwood, MA: Artech House.

22. Krohn, D. A. (2000). Fibre optic sensors: fundamentals and applications. Research Triangle, NC: ISA.

23. Kawasaki, B. S., Hill, K. O., Johnson, D. C., & Fujii, Y. (1978). Narrow-band Bragg reflectors in optical fibres. Optics Letters, 3(2), 66. doi: 10.1364/ol.3.000066.

24. Hill, K. O., Fujii, Y., Johnson, D. C., & Kawasaki, B. S. (1978). Photosensitivity in optical fibre waveguides: Application to reflection filter fabrication. Applied Physics Letters, 32(10), 647–649. doi: 10.1063/1.89881.

25. Hill, K. O., Fujii, Y., Johnson, D. C., & Kawasaki, B. S. (1978). Photosensitivity in optical fibre waveguides: Application to reflection filter fabrication. Applied Physics Letters, 32(10), 647–649. doi: 10.1063/1.89881.

26. Kersey, A., & Dandridge, A. (1989). Multiplexed Mach-Zehnder ladder array with ten sensor elements. Electronics Letters, 25(19), 1298. doi: 10.1049/el:19890868.

27. Agrawal, G. (1989). Crosstalk penalty in multichannel ASK heterodyne light wave systems. Journal of Lightwave Technology, 7(12), 2064–2071. doi: 10.1109/50.41631.

28. Kersey, A., Marrone, M., & Dandridge, A. (1991). Experimental investigation of polarisation-induced fading in interferometric fibre sensor arrays. Electronics Letters, 27(7), 562. doi: 10.1049/el:19910354.

29. Kersey, A., Marrone, M., & Davis, M. (1991). Polarisation-insensitive fibre optic Michelson interferometer. Electronics Letters, 27(6), 518. doi: 10.1049/el:19910325.

30. Marrone, M. J., Kersey, A. D., & Dandridge, A. (1992). Fibre Optic Michelson Array with Passive Elimination of Polarization Fading and Source Feedback Isolation. Optical Fibre Sensors. doi: 10.1364/ofs.1992.w36.

31. Yuan, L., Jin, W., Zhou, L., Hoo, Y., & Demokan, M. (n.d.). Enhanced multiplexing capacity of low coherence reflectometric sensors based on a loop topology. Proceedings of IEEE Sensors. doi: 10.1109/icsens.2002.1037354.

32. Tucker, R., Eisenstein, G., & Korotky, S. (1988). Optical time-division multiplexing for very high bit-rate transmission. Journal of Lightwave Technology, 6(11), 1737–1749. doi: 10.1109/50.9991.

33. Kersey, A., Davis, M., Patrick, H., Leblanc, M., Koo, K., Askins, C., … Friebele, E. (1997). Fibre grating sensors. Journal of Lightwave Technology, 15(8), 1442–1463. doi: 10.1109/50.618377.

34. Weber, H.-G., Ludwig, R., Ferber, S., Schmidt-Langhorst, C., Kroh, M., Marembert, V., … Schubert, C. (2006). Ultrahigh-Speed OTDM-Transmission Technology. Journal of Lightwave Technology, 24(12), 4616–4627. doi: 10.1109/jlt.2006.885784.

35. TDM Multiplexing. (n.d.). Retrieved November 28, 2019, from http://citeseerx.ist.psu.edu/viewdoc/download?doi=10.1.1.586.6210&rep=rep1&type=pdf,.

36. ¿Qué es WDM? (n.d.). Retrieved from http://es.opticalmodulemanufacturers.com/what-is-wdm_n17.

37. Rappaport, T. S. (2002). Wireless communicators: principles and practice. Upper Saddle River, NJ: Prentice-Hall PTR.

38. Agrawal, G. P. (2011). Fibre-optic communication systems. Oxford: Wiley-Blackwell.

39. Kersey, A., Dandridge, A., & Davis, M. (n.d.). Code-division Multiplexed Interferometric Array with Phase Noise Reduction And Low Crosstalk. 8th Optical Fibre Sensors Conference. doi: 10.1109/ofs.1992.763056.

40. Takeda, M., Ina, H., & Kobayashi, S. (1982). Fourier-transform method of fringe pattern analysis for computer-based topography and interferometry. Journal of the Optical Society of America, 72(1), 156. doi: 10.1364/josa.72.000156.

41. Find and share research. (n.d.). Retrieved from https://www.researchgate.net/figure/Measurement-principal-of-Fiber-Bragg-Grating-FBG-sensor_fig2_277892527.

42. (n.d.). Retrieved December 25, 2019, from http://www.bostoninstruments.com/technology.html.

43. P. (n.d.). Retrieved December 20, 2019, from https://uk.mathworks.com/help/matlab/ref/unwrap.html.

44. sys. (n.d.). Retrieved December 22, 2019, from https://uk.mathworks.com/help/control/ref/stepinfo.html.

45. Hargrave, M. (2019, November 18). Standard Deviation Definition. Retrieved December 30, 2019, from https://www.investopedia.com/terms/s/standarddeviation.asp.

46. Calibration Awareness. (n.d.). Retrieved January 2, 2020, from https://calibrationawareness.com/calibration-awareness-what-is-calibration.

47. Ronald. (n.d.). FIBER OPTIC. Retrieved January 12, 2020, from http://fibers-optics.blogspot.com/

48. Virginia Tech Scholarly Communication University Libraries. (n.d.). Retrieved January 12, 2020, from https://scholar.lib.vt.edu/

49. City Research Online. (n.d.). Retrieved January 14, 2020, from https://openaccess.city.ac.uk/.

50. Malekzadeh, Masoud, and F. Necati Catbas. "A comparative evaluation of two statistical analysis methods for damage detection using fibre optic sensor data", International Journal of Reliability and Safety, 2014.

(2014). "A Comparative Evaluation of Two Statistical Analysis Methods for Damage Detection Using Fibre Optic Sensor Data".

51. Home. (n.d.). Retrieved January 15, 2020, from http://www.fiso.com/.

52. fantastiek.com is available at DomainMarket.com. (n.d.). Retrieved January 14, 2020, from http://www.fantastiek.com/.

53. A Global Leader in Automated Test and Automated Measurement Systems. (n.d.). Retrieved January 15, 2020, from http://www.ni.com/.

54. Tutorial Scribd. (n.d.). Retrieved January 15, 2020, from https://es.scribd.com/presentation/3077260/Tutorial-Scribd.

55. Main Page. (2020, February 5). Retrieved January 15, 2020, from https://en.wikipedia.org/wiki/Main_Page.

56. Castaldo, L. (n.d.). CORISTA. Retrieved January 15, 2020, from http://www.corista.unina.it/.

57. Handle Proxy. (n.d.). Retrieved January 15, 2020, from http://hdl.handle.net/.

58. fantastiek.com is available at DomainMarket.com. (n.d.). Retrieved January 15, 2020, from http://www.fantastiek.com/.

59. BENVENUTO IN AIDIC. (n.d.). Retrieved January 15, 2020, from http://www.aidic.it/.

60. theses-and-dissertations Theses and Dissertations. (n.d.). Retrieved January 15, 2020, from https://www.uj.ac.za/library/research-support/Pages/theses-and-dissertations.aspx

61. Start. (n.d.). Retrieved January 15, 2020, from https://gfzpublic.gfz-potsdam.de/.

62. Wang, Z. (2006). Intrinsic Fabry-Perot Interferometric Fiber sensor based On ultra-short BRAGG gratings for Quasi-distributed strain and temperature measurements (Doctoral dissertation, 2006). Blacksburg, VA: University Libraries, Virginia Polytechnic Institute and State University.

63. Geib, D. C. (2003). Multiplexing of Extrinsic Fabry-perot optical fiber sensors for strain measurements (Doctoral dissertation, 2003). Blacksburg, VA: University Libraries, Virginia Polytechnic Institute and State University.

64. Karimi, M. (2014). Experimental and theoretical analysis of polarization-maintaining fibre for sensing applications (Unpublished doctoral dissertation). City University.